

DRUG RELEASE PROPERTIES OF NANOSTRUCTURED
LIPID, LIPOSOME, OIL-IN-WATER MICROEMULSION
AND κ -CARRAGEENAN-CHITOSAN NANOPARTICLE

YEW HAN CHOI

THESIS SUBMITTED IN FULFILMENT OF
THE REQUIREMENTS FOR THE DEGREE
OF DOCTOR OF PHILOSOPHY

FACULTY OF SCIENCE
UNIVERSITY OF MALAYA
KUALA LUMPUR

2017

UNIVERSITI MALAYA
ORIGINAL LITERARY WORK DECLARATION

Name of Candidate: **YEW HAN CHOI**

Registration/Matric No: **SHC 110101**

Name of Degree: **DOCTOR OF PHILOSOPHY**

Title of Project Paper/Research Report/Dissertation/Thesis ("this Work"):

DRUG RELEASE PROPERTIES OF NANOSTRUCTURED LIPID, LIPOSOME, OIL-IN-WATER MICROEMULSION AND κ -CARRAGEENAN-CHITOSAN NANOPARTICLE

Field of Study: **PHYSICAL CHEMISTRY/ BIOCOLLOID**

I do solemnly and sincerely declare that:

- (1) I am the sole author/writer of this Work;
- (2) This Work is original;
- (3) Any use of any work in which copyright exists was done by way of fair dealing and for permitted purposes and any excerpt or extract from, or reference to or reproduction of any copyright work has been disclosed expressly and sufficiently and the title of the Work and its authorship have been acknowledged in this Work;
- (4) I do not have any actual knowledge nor do I ought reasonably to know that the making of this work constitutes an infringement of any copyright work;
- (5) I hereby assign all and every rights in the copyright to this Work to the University of Malaya ("UM"), who henceforth shall be owner of the copyright in this Work and that any reproduction or use in any form or by any means whatsoever is prohibited without the written consent of UM having been first had and obtained;
- (6) I am fully aware that if in the course of making this Work I have infringed any copyright whether intentionally or otherwise, I may be subject to legal action or any other action as may be determined by UM.

Candidate's Signature

Date

Subscribed and solemnly declared before,

Witness's Signature

Date

Name:

Designation:

ABSTRACT

The dissolution and permeation of active ingredient from its carrier system are the key factors in affecting its efficacy. An ability to control active ingredient's rate of release not only enable optimum therapeutic effect but also lower the possibility of adverse effect. This study aimed to investigate the physicochemical properties, encapsulation efficiency and release profile of four types of nanocarrier with different disperse and continuous phases. The four nanocarriers include (i) nanostructured lipid whereby the lipid matrix is dispersed in aqueous phase; (ii) liposome consists of outer lipid bilayer and aqueous core which also dispersed in aqueous phase; (iii) water-in-oil microemulsion has water droplet as disperse phase and olive oil as continuous phase; last but not least, (iv) κ -carrageenan-chitosan nanoparticle which has hydrophilic polymer dispersed in aqueous phase. Three low molecular weight active ingredients with different solubility in water which are ascorbic acid, caffeine and lidocaine were then encapsulated in those nanocarriers. Based on the physicochemical evaluations, the formulated nanocarriers were stable for at least 30 days with polydispersity of < 0.4 when kept at 30 °C. The particle sizes of nanocarriers were in the ascending order of 30 nm, 100 nm, 250 nm, and 400 nm for microemulsion, liposome, nanostructured lipid, and κ -carrageenan-chitosan nanoparticle respectively. Encapsulation efficiency revealed that liposome and nanostructured lipid which have lipid surface, were excellent for lidocaine encapsulation up to 80% while water-in-oil microemulsion and κ -carrageenan-chitosan nanoparticle have better preference towards more water soluble ascorbic acid with 70% encapsulation efficiency. All nanocarriers exhibit controlled release property whereby the active ingredients' rates of release from those nanocarriers were slower than free active ingredients. The average time required for *in vitro* 50% active ingredients to be released from nanocarriers were in the order of liposome (7 hours), nanostructured lipid (9 hours), water-in-oil microemulsion (33 hours), and lastly, κ -

carrageenan-chitosan nanoparticle (more than 48 hours) irrespective to the types of active ingredients. The reason for a shorter time to achieve 50% release in liposome and nanostructured lipid is due to initial burst release from the surface of the nanocarrier which is then followed by sustained release from the matrix core. Nanostructured lipid which requires longer release time than liposome was accountable to the fact that longer diffusion path length for the homogenized nanocarrier to diffuse due to its larger size. The extended period of release time for water-in-oil microemulsion is plausibly due to interfacial barrier and different permeability coefficient of donor and receptor chamber in Franz diffusion cell. κ -carrageenan-chitosan nanoparticle which extensively prolonged the release time could be attributed by electrostatic interaction between the active ingredients and the polymer. The *in vitro* release profile of those nanocarriers showing that they could be tailored for different applications, hence aided in solving solubility and permeability problems, enhancing therapeutic effects and lastly, minimizing or eliminating possible side effects.

ABSTRAK

Kelarutan dan penelapan ramuan aktif adalah faktor-faktor utama yang mempengaruhi efikasi ramuan aktif dalam sistem penghantaran. Kebolehan untuk mengawal kadar pembebasan ramuan aktif bukan hanya memberi kesan terapeutik yang optimum tetapi juga membantu mengurangkan kesan sampingan. Objektif penyelidikan ini adalah untuk mengkaji sifat fisikokimia, kecekapan pengkapsulan dan profil pembebasan ramuan aktif daripada empat jenis sistem penghantaran yang mempunyai fasa sebaran dan fasa berterusan yang berbeza. Empat sistem penghantaran yang dikaji adalah (i) lipid struktur nano dimana matriks lipid tersebar dalam akues; (ii) liposom mempunyai lipid dwilapisan luar dan akues teras yang juga tersebar dalam akues; (iii) emulsimikro air dalam minyak terdiri daripada butiran air sebagai fasa sebar dan minyak zaitun sebagai fasa berterusan serta (iv) zarah nano κ -karagenan-kitosan dimana polimer hidrofilik tersebar dalam akues. Tiga ramuan aktif yang mempunyai berat molekul yang kecil serta keterlarutan air yang berbeza iaitu asid askorbik, kafein dan lidokain telah dikapsulkan dalam sistem penghantaran tersebut. Berdasarkan penilaian fisikokimia, apabila sistem penghantaran tersebut disimpan pada suhu 30 °C, ia adalah stabil dengan kepoliserakan yang kurang daripada 0.4 selama sekurang-kurangnya 30 hari. Purata saiz zarah sistem penghantaran emulsimikro, liposom, lipid struktur nano dan zarah nano κ -karagenan-kitosan adalah masing-masing 30 nm, 100 nm, 250 nm dan 400 nm. Kecekapan pengkapsulan menunjukkan bahawa liposom dan lipid struktur nano adalah sesuai untuk mengkapsul lidokain iaitu sebanyak 80% manakala emulsimikro air dalam minyak dan zarah nano κ -karagenan-kitosan yang lebih sesuai untuk asid askorbik yang lebih larut dalam air, mempunyai kecekapan pengkapsulan sebanyak 70%. Semua sistem penghantaran menunjukkan sifat pembebasan terkawal dimana kadar pembebasan ramuan aktif dari sistem penghantaran adalah lebih perlahan berbanding ramuan aktif yang tidak dikapsulkan. Purata masa yang diperlukan untuk membebaskan

50% ramuan aktif dari sistem penghantaran secara *in vitro* tanpa mengambil kira jenis ramuan aktif adalah meningkat daripada liposom (7 jam), lipid struktur nano (9 jam), emulsimikro air dalam minyak (33 jam) dan zarah nano κ -karagenan-kitosan (lebih daripada 48 jam). Liposom dan lipid struktur nano memerlukan masa yang lebih pendek berikutan peletusan awal dari permukaan sistem penghantaran seterusnya pembebasan tertahan dari matriks teras. Lipid struktur nano memerlukan masa yang lebih lama berbanding liposom dalam pembebasan ramuan aktif disebabkan oleh saiz partikel yang lebih besar maka laluan peresapan yang lebih panjang bagi sistem penghantaran tersebut. Masa pembebasan yang diperpanjangkan oleh emulsimikro air dalam minyak adalah berkemungkinan kerana sawar antara muka dan koefisien ketelapan yang berbeza pada bahagian penderma dan penerima 'Franz diffusion cell'. Zarah nano κ -karagenan-kitosan yang mempunyai masa pembebasan yang diperpanjangkan secara ekstensif adalah disebabkan oleh interaksi elektrostatik antara ramuan aktif dan polimer. Berlandaskan profil pembebasan *in vitro*, sistem penghantaran yang dikaji boleh dikhususkan untuk aplikasi yang berbeza supaya dapat menyelesaikan masalah kelarutan dan penelapan, mempertingkatkan kesan terapeutik dan juga mengurangkan atau menghapuskan kesan sampingan ramuan aktif.

ACKNOWLEDGEMENT

I would like to take this opportunity to thank my dearest family members for their moral support and unconditional love. I would also like to express my sincere appreciation to my supervisor, Prof. Dr. Misni Misran for his constant guidance, patience and encouragement from the beginning of proposal preparation until the final write up of this thesis. Meanwhile, not to forget a bunch of great lab mates from colloid and surface laboratory and friends, Dr. Teo Yin Yin, Dr. Tan Hsiao Wei, Madam Radziah Muhamad, Madam Hairani Tahir, Ms. Jane Gew Lai Ti, Mr. Vicit Rizal Eh Suk, Mr. Woo Juin Onn, Ms. Tiew Shu Xian, Ms. Premarayani Menon, Madam Sumaira Naeem, Ms. Ainnul Hamidah Syahadah and many more which I could not count individually. Many thanks to the staffs of Faculty of Science from both University Malaya and University Sains Malaysia, especially those technical staff for the usage of instruments in the faculty. Finally, without the financial support from MyBrain15 which offered me a scholarship along this studies, this work would not have been a success.

TABLE OF CONTENT

ABSTRACT	iii
ABSTRAK	v
ACKNOWLEDGEMENT	vii
TABLE OF CONTENT	viii
LIST OF FIGURES	xi
LIST OF TABLES	xvi
LIST OF SYMBOLS AND ABBREVIATIONS	xviii
CHAPTER 1: INTRODUCTION	1
1.1 Solvent solubility and bioavailability of active ingredients	1
1.2 Active ingredients' delivery pathways	3
1.3 Drug delivery carrier	5
1.4 Characterization of delivery carrier	6
1.5 Aims of research	8
1.6 Outline of research	8
CHAPTER 2: LITERATURE REVIEW	9
2.1 Nanostructured lipid	10
2.1.1 Lipids and emulsifier for NLC	11
2.1.2 Techniques applied in NLC's preparation	12
2.1.2.1 Hot and/or cold homogenization	12
2.1.2.2 Ultrasonication	13
2.1.2.3 Emulsification-solvent evaporation	13
2.1.3 Advantages of NLC's usage	14
2.2 Liposome	16
2.2.1 Surface modified liposome	16
2.2.2 Preparation of liposome	19
2.2.2.1 Physical dispersion	19
2.2.2.2 Solvent dispersion	20
2.2.2.3 Detergent solubilisation	20
2.2.3 Interaction of liposome with the body	21
2.3 Water-in-oil microemulsion	23
2.3.1 Compositions of microemulsion	24
2.3.2 Preparation of microemulsion	26
2.3.3 Advantages of microemulsion application	27
2.4 Polymeric nanocarrier	29
	viii

2.4.1 Polysaccharide based nanoparticles	29
2.4.1.1 Chitosan	30
2.4.1.2 Carrageenan	31
2.4.2 Synthesis of polysaccharide nanoparticle	31
2.4.3 Polymeric nanoparticle for active ingredients delivery	33
CHAPTER 3: MATERIALS AND METHODS	37
3.1 Materials	37
3.2 Preparation of delivery carriers	38
3.2.1 Preparation of NLC	38
3.2.2 Preparation of liposome	39
3.2.3 Preparation of water-in-oil microemulsion	39
3.2.4 Preparation of κ -carrageenan-chitosan nanoparticle	40
3.3 Principle and characterization of delivery carriers	41
3.3.1 Particle size and zeta potential	41
3.3.2 Transmission electron microscopy (TEM)	43
3.3.3 Differential scanning calorimetry (DSC)	44
3.3.4 Critical vesicular concentration (CVC)	45
3.3.5 FTIR	46
3.3.6 Swelling percentage	47
3.3.7 pH	48
3.3.8 Conductivity	48
3.3.9 Viscosity	49
3.4 Loading efficiency, encapsulation efficiency and release profile of nanocarrier	50
3.4.1 Loading and encapsulation of active ingredients	51
3.4.1.1 Preparation and evaluation of encapsulated NLC	51
3.4.1.2 Preparation and evaluation of encapsulated liposome	51
3.4.1.3 Preparation and evaluation of water-in-oil microemulsion	52
3.4.1.4 Preparation and evaluation of encapsulated κ -carrageenan-chitosan nanoparticle	52
3.4.2 Franz diffusion cell for active ingredient's release profile	53
3.4.3 Kinetic models	54
3.4.3.1 Zero-order model	54
3.4.3.2 First-order model	54
3.4.3.3 Higuchi model	55
3.4.3.4 Hixson-Crowell model	55

3.4.3.5 Korsmeyer-Peppas model	56
CHAPTER 4: RESULTS AND DISCUSSION	57
4.1 Physical characterization of delivery carriers	57
4.1.1 Characterization of NLC	57
4.1.2 Characterization of Liposome	62
4.1.3 Characterization of water-in-oil microemulsion	67
4.1.4 Characterization of κ -carrageenan-chitosan nanoparticle	73
4.2 Loading and encapsulation efficiency of active ingredients	80
4.2.1 Encapsulated NLC	81
4.2.2 Encapsulated liposome	84
4.2.3 Encapsulated water-in-oil microemulsion	88
4.2.4 Encapsulated κ -carrageenan-chitosan nanoparticle	90
4.3 Release profile of active ingredients from delivery vehicles	93
4.3.1 Release profile of unencapsulated ingredients	93
4.3.2 Release profile of NLC	97
4.3.3 Release profile of liposome	102
4.3.4 Release profile of water-in-oil microemulsion	107
4.3.5 Release profile of κ -carrageenan-chitosan nanoparticle	112
CHAPTER 5: CONCLUSION	118
5.1 Summary	118
5.2 Future work	122
REFERENCE	123
LIST OF PUBLICATIONS AND PAPERS PRESENTED	150

LIST OF FIGURES

Figure 1.1	General pathways for active ingredients' delivery	3
Figure 2.1	Delivery vehicles for active ingredients' solubilisation and permeation	9
Figure 2.2	Effect of surfactant packing parameters on the structure of microemulsion. The packing parameter of a surfactant is affected by the area of hydrophilic head group (a_o), length of hydrophobic tail (l_c) and the volume of the surfactant's tail (v). The larger the value of packing parameters, the structure will be more prone to the formation of water-in-oil microemulsion.	25
Figure 4.1	Changes in particle size of NLC samples prepared by using different fatty acid compositions for a storage period of 28 days at 30 °C. The symbols ▽ = NLC 1, ○ = NLC 2, ◇ = NLC 3, △ = NLC 4, □ = NLC 5.	58
Figure 4.2	Changes in zeta potential of NLC aqueous suspension with varied fatty acid compositions as a function storage time of 28 days at 30 °C. The symbols ▽ = NLC 1, ○ = NLC 2, ◇ = NLC 3, △ = NLC 4, □ = NLC 5.	59
Figure 4.3	Differential scanning calorimetry thermogram of NLC. The experiment was performed from 25 °C to 100 °C at a scan rate of 5 °C per minute.	61
Figure 4.4	TEM micrographs of NLC where (a) is NLC 1, (b) is NLC 3, and (c) is NLC 5. All micrographs were taken at 10, 000 × magnification using Carl Zeiss LIBRA® 120.	62
Figure 4.5	Surface tension of fatty acids liposome solution with different concentrations evaluated at pH 8.6 with a temperature of 30 °C. □ = oleic acid, ○ = linoleic acid, △ = linolenic acid. The arrow indicates the critical vesicular concentration of fatty acid liposomes.	63
Figure 4.6	TEM micrographs of liposome where (a) represents oleic acid, (b) represents linoleic acid, and (c) represents linolenic acid liposome. For those micrographs, all were taken at 8,000 × magnification by using JOEL JEM-2100F.	66
Figure 4.7	Ternary phase diagram of microemulsion prepared by olive oil, water and mixed surfactants of Span 80 with various types of Tween surfactants, namely (a) Tween 40, (b) Tween 60, (c) Tween 80 and (d) Tween 85. The shadowed region indicates the presence of microemulsion.	68

Figure 4.8	Rheological behaviour of microemulsions prepared with different types of Tween surfactants in a shear rate of $0.1 - 100 \text{ s}^{-1}$. The symbols $\square = \text{ST40}$, $\circ = \text{ST60}$, $\nabla = \text{ST80}$, and $\Delta = \text{ST85}$ where opened symbols represent viscosity while solid symbols represent shear stress.	72
Figure 4.9	TEM micrographs of ST80 microemulsion taken at different magnifications of (a) $10,000 \times$ and (b) $20,000 \times$ magnification. In this visualization, Carl Zeiss LIBRA [®] 120 is being employed.	73
Figure 4.10	Particle size of κ -carrageenan-chitosan nanoparticle prepared at 30°C using pre-dissolved 1% κ -carrageenan and 1% chitosan at different mass ratios in a pH ranged from 3 to 6. The symbols $\square = \text{pH } 3$, $\circ = \text{pH } 4$, $\Delta = \text{pH } 5$, $\diamond = \text{pH } 6$.	74
Figure 4.11	Schematic diagram of polyelectrolyte complexation for κ -carrageenan and chitosan. The positively charged amino group (red) of chitosan will react with negatively charged sulphate group (blue) of κ -carrageenan.	75
Figure 4.12	Zeta potential of κ -carrageenan-chitosan nanoparticle prepared at 30°C using pre-dissolved 1% κ -carrageenan and 1% chitosan at different mass ratios in a pH ranged from 3 to 6. The symbols $\square = \text{pH } 3$, $\circ = \text{pH } 4$, $\Delta = \text{pH } 5$, $\diamond = \text{pH } 6$.	76
Figure 4.13	FTIR spectrum of (a) chitosan powder, (b) κ -carrageenan powder, (c) mixture of 1:1 κ -carrageenan with chitosan powder and (d) κ -carrageenan-chitosan nanoparticle at a wavelength of $4000\text{-}450 \text{ cm}^{-1}$.	79
Figure 4.14	Morphology of κ -carrageenan-chitosan nanoparticle prepared at 1:1 mass ratio of κ -carrageenan and chitosan. The micrographs were taken at (a) $30,000 \times$ and (b) $120,000 \times$ magnification by using JOEL JEM-2100F.	80
Figure 4.15	Active ingredients loaded NLC at different weight ratios of active ingredients to NLC. Where symbol $\square = \text{ascorbic acid}$, $\circ = \text{caffeine}$, $\Delta = \text{lidocaine}$ while AI = active ingredients, AI ^c = loaded active ingredients.	81
Figure 4.16	Encapsulation efficiency of active ingredients in varied weight ratios of active ingredients to NLC. Where symbol $\square = \text{ascorbic acid}$, $\circ = \text{caffeine}$, $\Delta = \text{lidocaine}$ while W= weight, AI= active ingredients.	82
Figure 4.17	Effect of active ingredients towards the stability of NLC with respect to storage time at 30°C . Where symbols $\blacksquare = \text{unloaded NLC}$, $\nabla = \text{ascorbic acid}$, $\Delta = \text{caffeine}$, $\circ = \text{lidocaine}$.	83

Figure 4.18	Changes in zeta potential and stability of active ingredients loaded NLC as a function of storage time at 30 °C. Where symbols ■ = unloaded NLC, ▽ = ascorbic acid, Δ = caffeine, ○ = lidocaine.	84
Figure 4.19	Particle size of oleic acid liposomes after loaded with different active ingredients at mole ratios of 0.1 to 0.5 active ingredients to fatty acid (n_{AI}/n_{FA}). Where symbol □ = ascorbic acid, ○ = caffeine, Δ = lidocaine.	86
Figure 4.20	Zeta potential of oleic acid liposomes after loaded with different active ingredients at mole ratios of 0.1 to 0.5 active ingredients to fatty acid (n_{AI}/n_{FA}). Where symbol □ = ascorbic acid, ○ = caffeine, Δ = lidocaine.	87
Figure 4.21	Mass ratio of active ingredients loaded into κ -carregeenan-chitosan nanoparticle. Where symbol □ = ascorbic acid, ○ = caffeine, Δ = lidocaine while M_{AI}/M_{CNP} is the mass ratio of active ingredients to the weight of κ -carregeenan and chitosan and M_{AI}^e is the mass of loaded active ingredients.	90
Figure 4.22	Encapsulation efficiency of active ingredients in κ -carregeenan-chitosan nanoparticle. Where symbol □ = ascorbic acid, ○ = caffeine, Δ = lidocaine while M_{AI}/M_{CNP} is the mass ratio of active ingredients to the weight of κ -carregeenan and chitosan.	91
Figure 4.23	Release profile of unencapsulated active ingredients for 24 hours. Where symbol □ = ascorbic acid, ○ = caffeine, Δ = lidocaine.	93
Figure 4.24	Curve fitting of unencapsulated active ingredients release profile in different kinetic models. Where symbol □ = ascorbic acid, ○ = caffeine, Δ = lidocaine. The solid symbol represents the experimental plot while the opened symbol with line represents the predicted plot.	95
Figure 4.25	Curve fitting of unencapsulated active ingredients release profile for the first 12 hours in different kinetic models. Where symbol □ = ascorbic acid, ○ = caffeine, Δ = lidocaine. The solid symbol represents the experimental plot while the opened symbol with line represents the predicted plot.	97
Figure 4.26	Release profile of active ingredients from NLC for 24 hours. Where symbol □ = ascorbic acid, ○ = caffeine, Δ = lidocaine.	98
Figure 4.27	Curve fitting of active ingredients' release profile from NLC in different kinetic models for 24 hours. Where symbol □ = ascorbic acid, ○ = caffeine, Δ = lidocaine. The solid symbol represents the experimental plot while the opened symbol with line represents the predicted plot.	100

Figure 4.28	Curve fitting of active ingredients' release profile from NLC in different kinetic models for the first 12 hours. Where symbol \square = ascorbic acid, \circ = caffeine, Δ = lidocaine. The solid symbol represents the experimental plot while the opened symbol with line represents the predicted plot.	102
Figure 4.29	Release profile of active ingredients from liposome for 24 hours. Where symbol \square = ascorbic acid, \circ = caffeine, Δ = lidocaine.	103
Figure 4.30	Curve fitting of active ingredients' release profile from oleic acid liposome in different kinetic models for 24 hours. Where symbol \square = ascorbic acid, \circ = caffeine, Δ = lidocaine. The solid symbol represents the experimental plot while the opened symbol with line represents the predicted plot.	105
Figure 4.31	Curve fitting of active ingredients' release profile from liposome in different kinetic models for the first 12 hours. Where symbol \square = ascorbic acid, \circ = caffeine, Δ = lidocaine. The solid symbol represents the experimental plot while the opened symbol with line represents the predicted plot.	107
Figure 4.32	Release profile of active ingredients from water-in-oil microemulsion for 24 hours. Where symbol \square = ascorbic acid, \circ = caffeine, Δ = lidocaine.	108
Figure 4.33	Curve fitting of active ingredients' release profile from water-in-oil microemulsion in different kinetic models for 24 hours. Where symbol \square = ascorbic acid, \circ = caffeine, Δ = lidocaine. The solid symbol represents the experimental plot while the opened symbol with line represents the predicted plot.	110
Figure 4.34	Curve fitting of active ingredients' release profile from microemulsion in different kinetic models for the first 12 hours. Where symbol \square = ascorbic acid, \circ = caffeine, Δ = lidocaine. The solid symbol represents the experimental plot while the opened symbol with line represents the predicted plot.	112
Figure 4.35	Release profile of active ingredients from κ -carrageenan-chitosan nanoparticle for 24 hours. Where symbol \square = ascorbic acid, \circ = caffeine, Δ = lidocaine.	113
Figure 4.36	Curve fitting of active ingredients' release profile from κ -carrageenan-chitosan nanoparticle in different kinetic models for 24 hours. Where symbol \square = ascorbic acid, \circ = caffeine, Δ = lidocaine. The solid symbol represents the experimental plot while the opened symbol with line represents the predicted plot.	115

- Figure 4.37** Curve fitting of active ingredients' release profile from κ -carrageenan-chitosan nanoparticle in different kinetic models for the first 12 hours. Where symbol \square = ascorbic acid, \circ = caffeine, Δ = lidocaine. The solid symbol represents the experimental plot while the opened symbol with line represents the predicted plot. 117
- Figure 5.1** The proposed mechanism of the release of sparingly water soluble active ingredients in different delivery system. k_0 with red arrow indicates the release of unencapsulated active ingredients from donor chamber into receptor chamber. k_1 , k_2 , and k_3 with black arrow indicate the release of encapsulated active ingredients released from the respective delivery carrier. The color blue indicate aqueous phase whereas yellow color indicate oil phase. The size of the particle is in correlation to the size obtained from DLS. 121

LIST OF TABLES

Table 1.1	Biopharmaceutical classification system of active ingredients	2
Table 1.2	Amount of solvent needed to dissolve 1 g of solute	2
Table 3.1	Compositions of lipid components for the preparation of NLC	38
Table 3.2	Chemical structure and properties of active ingredients	51
Table 4.1	Thermal parameters of fatty acids based NLC	60
Table 4.2	Particle size, polydispersity index and zeta potential of fatty acid liposome and their stability for two weeks at 30 °C	65
Table 4.3	Physical properties of water-in-oil microemulsions prepared with different types of Tween surfactants measured at 30 °C	70
Table 4.4	Percentage yield of dried κ -carrageenan-chitosan nanoparticle prepared at different pH	77
Table 4.5	Swelling percentage of dried κ -carrageenan-chitosan nanoparticle in pH 7.4 phosphate buffer solution	78
Table 4.6	Loading efficiency of oleic acid liposome prepared by using active ingredients with different water solubilities as a model to predict the capability of liposome in encapsulating active ingredients	85
Table 4.7	Encapsulation efficiency of C18 unsaturated fatty acid liposome using three different active ingredients with varied water solubilities	85
Table 4.8	Changes in particle size of active ingredients loaded oleic acid liposome after 2 weeks of storage at 30 °C	87
Table 4.9	Changes in zeta potential of active ingredients loaded oleic acid liposome after 2 weeks of storage at 30 °C	88
Table 4.10	Optimum weight of active ingredients solubilized in 1 ml of deionized water	88
Table 4.11	Physical properties of active ingredients loaded ST80 microemulsions	89
Table 4.12	Particle size and zeta potential of active ingredients loaded κ -carrageenan-chitosan nanoparticle	92
Table 4.13	Unencapsulated active ingredients' rate constant and the linear regression of release curve after curve fit in different kinetic models for 24 hours	94

Table 4.14	Unencapsulated active ingredients' rate constant and the linear regression of release curve after curve fit in different kinetic models for the first 12 hours	96
Table 4.15	Active ingredients' rate constant and the linear regression of release curve from NLC after curve fit in different kinetic models for 24 hours	99
Table 4.16	Active ingredients' rate constant and the linear regression of release curve from NLC after curve fit in different kinetic models for the first 12 hours	101
Table 4.17	Active ingredients' rate constant and the linear regression of release curve from oleic acid liposome after curve fit in different kinetic models for 24 hours	104
Table 4.18	Active ingredients' rate constant and the linear regression of release curve from oleic acid liposome after curve fit in different kinetic models for the first 12 hours	106
Table 4.19	Active ingredients' rate constant and the linear regression of release curve from microemulsion after curve fit in different kinetic models for 24 hours	109
Table 4.20	Active ingredients' rate constant and the linear regression of release curve from microemulsion after curve fit in different kinetic models for first 12 hours	111
Table 4.21	Active ingredients' rate constant and the linear regression of release curve from κ -carrageenan-chitosan nanoparticle after curve fit in different kinetic models for 24 hours	114
Table 4.22	Active ingredients' rate of release from κ -carrageenan-chitosan nanoparticle after curve fitting in different kinetic models for the first 12 hours	116
Table 5.1	The properties of each active ingredient's delivery vehicles	120

LIST OF SYMBOLS AND ABBREVIATIONS

Symbols

T	Absolute temperature
Q_t	Amount of drug dissolved in time t
Q	Amount of drug released in time t per unit area
ω	Angular frequency
a	Area
k	Boltzmann constant
G	Conductance
I	Current
Δ	Delta, change of any changeable quantity
ϵ	Dielectric constant
e	Electron charge
U_E	Electrophoretic mobility
F	Faraday's constant
K	First order rate constant
M_t/M_∞	Fraction of drug released at time t
R	Gas constant
$f(\kappa a)$	Henry's function
K_H	Higuchi dissolution constant
R_h	Hydrodynamic radius of particle
$[H^+]$	Hydrogen ion concentration
W_0	Initial amount of drug in the pharmaceutical dosage form
Q_0	Initial amount of drug in the solution
C_0	Initial concentration of drug

ι	Iota
κ	Kappa
l	Length
m	Mass
n	Number of mole
π	Pi
h	Planck's constant
E	Potential difference
E_r	Reference potential
W_t	Remaining amount of drug in pharmaceutical dosage form at time t
γ	Shear rate (Velocity per unit height)
τ	Shear stress (Amount of force applied to sample per unit area)
Γ	Surface concentration
γ	Surface tension
D_t	Translational diffusion constant
η	Viscosity of solution
V	Voltage
v	Volume
ϕ	Volume fraction
λ	Wavelength or lambda
w/w	Weight to weight ratio
K_0	Zero order release constant
ζ	Zeta potential

Units

cm	Centimeter
C	Columbus
Da	Dalton
°C	Degree Celcius
g	Gram
K	Kelvin
kg	Kilogram
m	Meter
mbar	Millibar
mg	Milligram
ml	Millilitre
mM	Millimolar
mS	Milli-Siemen
mV	Millivolt
mW	Milliwatt
µm	Microliter
µm	Micrometer
mol	Mole
nm	Nanometer
N	Newton
Ω	Ohm
Pa	Pascal
%	Percent
rpm	Round per minute
S	Siemen

Abbreviation

CDP-choline	Cytidine-5'-diphosphocholine
CHEMS	cholesteryl hemisuccinate
CMC	Critical micelle concentration
CVC	Critical vesicle concentration
DC-Chol	3-(N-(N',N'-dimethylaminoethane) carbonyl) cholesterol
DDAB	Dimethyldioctadecylammonium bromide
DLP	Dermis localizing peptide
DLS	Dynamic light scattering
DNA	Deoxyribonucleic acid
DOPE	Dioleylphosphatidylethanolamine
DOTAP	1,2-dioleyl-3-trimethylammonium-propane
DSC	Differential scanning calorimetry
EE	Encapsulation efficiency
EGCG	Epigallocatechin
EPR	Enhanced permeability and retention
ETP	Economic Transfer Program
FTIR	Fourier transform infrared spectroscopy
HER-2	Human epidermal growth factor receptor-2
HPG	Hyperbranched polyglycerol
IFN- γ	Interferon- γ
LCST	Lower critical solution temperature
LE	Loading efficiency
LP-12	Linear peptide-12mer
LUV	Large unilamellar vesicle
MLV	Multilamellar vesicle
MPS	mononuclear phagocyte system
mRNA	Messenger RNA

MUV	Medium unilamellar vesicle
MWCO	Molecular weight cut off
NLC	Nanostructured lipid carrier
OPM	Optical polarizing microscope
PDI	Polydispersity index
PEC	Polyelectrolyte complex
PEG	Polyethylene glycol
PMN	Polymorphonuclear leukocyte
RNA	Ribonucleic acid
SP	Swelling percentage
siRNA	small interference RNA
SLN	Solid lipid nanoparticle
Span 40	Sorbitan monopalmitate
Span 80	Sorbitan monooleate
SPP	Skin penetrating peptide
SUV	Small unilamellar
TEM	Transmission electron microscopy
TEWL	Transepidermal water loss
TPP	Tripolyphosphate
Tween 40	Polyoxyethylene sorbitan monopalmitate
Tween 60	Polyoxyethylene sorbitan monostearate
Tween 80	Polyoxyethylene sorbitan monooleate
Tween 85	Polyoxyethylene sorbitan trioleate

CHAPTER 1: INTRODUCTION

The term nanotechnology was first used in 1974 by Norio Taniguchi (Dusastre, 2008) whilst the massive advancement of nanotechnology was advocated by Bill Clinton in National Nanotechnology Initiative program in year 2000. Malaysia introduced Economic Transformation Program (ETP) in 2009 while nanotechnology was given a high level of attention in this plan. Through this initiative, there is a breakthrough in the field of medical therapy. The attention is mainly focused on solving the solubility and permeability problems of active ingredients using specially designed vehicles for specific and safer treatment. In earlier days, treatment is limited to direct application of active ingredient which blended in matrix or as colloidal dispersion in the form of tablet, emulsion, gel and/or aerosol. Nevertheless, these treatments sometimes could not reach its optimum efficacy as well as generate adverse effects after chronic exposure to the potent active ingredients. Thus, more sophisticated nano-sized carriers such as liposome, dendrimer, nanocrystal, hydrogel were fabricated to address the issues and modulate active ingredients' delivery.

1.1 Solvent solubility and bioavailability of active ingredients

Despite that the human's body is made up of 70% water, the skin is covered by hydrophobic layer of cells. For this reason, it is crucial that the active ingredient will be able to solubilize in aqueous phase when its presence in the body or permeate through hydrophobic layer of the skin, which then followed by absorption into systemic circulation until it reaches site of action. This mechanism is known as the active ingredients solubility and bioavailability. The term solubility, is defined as the amount of solvent required to dissolve 1 g of solute while bioavailability, is the amount and rate at which a substance is absorbed and available at the site of physiological activity in living system. Based on the solubility and permeability, active ingredients were

categorized into four groups in biopharmaceutical classification as in Table 1.1 while the amount of solvent required to dissolve 1 g of solute is shown in Table 1.2 (Dahan *et al.*, 2009; Kawabata *et al.*, 2011).

Table 1.1: Biopharmaceutical classification system of active ingredients

Class	Solubility	Permeability	Absorption
I	High	High	Good
II	Low	High	Variable
III	High	Low	Variable
IV	Low	Low	Poor

Table 1.2: Amount of solvent needed to dissolve 1 g of solute

Solubility	Amount of solvent required (ml)
Very soluble	Less than 1
Freely soluble	1 to 10
Soluble	10 to 30
Sparingly soluble	30 to 100
Slightly soluble	100 to 1000
Very slightly soluble	1000 to 10000
Practically insoluble	Greater than 10000

For Class I active ingredient that has the properties of high solubility and permeability, it gives rise to a greater absorption rate than excretion rate. Thus, Class I active ingredient has a higher bioavailability over time. For Class II active ingredient with the properties of low solubility but high permeability, problems arise many times because of inadequate dissolution rate. As a consequence, further understanding in the enhancement of active ingredients' solubility is required. For Class III active ingredient with the properties of high solubility but low permeability, its bioavailability gets limited at the site of action. Hence, attention is being focused on the materials as well as methods for the preparation of formulation. Finally, Class IV active ingredient with the properties of low solubility and permeability, requires both approaches taken for both Class II and III active ingredient to enhance dissolution rate and improve its bioavailability. The classification is essential for oral delivery. However, for topical

delivery, the ability of active ingredient to penetrate through hydrophobic skin cell layer is important for its absorption. As a consequence, active ingredient classified in both Class III and IV in reverse could have a better permeability than those of Class I and II.

The rate of release of active ingredient depends on the features of the nanocarrier to encapsulate and control active ingredient's release. For instance, fast dissolution rate of Class I active ingredient could be regulated by trapping it in three dimensional hydrogel while enhancement of solubility and permeability of Class IV active ingredient can be achieved by using lipid nanoparticle. These innovations could contribute to more targeted delivery depending on its pathway and so reduce the possibilities of adverse effects that arise from active ingredients' accumulation.

1.2 Active ingredients' delivery pathways

The therapeutic effect of active ingredients can be either localized or systemic depending on its delivery pathways. Most of the time, localized effect implicates topical delivery while systemic effect can be carry out via oral, parenteral, nasal or ophthalmic pathway (Figure 1.1).

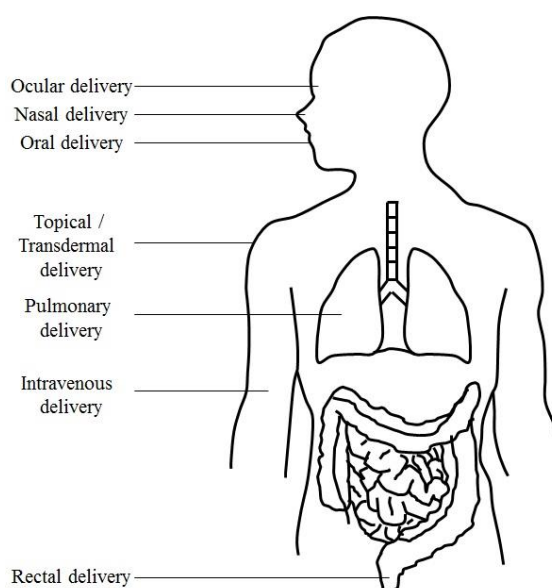


Figure 1.1: General pathways for active ingredients' delivery

Among the various types of delivery pathways, topical delivery gains a lot of attention as it could avoid first-pass metabolism and enzymatic breakdown. Hence, it will indirectly minimize the possible degradation of active ingredients that experienced in oral delivery as well as pain that caused by injection in intravenous delivery. Therefore, the major challenge in topical delivery is the route of active ingredients to penetrate through the skin down into the circulatory system. If active ingredients could easily permeate through the skin, this delivery might be one of the best ways for treatment.

The skin is the largest organ of the body. It consists of three main layers which include epidermis, dermis and subcutaneous tissue with different structures and functions. In topical delivery, the main barrier to overcome during active ingredient's permeation is the topmost epidermis layer. Epidermis is a multi-layered membrane with a thickness of 60-80 μm . This complex membrane is made up of four distinct layers, which are stratum corneum, stratum granulosum, stratum spinosum and stratum basale counted from the outer layer. Stratum corneum, the protective layer of the skin is roughly 10 μm thick. Nevertheless, due to its unique constituents, the hydrophobic layer sets as a barrier in preventing the penetration of substance with a particle size larger than 40 nm (William, 2003).

In topical delivery, active ingredients can permeate through the epidermis via shunt, intracellular and intercellular route. Shunt route allows diffusion of active ingredients bypassing stratum corneum, thus directly into dermis layer via pores of hair follicle and sweat ducts. Intracellular pathway requires multiple partitioning and diffusion steps throughout the epidermis. Intercellular route enables components to directly diffuse and reach dermis layer without those steps in intracellular pathway (Prow *et al.*, 2011). On that account, a suitable delivery carrier could be prepared to suit those permeation

routes, for examples, by formulating delivery carrier with a size below 40 nm or particle with lipophilic properties.

1.3 Drug delivery carrier

Numerous delivery carriers such as micelle, vesicle, lipid dispersion and nanoparticle dispersion with a particle size less than 500 nm were developed to enhance active ingredient's encapsulation, control the rate of release and provide better penetration to the targeted site. This could reduce active ingredient's wastage, prevent possible adverse effect and decrease the degradation of active ingredients through high encapsulation and controlled release.

Effective encapsulation and sustained release of active ingredients could reduce the dosage that required for effective therapeutics. Polymeric micelle which consists of hydrophobic core-shell and hydrophilic surface, is suitable for the encapsulation of hydrophobic active ingredients (Zhang *et al.*, 2012) while hydrogel with polymeric networks could be more effective in the entrapment of hydrophilic active ingredients (Chen *et al.*, 2011). Apart from that, sustained release of active ingredients can reduce cell cytotoxicity by improving their distribution and prevent their accumulation in the body. Zhang *et al.* (2012) proved that nanostructured lipid-dextran sulfate hybrid carriers with high encapsulation efficiency can sustain the release of mitoxantrone hydrochloride for 72 hours and thus enhance the therapeutic effect as compared to the free active ingredient.

Active ingredients can be easily metabolized, degraded or cleared by the body system through enzymatic digestion, oxidation and mononuclear phagocytic system (MPS) uptake respectively (Li and Huang, 2008). For that reason, delivery carrier which coated

with polyethylene glycol (PEG) or hyperbranched polyglycerol (HPG) can prolong its circulation time by increasing surface hydrophilicity, hindrance of negative surface charge and improving resistance to adsorption (Allen and Martin, 2004; Deng *et al.*, 2014). Besides that, nanocarrier with a multi-layered structure such as aquasomes, could prolong the release time of recombinant human interferon- α -2b for combating ovarian cancer cells (Kaur *et al.*, 2015). Other than that, matrix core of delivery carrier acts as a barrier to prevent active ingredient from environment degradation, thereby extends its shelf-life. Solid lipid nanocarrier (SLN) with a flexibility in modulating the rate of active ingredient's release, hence protecting the active ingredient from chemicals, photochemical and oxidative degradation (Chinsriwongkul *et al.*, 2011).

1.4 Characterization of delivery carrier

Delivery carrier usually presents in the form of colloidal system, whereby the particle is evenly distributed in the continuous phase. Physicochemical characteristics of a prepared formulation will highly affect its stability and efficacy. On that account, an easy yet significant way to evaluate the stability of a formulation is through visual observation. Destabilization of colloidal system will induce separation of the formulation into respective immiscible phases via coalescence, flocculation and/or Ostwald ripening (Badolato *et al.*, 2008; Somasundaran *et al.*, 2007). Besides that, changes in the turbidity of the suspension also may be taken as an indication of instability. When lipid nanoparticle was monitored using spectrophotometer at the wavelength of 200-800 nm hourly for 72 hours, it was shown that the transmittance increased after 24 hours. This is a phenomenon whereby the lipid nanoparticle becomes unstable and it flocculates to form an oil layer on top of the formulation.

Apart from visual observation, a more accurate way to evaluate the stability of a formulation is through the determination of particle size and zeta potential by employing zetasizer. Small particle size and zeta potential with a magnitude which is higher or lower than ± 30 mV are usually categorized as highly stable. This stability is attributed by net forces of attraction and repulsion between the particle, vesicle or droplet. These net forces are contributed by electrostatic force, van der Waals force, hydrophobic and hydrophilic forces. When the particle, vesicle or droplet comes closer to each other, electrical double layer surrounding its surface may acts as a barrier to prevent destabilization of the formulation. Other than that, thermal stability is an important feature especially for topical formulation. The delivery carrier can be designed as a thermal sensitive carrier, whereby those encapsulated active ingredients will be released at the designated temperature. On account of that, during logistic and storage, we have to ensure that the storage temperature is kept below 30 °C to prevent the destabilization of formulation. In addition, by examining the morphology of sample under optical polarizing microscope (OPM) or transmission electron microscope (TEM), it could be confirmed that the sample is well dispersed without any possible aggregation.

Apart from physicochemical characteristics, a major concern in the design of delivery carrier is its abilities to encapsulate and release active ingredients. The encapsulation efficiencies of active ingredients depend on their compatibility with delivery carrier. Oil-in-water emulsion and lipid nanoparticle which entrapped active ingredients in the oil droplet and lipid core respectively, is a better approach for the encapsulation of hydrophobic active ingredients. On the other hand, an active ingredient which is more hydrophilic has a higher tendency to be entrapped in hydrogels and water-in-oil emulsion. Other than that, bilayer vesicle and double emulsion could incorporate both the hydrophobic and hydrophilic active ingredients. Through the understanding of those

chemical constituents, we also can encapsulate water soluble active ingredients in lipid core and vice versa. Apart from encapsulation, the ability of delivery carrier to control rate of active ingredients' release, makes it promising for different applications. The release can be either in the form of fast release, controlled release or prolonged release. A good understanding of the release profile could provide insight on the most preferable route for delivery, thereby optimized the therapeutic effects.

1.5 Aims of research

The aims of our studies are:

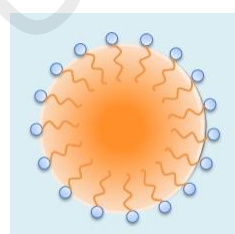
- To formulate or fabricate different types of drug carrier systems for delivery;
- To determine and select the best formulation in each system based on their physicochemical properties;
- To encapsulate active ingredients with varied solubility in water into carrier system and determine their release profile;
- To compare, select and comment on the system prepared based on the results obtained.

1.6 Outline of research

There are five main chapters in this thesis. The first chapter includes the introduction of this research and aims to be achieved. Chapter 2 describes about the delivery system and their advantages for application. Chapter 3 presents the methods and approaches used in the design of experiments. Chapter 4 displays the results obtained via different characterization and discusses the significance of those results. Chapter 5 summarizes the findings and proposes potential future work that can be done.

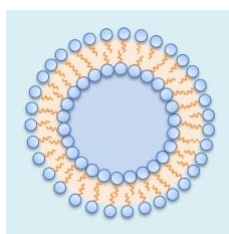
CHAPTER 2: LITERATURE REVIEW

Colloid is any particle with typical dimensions ranging from 10 to 1000 nm that dispersed throughout another substance. The particles are too small to be viewed with an ordinary light microscope, nonetheless, they are incapable of passing through the semi-permeable membrane. One of the commonly found colloid is emulsion in the form of either oil-in-water or water-in-oil dispersion of two immiscible liquids. Oil-in-water dispersion has refreshing and oil-free texture while water-in-oil dispersion could enhance penetration and reduce transepidermal water loss (TEWL). Thus, delivery carriers with different dispersed and continuous phase were explored for their physicochemical properties, active ingredients' encapsulation efficiency and active ingredients' release profile. In this research, four types of delivery carriers, namely nanostructured lipid, liposome, water-in-oil microemulsion and κ -carrageenan-chitosan nanoparticle were prepared. Nanostructured lipid is lipid matrixes disperse in aqueous solution; liposome is lipid bilayers with aqueous core disperse in aqueous solution; water-in-oil microemulsion has aqueous droplets disperse in oil continuous phase while κ -carrageenan-chitosan nanoparticle has hydrophilic polymer stabilized in aqueous surrounding. The carriers were encapsulated with active ingredients of varied solubility in water to evaluate the most suitable carrier for higher encapsulation efficiency. Release profile provides the rate of release for prediction of possible delivery pathways.



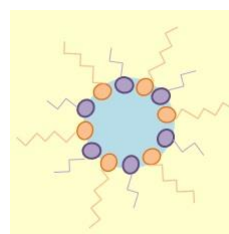
NLC

Oil-in-water



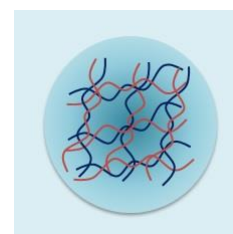
Liposome

Water-oil-water



**Water-in-oil
microemulsion**

Water-in-oil



**κ -carrageenan-
chitosan nanoparticle**

Hydrophilic polymer in
water

Figure 2.1: Delivery vehicles for active ingredients' solubilisation and permeation

2.1 Nanostructured lipid

The concept of lipid nanocarrier arises from oil-in-water emulsion, whereby the oil is fully or partially replaced by crystallized lipid that stabilized by surfactants (Müller *et al.*, 2002a). Lipid nanoparticle is either in the form of solid lipid nanoparticle or nanostructured lipid carrier (NLC), bearing particle size less than 1000 nm. SLN being the first generation lipid nanoparticle, was prepared by single or blend type of solid lipids (Müller *et al.*, 2007). SLN with high ordered crystalline is capable to encapsulate both hydrophobic and hydrophilic active ingredients for prolonged release. The slow release kinetic is plausibly due to lower diffusion rate of active ingredients from the crystallized matrix core (Müller *et al.*, 2002b; Weiss *et al.*, 2008). Nevertheless, the crystallinity limits the loading capacity and stability of SLN. This is plausibly due to the perfect arrangement in SLN which leads to drug expulsion. In order to overcome the problems, second generation lipid nanoparticles known as NLC was introduced (Pardeike *et al.*, 2009).

NLC is derived from SLN by replacing certain percentage of solid lipid with liquid lipid. This substitution creates an imperfect lipid matrix with higher fluidity, aid in enhancing active ingredients' loading capacity (Yuan *et al.*, 2007). This was observed in clotrimazole encapsulated SLN and NLC, whereby NLC showed higher entrapment efficiency compared to SLN (Souto *et al.*, 2004a). In conjunction with the imperfection, liquid lipid reduces the melting temperature of lipid nanoparticle. Even so, there is always a limitation in the amount of liquid lipid that could be introduced into the NLC due to temperature factor. As a consequence, it is important to ensure that NLC still remains as solid particle at least at body temperature of 37 °C; otherwise it could be just an oil-in-water dispersion (Severino *et al.*, 2011; Souto and Müller, 2008). Besides that, NLC works well in encapsulating Class II active ingredients. Lutein which falls in this

class has better solubility and permeability across synthetic membranes while prepared lipid nanoparticle with small particle size further enhance the permeation process (Mitri *et al.*, 2011).

2.1.1 Lipids and emulsifier for NLC

Cetyl palmitate, glyceryl monostearate and stearic acid are commonly used as solid lipid in preparation of NLC. Cetyl palmitate, an ester derived from palmitic acid and cetyl alcohol, has good moisturizing effect. Thus, it serves as emollient to keep the skin moist and comfortable (Carbone *et al.*, 2014; Kovacevic *et al.*, 2011; Teeranachaideekul *et al.*, 2008). Glyceryl monostearate which is a glycerol ester of stearic acid, gives lubricant effect thereby reduces friction and eases spreading of formulation (Bhalekar *et al.*, 2009; Kotikalapudi *et al.*, 2012; Nayak *et al.*, 2010; Ranpise *et al.*, 2014). Stearic acid, a fatty acid with smoothing effect on the skin and neutral effect on both the cholesterol and blood lipids, is suitable as solid lipid in NLC (Pandita *et al.*, 2014; Rahman *et al.*, 2014; Woo *et al.*, 2014).

Medium chain triglyceride and oleic acid are liquid lipids found in NLC formulation. Medium chain triglycerides such as caprylic- and capric-triglyceride have many nutritional benefits, especially for the purposes of fat mass reduction and therapeutic effect for brain disorder (Doktorovová *et al.*, 2010; Freemantle *et al.*, 2006; Hu *et al.*, 2008; Severino *et al.*, 2011; Zhang *et al.*, 2015). Oleic acid, which helps in modulating immune responses thereby enhancing cutaneous wound healing, is suitable for topical applications (Agrawal *et al.*, 2010; Chen *et al.*, 2014; Patel *et al.*, 2012; Souza *et al.*, 2011).

Emulsifier can be small molecule surfactants, phospholipids or even macromolecules such as protein and polysaccharides. It is applied for dispersing and stabilizing lipid nanoparticles in aqueous medium. Polyoxyethylene sorbitan monooleate, which is known as Tween 80, is a non-ionic and non-toxic surfactant that presents in food and cosmetic products. Due to its properties, Tween 80 does not dramatically affect surface charge of lipid nanoparticle (Gonzalez-Mira *et al.*, 2010; Keck *et al.*, 2014; Teeranachaideekul *et al.*, 2007; Üner *et al.*, 2004). Lecithin which is an excellent lubricant, can be fully metabolized by the body. Its zwitterionic effect works well as a charge neutralizer, aids in modifying surface charge of lipid nanoparticle for specific application (Han *et al.*, 2012; Jia *et al.*, 2010; Luan *et al.*, 2014; Zhang *et al.*, 2008).

2.1.2 Techniques applied in NLC's preparation

The approaches taken in preparation of NLC could dramatically affect its properties. Solid lipid and/or emulsifier is required to be in the molten state in order to produce homogenized formulation. In spite of that, labile materials should be prevented from high temperature and sometimes solvent is required for better encapsulation efficiency. The techniques that are usually employed in the preparation of NLC include hot and/or cold homogenization, ultrasonication, and emulsification-solvent evaporation method (Almeida and Souto, 2007; Ekambaram *et al.*, 2012; Patidar *et al.*, 2010; Wissing *et al.*, 2004).

2.1.2.1 Hot and/or cold homogenization

In hot homogenization method, the lipid and/or surfactant are first melted at a temperature of 5 to 10 °C higher than the melting point of the materials. The molten mixture is then mixed with aqueous phase at the same temperature, followed by homogenization at a high speed to disperse and subsequently reduce the size of lipid

droplet. The evenly dispersed droplets will then crystallized in cold environment to form lipid nanoparticles. Further reduction and more uniform particle size can be obtained by passing through homogenized pre-emulsion in a high pressure homogenizer (Araújo *et al.*, 2012; Fan *et al.*, 2014; Liu *et al.*, 2007; Souto *et al.*, 2004b; Üner *et al.*, 2005). In cold homogenization method, the preparation procedure is similar as hot homogenization method. The difference between the two preparation methods is that in cold homogenization method, hot molten is being cooled down and ground into lipid microparticle before being dispersed in cold aqueous phase and finally passed through the high pressure homogenizer (Dangi *et al.*, 2011; Neupane *et al.*, 2014). Nevertheless, hot homogenization method is preferred to produce small and uniform particle (Mukherjee *et al.*, 2009).

2.1.2.2 Ultrasonication

In ultrasonication method, lipid components are first dissolved in organic solvent, followed by solvent evaporation to form a thin layer of lipid film. The lipid thin film is then hydrated in emulsifier supplemented aqueous phase, followed by some agitation to disperse the lipid thin film and thereby lipid particle is formed. In most cases, the agitation is achieved by homogenization, followed by ultrasonication to ensure that the particles are in uniform size (Brugè *et al.*, 2013; Castelli *et al.*, 2005; Cirri *et al.*, 2012; Pinto *et al.*, 2014; Puglia *et al.*, 2008).

2.1.2.3 Emulsification-solvent evaporation

In emulsification-solvent evaporation method, lipid matrix is first solubilized in water immiscible solvent and then added into an emulsified aqueous medium. The solvent will undergo evaporation and nanoparticle dispersion is formed when the lipid gradually precipitated into the aqueous phase (Sadiq and Rassol, 2014; Trotta *et al.*, 2003;

Varshosaz *et al.*, 2014). This method is suitable for labile active ingredients as it is free from high temperature heating.

2.1.3 Advantages of NLC's usage

Lipid nanoparticle could enhance loading and encapsulation efficiency, improve active ingredient's stability, allow deeper skin penetration and increase skin hydration. The imperfect amorphous structure of NLC gives more room for the accommodation of active ingredients than perfect structured SLN (Pople and Singh, 2011; Souto *et al.*, 2004a). Quercetin loaded NLC showed a higher encapsulation efficiency and loading capacity as compared to SLN (Aditya *et al.*, 2014). Apart from that, lipid nanoparticle could encapsulate various types of active ingredients including coenzyme Q₁₀ (Pardeike and Müller, 2007), psoralen (Fang *et al.*, 2008), retinoic acid (Castro *et al.*, 2009), flurbiprofen (Gonzalez-Mira *et al.*, 2010), itraconazole (Pardeike *et al.*, 2011), curcumin (Puglia *et al.*, 2012), miconazole (Mendes *et al.*, 2013), artemether (Nnamani *et al.*, 2014) and recombinant human epidermal growth factor (Gainza *et al.*, 2015). Lipid nanoparticle could also protect labile active ingredient from oxidation and degradation by reducing its contact with the external environment (Puglia *et al.*, 2014). The work done by Junyaprasert *et al.* (2009) showed that Q₁₀ loaded NLC has better particle size, zeta potential and higher Q₁₀ remained after one year storage as compared to nanoemulsion. Besides that, the amount of phenylethyl resorcinol loaded in NLC reduced by 1.3% only even though it was exposed to natural daylight for a period of 90 days (Fan *et al.*, 2014).

Lipid nanoparticle helps to enhance active ingredient's penetration, prevent skin dehydration and reduce adverse effect. Penetration enhancement is attributed by its lipophilic nature whereby lipid nanoparticle can partition into the skin layer more

efficiently. Glyceryl behenate/capric caprylic triglyceride genistein loaded NLC favours deeper skin layer penetration as compared to glyceryl behenate genistein loaded SLN because the fluidity of liquid lipid eases the penetration process (Andrade *et al.*, 2014). Idebenone loaded NLC improved the permeation of active ingredient in guinea pig's skin as compared to nanoemulsion and oil solution (Li and Ge, 2012). This was further supported by the work done by Schwarz *et al.* (2013), whereby Q₁₀ with smaller particle size could penetrate into the deeper skin layer and it gave a higher penetration rate as compared to those with larger particle size.

The occlusion effect of NLC is achieved by the formation of lipid thin film on top of the skin after the application of the formulation. Lipid thin film helps to repair and prevent water loss from the skin. In a comparison study done by Pardeike *et al.* (2010), it showed that Cutanova Nanorepair Q10 cream which consists of NLC has better skin hydration effect as compared to NLC free cream. Other than that, application of NLC-silver complex on mild to medium severe atopic dermatitis patient not only hydrates the skin but also prevents the growth of bacteria which worsen the condition of atopic dermatitis (Keck *et al.*, 2014).

In hazardous prevention, molecular oxybenzone which presents in sunscreen, was shown to have a slower release rate by 50% in lipid nanoparticles as compared to similar size emulsion. Thus, amount of oxybenzone which accumulated on the skin could be reduced yet prolonged sun protection factor was achieved (Wissing and Müller, 2002). Celecoxib loaded NLC can be modulated to achieve prolonged release of the active ingredients for the lessening of pain and inflammation that caused by rheumatoid arthritis, thus reduced the frequency of application of medicine (Joshi and Patravale, 2008).

2.2 Liposome

Liposome is a small spherical vesicle which composed of one or more lipid bilayer surrounding an aqueous inner core. This enables liposome to encapsulate both hydrophobic and hydrophilic active ingredients. The hydrophobic components are usually embedded in the lipid core while the hydrophilic components are entrapped in the aqueous interior, hence forming a protection layer for labile active ingredients from external environment (Immordino *et al.*, 2006). That being the case, liposome is used as a carrier to encapsulate small molecules, peptides, hormones, genetic materials, antibiotics and anticancer agents (Chang and Yeh, 2012).

Liposome can be classified into different categories based on their structural parameters and components for applications. Depending on the lamellar layer, liposome is structurally grouped as unilamellar and multilamellar vesicles (MLV). Unilamellar vesicles consist of single phospholipid bilayer while multilamellar vesicle has onion-like arrangements. Based on their size, unilamellar vesicle can be further categorized into small unilamellar vesicle (SUV), medium unilamellar vesicle (MUV) and large unilamellar vesicle (LUV) with size around 20-40 nm, 40-80 nm and 100-1000 nm respectively (Akbarzadeh *et al.*, 2013). Depending on its components for application, liposomes can be either conventional liposome, long circulatory liposome, fusogenic liposome, pH sensitive liposome, cationic liposome or immuno-liposome.

2.2.1 Surface modified liposome

Conventional liposome is the most basic liposome that made up of neutral or negatively charged phospholipids and cholesterol. Diacylglyceride such as phosphatidyl choline (lecithin), phosphatidyl ethanolamine (cephalin), phosphatidyl serine or phosphatidyl inositol is the commonly used phospholipids (Mansoori *et al.*, 2010). In order to

enhance the rigidity of lipid bilayer (Sulkowski *et al.*, 2005) and provide signal transduction (Chattopadhyay and Paila, 2007), cholesterol is often added. Despite that, conventional liposome is recognized as an exogenous substance, thus it gets eliminated by the reticuloendothelial system of the body (Maruyama, 2011). As a result, stealth liposome or long circulatory liposome is being introduced.

Stealth liposome has longer circulation time as a consequence of increase surface hydrophilicity and hindrance of negative surface charge by materials coated on liposome (Allen and Martin, 2004). Stearic stabilization is achieved when the coated PEG attracts water, in turn reduces both the adsorption of opsonins and recognition of liposome by MPS (Ishida *et al.*, 2006; Yang *et al.*, 2007). Doxorubicin encapsulated PEGylated liposome which marketed as Caelyx or Doxil, was introduced for cancer treatment (Ishida and Kiwada, 2008). Polysaccharide, *O*-palmitoylscleroglucan anchored liposome showed improved stability as compared to conventional liposome when being suspended in simulated gastric fluid and bile salt solutions (Carafa *et al.*, 2006).

Fusogenic liposome is a liposome coated with Sendai virus envelope glycoproteins, either by natural or synthetic lipid for targeted delivery (Nicolosi *et al.*, 2015). It can efficiently fuses through plasma membrane to deliver nucleotides and/or proteins (Kunisawa *et al.*, 2005) and protects siRNA from degradation (Auguste *et al.*, 2008). Fusogenic liposome was being shown to success in facilitating siRNA endosomal escape and enhancing gene silencing (Hatakeyama *et al.*, 2009).

Immuno-liposomes formed when monoclonal or polyclonal antibodies are attached on the surface of liposomes for cell specific targeting (Park *et al.*, 2004). Transmembrane glycoprotein, human epidermal growth factor receptor-2 (HER2) which over-expressed in breast cancer cells, serves as a receptor for recombinant humanized monoclonal anti-HER2 antibody, Herceptin. When Herceptin is bound to liposomes, targeted delivery of immune-liposome to breast cancer cells could be achieved (Yang *et al.*, 2007; Barraón-Catalán *et al.*, 2010).

pH sensitive liposome is designed to undergo acid-triggered destabilization and promote the release of active ingredients into cytosol (Sudimack *et al.*, 2002; Torchilin, 2011). It is usually composed of dioleoylphosphatidylethanolamine (DOPE) with cholesteryl hemisuccinate (CHEMS) or oleic acid. In acidic condition, the lipids become partially protonated and lose its negative charge, attributed to the loss of bilayer structure's stability by electrostatic repulsion (Cho *et al.*, 2009; Ishida *et al.*, 2006). Gemcitabine encapsulated pH sensitive liposome significantly increases cell apoptosis of non-small cell lung cancer as compared to free gemcitabine (Kim *et al.*, 2009).

Cationic liposome is widely explored as a mediator for proteins, peptides and DNA into cell. Cationic lipid including 3-(N-(N',N'-dimethylaminoethane) carbonyl) cholesterol (DC-Chol), 1,2-dioleoyl-3-trimethylammonium-propane (DOTAP), and dimethyldioctadecylammonium bromide (DDAB), with low immunogenicity and toxicity, has high potential for targeted delivery (Inoh *et al.*, 2013; Maitani *et al.*, 2007; Yan *et al.*, 2007; Zhuang *et al.*, 2012). Cationic liposome which forms a complex with siRNA, could enhance its cellular uptake as a consequence of electrostatic interaction between the complex and plasma membrane (Tagami *et al.*, 2012). In a recent research

done by Saengkrit *et al.* (2014), curcumin loaded cationic liposome was shown to have improved surface charge by DDAB, thus enhanced the effect for cervical cancer therapy.

2.2.2 Preparation of liposome

Liposome can be easily prepared via dry lipid membrane technique. This was done by drying the dissolved lipid components from organic solvent followed by dispersing the dried lipid in aqueous media. The more specific preparation methods such as physical dispersion, solvent dispersion and detergent solubilisation were introduced.

2.2.2.1 Physical dispersion

Physical dispersion method can be carried out by sonication, membrane extrusion, micro-emulsification or freeze-thawing of liposomes. In sonication, bath sonicator or probe sonicator is employed to reduce the particle size of liposomes (Ćurić *et al.*, 2013; Jiang *et al.*, 2015). In membrane extrusion, liposome was passed through a membrane filter with specific pore size. Those with larger particle size will either retain on the upper part of the membrane or fuse through the membrane to form liposome with smaller particle size (Franzen *et al.*, 2011; Nguyen *et al.*, 2013). Micro-emulsification is executed under a high pressure micro fluidizer. The emulsified sample is brought to collide at a high velocity to produce liposomes with narrow particle size distribution (Lajunen *et al.*, 2014; Tang *et al.*, 2013). In freeze-thawing method, opposite result is achieved. During liposome's rupture and reformation, small vesicles are formed within a larger vesicle. Hence, this method could increase the encapsulation efficiency of active ingredients (Guo *et al.*, 2011; Xu *et al.*, 2012).

2.2.2.2 Solvent dispersion

In solvent dispersion method, the lipids are dissolved in ethanol or ether, followed by injection of the solution in aqueous phase which contains active materials (Meure *et al.*, 2008). In ethanol injection, ethanol dissolved lipids are rapidly injected into aqueous medium using fine needle. Ethanol is diluted while lipids is dispersed in aqueous phase to form liposomes (Justo and Moraes, 2011; Padamwar and Pokharkar, 2006). On the other hand, ether injection requires slower injection of water immiscible solvent into aqueous phase at vaporizing temperature of the solvent (Guan *et al.*, 2012; Pham *et al.*, 2006). By using the solvent dispersion method, large scale of liposomes could be produced without degrading and oxidizing the lipids (Charcosset *et al.*, 2014).

2.2.2.3 Detergent solubilisation

In detergent solubilisation method, liposome is formed through self-assembly of lipid-detergent mixture. This method involved bilayer solubilisation by detergent from low to high concentration until critical micelle concentration (CMC) is reached. Below CMC, detergent molecules exist as free molecule in the solution. Gradual increase of detergent's concentration in solution forms lamellar layer or known as detergent containing bilayer. When the concentration of detergent is further increased until it reaches CMC, lamellar layer undergoes dissolution and assembles into spherical vesicle known as lipid-detergent mixed micelle (Lichtenberg *et al.*, 2013a; Lichtenberg *et al.*, 2013b). This method is applied in octylglucoside mediated solubilisation and reconstruction into unilamellar vesicle that composed of lipids extracted from *E.coli* membranes (Krylova *et al.*, 2010).

2.2.3 Interaction of liposome with the body

Liposome has the potential as a delivery carrier, owing to its features of specific targeting through surface modification, regulating distribution by liposomal size, prolonged release depending on the composition and protecting active ingredients from degradation and preventing body from adverse effects.

During inflammation or presence of tumor, vascular pathophysiology would have some structural changes. The defect in blood vessel however enable the accumulation of small particle size materials in the interstitial space by fusing through endothelial cell and accumulating more particles in tumor tissue than normal cell. This phenomenon is also known as enhanced permeability and retention (EPR) effect (Danhier *et al.*, 2010). Thus, liposome which undergoes surface modification, can retain in the bloodstream for a longer period without being phagocytized by macrophages. This modification could enhance the chance of liposome to fuse passively and accumulate at the targeted site (Nakano *et al.*, 2008). Active targeting involves ligands that attached on liposome, bind specifically to receptor on the targeted cell (Noble *et al.*, 2014). Active targeting of peptide ligand PH1 towards Tie2 receptor is proven when cisplatin loaded liposome down-regulates Tie2 which is linked to angiogenesis in cancer cell (Mai *et al.*, 2009).

The active ingredients' release rate can be regulated depending on the surface composition of liposome. PEG coated liposome has prolonged circulation time in the body (Elbayoumi and Torchilin, 2008; Ishida *et al.*, 2007; Kim *et al.*, 2009). Sometimes, we could enhance the release of active ingredients by providing an acidic environment to pH sensitive liposome. DOPE liposome coated with acid labile PEG conjugated vinyl ether lipids was destabilized, thus induced release of calcein (Shin *et al.*, 2003). Additionally, enhancement in doxorubicin release was being demonstrated in

thermosensitive liposomes that attached to poly(N-isopropylacrylamide-co-acrylamide) and PEG (Han *et al.*, 2006). Targeted delivery of liposomes involves the mechanism of receptor mediated internalization whereby ligands targeted liposomes can deliver high amount of drugs to the targeted sites (Sapra and Allen, 2003). This is proven by Adibhatla *et al.* (2005) in phase III stroke clinical trials whereby cytidine-5'-diphosphocholine (CDP-choline) loaded liposome has a better reduction in infarction as compared to free CDP-choline with equivalent dose.

The size of liposome and active ingredients affect the therapeutic efficacy whereby small molecule drug loaded liposomes have better retention at active sites (Mirahmadi *et al.*, 2010). It is plausibly related to the capability of liposomes to accumulate at the fiber network of tumors while free active ingredients can be easily diffused away and metabolized by the body. Epigallocatechin (EGCG) and catechin encapsulated liposome have higher local retention in basal cell carcinomas for the treatment of skin disorders (Fang *et al.*, 2006).

Liposome has a good protection layer to preserve labile active ingredients (Kim *et al.*, 2013; Kulkarni *et al.*, 2011). In the work done by Coimbra *et al.* (2011), resveratrol which is prone to cis-trans isomerization under light, exhibits photostability property when being encapsulated in liposome's lipid bilayer while carvacol disodium phosphate has a high loading efficiency in the aqueous core. Apart from small molecules, synthetic peptide which is bound with DNAhsp65 for loading into cationic liposome, functions as gene vaccine for therapeutic effects against diseases like tuberculosis (Rosada *et al.*, 2012).

Even though liposome has many benefits for application, but side effects might arise from potent active ingredients, thereby limits its usage and duration taken for therapeutic (Fang *et al.*, 2001; Koudelka and Turánek, 2012). Acute and chronic cardiotoxicity were observed in breast cancer patients when being treated with anthracycline but there was a reduction of side effect when anthracycline was encapsulated in PEGylated liposomes (Jurcut *et al.*, 2008). Reduction in adverse effect was also proven in the treatment of hepatic fibrosis, whereby interferon- γ (IFN- γ) liposome with prolonged release rate and targeted delivery towards hepatic stellate cell could enhance anti-fibrotic effects, thereby decreased the expression of ubiquitous receptor (Li *et al.*, 2012). Apart from that, reduction of effective therapeutic dose could as well reduce the possible side effect. Decrease in toxicity is being observed in liposome complex encapsulated with amphotericin B for the treatment of leishmaniasis (Daftarian *et al.*, 2013).

2.3 Water-in-oil microemulsion

Emulsion is a dispersion of two immiscible liquid of oil and water which stabilized by surfactants at the oil-water interface. It can be classified as microemulsion, nanoemulsion or macroemulsion. Microemulsion appear to be translucent or clear with a particle size less than 100 nm, nanoemulsion has a particle size up to 200 nm while macroemulsion is generally larger than 500 nm. Microemulsions are typically thermodynamically stable. Nevertheless, microemulsion's formation is not necessarily spontaneous but it requires an input of external energy. On the other hand, nanoemulsion and macroemulsion which require high energy input either by sonication or homogenization are considered kinetically stable yet have the tendency to phase separate (Kogan and Garti, 2006; Lawrence and Rees, 2000; Okur *et al.*, 2011; Yuan *et al.*, 2006). Based on Winsor's classification, microemulsion which fluctuates

dynamically can be structurally divided into Winsor type I, oil-in-water microemulsion; Winsor type II, water-in-oil microemulsion; Winsor type III, bicontinuous middle-phase microemulsion and Winsor type IV, single phase micellar solution (Eastoe, 2005). In oil-in-water microemulsion, globular-liked oil droplets are dispersed in aqueous continuous phase while opposite scenario happens in water-in-oil microemulsion. Currently, marketed products in the form of microemulsion or self-dispersing lipid formulation include Neoral[®] (cyclosporin A for immunosuppressant); Aptivus[®], Norvir[®] and Fortovase[®] (consist of tipranavir, ritonavir and saquinavir respectively works as protease inhibitor in HIV therapy) (Kalepu *et al.*, 2013; Muzaffar *et al.*, 2013).

2.3.1 Compositions of microemulsion

Microemulsion is made up of aqueous, oil, surfactant and co-surfactant. The selection of oil, surfactant and co-surfactant is limited to those which are non-toxic and non-irritant. Oil could protect the skin from dehydration (Telofski *et al.*, 2012) and act as a penetration enhancer across epidermis (Wang *et al.*, 2007). In most formulations, medium chain mono- and di-glyceride extracted from plant and animal is used as the excipients. In most cases naturally found plant-based oil such as almond oil, olive oil and jojoba oil is more preferable owing to its topical and oral benefits. Almond oil has numerous health and beauty benefits as it elevates high-density lipoproteins and serves as a natural emollient for skin rejuvenation (Ahmad, 2010). Olive oil helps to minimize the chances of persistent skin condition such as psoriasis, acne and eczema (Viola and Viola, 2009). On the other hand, Urpi-Sarda *et al.* (2012) proved that daily intake of olive oil helps to reduce the inflammatory biomarker such as interleukin-6, C-reactive protein and chemokine which is related to atherosclerosis. Jojoba oil which has similar chemical constituents as human sebum, helps to retain moisture without clogging the pores and has excellent oxidative stability (Sandha and Swami, 2009).

As an emulsifying agent, surfactants affect the structure of microemulsion by changing its molecular structure packing parameter. The critical packing parameter ($v/a_o l_c$) of less than 1, favours oil-in-water micelle; equals to 1, favours bilayer vesicle; while more than 1, favours water-in-oil inverted micelle (Figure 2.2). It is classified into different classes namely non-ionic, anionic, cationic and amphoteric depending on the surfactant's head group composition. Non-ionic surfactant does not carry charge while the other three surfactants are negatively, positively and oppositely charged respectively. Non-ionic surfactant such as sorbitan monooleate and polyoxyethylene sorbitan fatty acid ester is the preferred surfactant as it is non-toxic, non-irritant, biodegradable, stable towards changes of pH and ionic ingredients (Rowe *et al.*, 2009).

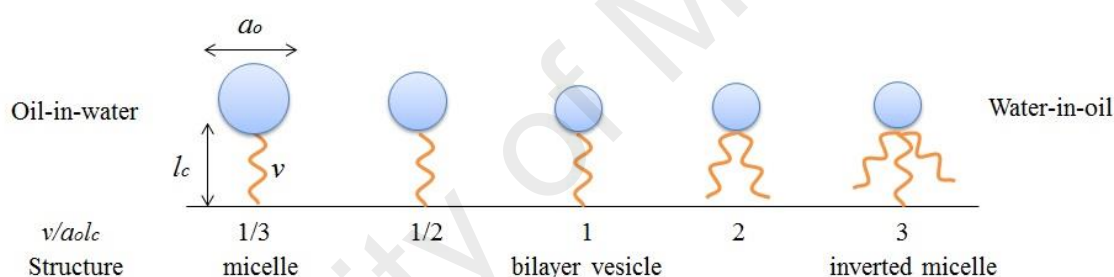


Figure 2.2: Effect of surfactant packing parameters on the structure of microemulsion. The packing parameter of a surfactant is affected by the area of hydrophilic head group (a_o), length of hydrophobic tail (l_c) and the volume of the surfactant's tail (v). The larger the value of packing parameters, the structure will be more prone to the formation of water-in-oil microemulsion.

In order to improve the wetting ability, co-surfactants such as ethanol and propylene glycol were usually added in the formulation. Co-surfactants enhance the solubilisation process by forming flexible interfacial film (Kreilgaard, 2002; Morozowich and Gao, 2009), reducing interfacial tension via increment of interface fluidity (Sripriya *et al.*, 2007; Zhang *et al.*, 2012) and enhancing permeability capacity of active ingredients for delivery (Ahmad *et al.*, 2014; Tsai *et al.*, 2010).

2.3.2 Preparation of microemulsion

The microemulsion is prepared either through phase titration or phase inversion temperature method. Several parameters such as temperature, types of oil, volume fraction of the droplets (ϕ) and molar ratio (R) of water to surfactant will affect the types of microemulsion being prepared. This can be evaluated by monitoring the density, viscosity and conductivity of the samples when those parameters are being manipulated during the preparation of microemulsion.

In phase titration method, phase diagram is constructed in order to determine the region of microemulsion formation in the presence of oil, aqueous and surfactant phase. The three components are varied at different percentages to make up 100% of ingredients in either v/v or w/w ratio. The mixture is agitated for complete mixing and the phase is determined through visual observation. Only those with clear, single phase solution are labelled as microemulsion thence being marked in the phase diagram to form a microemulsion region. In this preparation, the selection of oil type selected is crucial as increment of chain length will produce more positive curvature as the penetration of the surfactant tails will decrease relatively (Oldfield, 1994).

In phase inversion method, water-in-oil microemulsion is inverted into oil-in-water microemulsion or vice versa due to changes of temperature or continuous phase at the optimum surfactant concentration. If it is due to temperature changes, then inversion of oil-in-water microemulsion into water-in-oil microemulsion will depend on the cloud point of the surfactant in the mixture. It corresponds to temperature changes of surfactant's hydrophilic-hydrophobic characteristics, whereby hydrophilic head group was dehydrated during heating (Ontiveros *et al.*, 2014). On the other hand, changes of continuous phase can also cause phase inversion which was attributed by dilution. It

was observed that water-in-oil microemulsion loaded peptide for enhanced intestinal delivery slowly formed inverted oil-in-water microemulsion when the sample undergone a series of dilution with water up to 250-fold dilution (Liu *et al.*, 2013).

2.3.3 Advantages of microemulsion application

Microemulsion gained more attention as compared to other emulsions as it helped to enhance drug solubility, better thermodynamic stability, ease in scale up and higher drug permeability (Chen *et al.*, 2004; Okur *et al.*, 2014). Thus, this system is widely used in transdermal, oral, nasal and ocular delivery. It was shown that curcumin loaded water-in-oil microemulsion has better transdermal permeation as compared to micellar and surfactant-oil mixture (Sintov, 2015). When being treated orally, the symptoms of enhancement in pharmacological activity and no sign of intestinal mucosa damage were observed in rats when they were treated with multiple doses of earthworm fibrinolytic enzyme loaded water-in-oil microemulsion (Cheng *et al.*, 2008). The uses of microemulsion in the management of epilepsy through transnasal delivery is a breakthrough when carbamazepine loaded microemulsion with mucoadhesive not only displayed a better mucoadhesive effect and permeation rate but also free from nasal ciliotoxicity (Patel *et al.*, 2013). Besides that, voriconazole with broad range antifungal properties has better corneal permeation and drug accumulation when being loaded in oil-in-water microemulsion for ocular delivery than only active ingredient itself (Kumar and Sinha, 2014).

Active ingredients solubilisation in microemulsion is subject to the partition ability of active ingredients into the oil and aqueous phase. In water-in-oil microemulsion, it depends on the ability of active ingredients to dissolve in the aqueous phase (Porter *et al.*, 2008). Microemulsion with particle size which is less than 100 nm could enhance

permeability of active ingredients, thereby increasing its bioavailability in the system. In a comparison between microemulsion and tablet formulation, the results proved that the former has 12-fold higher bioavailability of saquinavir than the latter (Hosny and Hassan, 2014). The absorption rate could be improved by selecting lipids with similar properties as biological membrane, whereby phospholipids enhanced the permeability of poorly soluble active ingredients (Wu *et al.*, 2014). Another emerging finding is the use of skin penetrating peptide (SPP) such as poly-arginine, dermis localizing peptide (DLP) and linear peptide-12mer (LP-12) to act as a penetration enhancer for topical delivery. The peptide acts as the mediator between the active ingredients and the keratin present in the stratum corneum (Chen *et al.*, 2015; Kumar *et al.*, 2015).

The stability of the active ingredients in a delivery vehicle is highly dependent on its initial concentration, partition phase, and amount of external stimuli such as oxygen, light, pH, salt and temperature. In an experiment conducted by Špiclin *et al.* (2001), it showed that in the presence of oxygen, hydrophilic sodium ascorbyl phosphate is stable in water-in-oil microemulsion whereby 95% of active ingredients being remained after 2 months of storage. The protection layer can be enhanced by forming a double layer microemulsion whereby the initial microemulsion was coated with another layer of component. Lycopene loaded double layer microemulsion has better stability than single layer microemulsion when the formulation was challenged by the changes in pH, salt and temperature (Shi *et al.*, 2015).

Apart from that, microemulsion is easy to scale up. The step of warming up an oil-in-water microemulsion sometimes was being selected as the initial step to synthesize SLN with a monodispersed distribution (Marengo *et al.*, 2000). This enables researcher to overcome the shortage in the up-scaling during preparation of SLN or NLC

(Mojahedian *et al.*, 2013). It benefits the manufacturers due to the factors of cost effective, energy saving and ease in preparation.

2.4 Polymeric nanocarrier

Polymeric carrier as delivery vehicle has captured the attention of many researchers as it is biocompatible, biodegradable, cost effective and wide application. The polymeric material includes natural or synthetic polymers such as polylactic acid, polyvinylpyrrolidones, polysaccharides, proteins and peptides (Gong *et al.*, 2011; Kaneda *et al.*, 2004; van Zutphen and Reedijk, 2005). Depending on their structure and composition, they can be classified into hydrogel particle, filled hydrogel particle, biopolymeric particle, inclusion complexes and polyelectrolyte complexes for different functional performance (Hamidi *et al.*, 2008; Hamman, 2010; Joye and McClements, 2014). Among the polymeric material, polysaccharides are still the most favourable as they are abundantly found from natural sources and feasible for modification.

2.4.1 Polysaccharide based nanoparticles

Polysaccharides are composed of long chains homogeneous monosaccharide or heterogeneous copolymer units linked by glycosidic bonds. Naturally found polysaccharides usually originate from plants, algae, microbes and animals while synthetic polysaccharides are derived from naturally found polysaccharides. Among the naturally found polysaccharides, plant sources include cellulose, pectin, amylose; algae sources include alginate, carrageenan, fucoidan; microbe sources include xanthan gum, dextran, pullulan while animal sources include chitosan, heparin, chondroitin (Giri *et al.*, 2012; Linhardt and Liu, 2012; Liu *et al.*, 2008; Szu *et al.*, 2014). On the other hand, synthetic polysaccharide can be hydroxypropyl cellulose, methyl cellulose, hydroxypropylmethyl cellulose, N-trimethyl chitosan (Alves and Mano, 2008; Fettaka

et al., 2011). These polysaccharides with different chemical compositions or reactive groups serve as the main sources for synthesis of polysaccharide based nanoparticles. Negatively charged sodium alginate forms calcium alginate nanoparticles in the presence of positively charged calcium ions (Sugiura *et al.*, 2005). When β -D-glucan is crosslinked with sodium tripolyphosphate, nanoparticles with anti-fungal properties were being synthesised (Anusuya and Sathiyabama, 2014).

2.4.1.1 Chitosan

Chitosan is a linear aminopolysaccharide consisting of N-acetyl-D-glucosamine and D-glucosamine linked randomly by β -(1, 4) glycosidic bonds. This semi-crystalline polysaccharide is partially deacetylated derivative of chitin, found in crustacean shells such as crabs and shrimps (Patel *et al.*, 2010; Tiyaaboonchai, 2013). The crystallinity of chitosan is affected by the degree of deacetylated chitosan. Nevertheless, maximum crystallinity appears in 0% of deacetylation of chitin and minimum crystallinity in 100% of deacetylation of chitosan. The commercially available chitosan usually have 50 to 90% degree of deacetylation. Chitosan with high molecular weight is insoluble in neutral and alkaline conditions but soluble in mild acidic conditions. This is caused by protonation of free amino groups in the presence of acids (Suh and Matthew, 2000). Even so, chitosan can be soluble in water in the circumstances of low molecular weight or high degree of deacetylation of chitosan for different application (Malmo *et al.*, 2012; Tan and Misran, 2013). Chitosan which is positively charged reacts more responsive towards anionic materials to form ionic complexes. Owing to its pH dependent properties, chitosan nanoparticles is stable in acidic pH while adhesion and penetration is enhanced in alkaline pH (Makhlof *et al.*, 2011).

2.4.1.2 Carrageenan

Carrageenan is extracted from algae of class Rhodophyta (red algae) using water or alkaline water followed by alcohol precipitation. It is abundantly found in the genus of *Chondrus*, *Eucheuma* and *Kappaphycus* and classified into kappa (κ), iota (ι) and lambda (λ) carrageenan. These linear polysaccharides which linked by glycosidic bonds are composed of galactose and/or anhydrogalactose units. The major dissimilarity among those carrageenans is their negatively charged sulphated ester group. κ -carrageenan, ι -carrageenan and λ -carrageenan have one, two and three sulphated ester groups respectively. λ -carrageenan with three sulphated ester groups dissolve easily in hot and cold water but do not form gel while the other two carrageenans which are soluble at temperature higher than 60 °C or in the presence of sodium salt, form gel easily in the presence of gelling cations. As a consequence, carrageenan is a good excipient for gel formulation, suspension stabilizer, thickening agent in food and cosmeceutical products and suitable as controlled and sustained release delivery carrier. Mimicked release of methylene blue carrageenan hydrogel in gastrointestinal tract was shown to be minimized in the stomach and improved in the intestine (Hezaveh and Muhamad, 2012).

2.4.2 Synthesis of polysaccharide nanoparticle

Polysaccharide nanoparticles can be synthesized mainly by covalent crosslinking, ionic cross-linking, polyelectrolyte complexation or self-assembly of hydrophobically modified polysaccharide.

In cross-link method, cross-linker or condensing agent such as glutaraldehyde is required to connect the polysaccharide chains. Nevertheless, many researchers limit the usage of glutaraldehyde because of its toxicity that could induces reduction in cell

viability (Gan and Wang, 2007). In most cases, biocompatible dicarboxylic acid such as malic acid, succinic acid and citric acid are much preferred as the cross-linker. The rationale in cross-linking depends on the condensation of amino group of polysaccharide with aldehyde or carboxylic group of the cross-linker (Wang *et al.*, 2011). Cross-linking particle is stable and less likely to degrade (Banerjee *et al.*, 2002). The encapsulation of dextran-doxorubicin conjugate in chitosan nanoparticle by covalent linker has enhanced therapeutic effects and increased the survival rate of cancer patients (Mitra *et al.*, 2001).

Ionic cross-link depends on the interaction between charged functional group present in polysaccharide and small ionic molecules. Chitosan, guar gum and hydroxyethyl cellulose are positively charged while alginate, hyaluronic acid and carrageenan are negatively charged. In the presence of small anion molecule of tripolyphosphate (TPP) or cations of calcium ions, cross-linking occurs naturally in the presence of polysaccharide. Negatively charged TPP reacts with positively charged chitosan, forming particles for gene and small molecule delivery (Berger *et al.*, 2004; Gan *et al.*, 2005; Ko *et al.*, 2002; Luo *et al.*, 2010). Calcium as divalent cations, co-precipitate with carrageenan to form biodegradable and non-toxic porous nanocomposite for bone tissue engineering (Daniel-da-Silva *et al.*, 2007).

In polyelectrolyte complexation, the mechanism is through intermolecular electrostatic interaction whereby positively charged polysaccharides react with negatively charged polymeric molecules (Xu *et al.*, 2005). Since biocompatibility is one of the concern, chitosan with positively charged amino group could act as the natural polysaccharide (Luo and Wang, 2014; Wang *et al.*, 2011). Chitosan can freely interact with negatively charged polysaccharides, peptides and other polyelectrolytes. The ratio of two

oppositely charged polysaccharides, pH and temperature can affect the properties of the complexes prepared (Kim *et al.*, 2004). pH sensitive carboxymethyl Konjac glucomannan-chitosan beads which entrapped protein has site specific bioactive for delivery (Du *et al.*, 2006). Chitosan interacts with pectin to form porous scaffold, which is suitable for tissue regeneration application (Coimbra *et al.*, 2011).

Polysaccharides' self-assembly occurs when segments of hydrophilic part are modified with hydrophobic part to form amphiphilic polysaccharides. At the moment when amphiphilic polysaccharides come into contact with aqueous, they will aggregate spontaneously to form micelle or nanoparticles. This is ascribed to intra- and/or intermolecular hydrophobic interaction whereby hydrophobic segment aggregates to form inner core surrounded by hydrophilic segments. Thus, it is suitable for the entrapment of hydrophobic molecules (Liu *et al.*, 2005; Park *et al.*, 2006; Wang *et al.*, 2007). Hydrophobically modified glycol chitosan nanoparticles derived from glycol chitosan with 5 β -cholanic acid has enhanced the distribution in whole cells through endocytic pathways as compared to unmodified glycol chitosan nanoparticle for gene delivery (Nam *et al.*, 2009; Yoo *et al.*, 2005).

2.4.3 Polymeric nanoparticle for active ingredients delivery

Chitosan is a natural wound healing accelerator which promotes granulation and organization of cell through activation of inflammatory cells such as polymorphonuclear leukocytes (PMN), macrophage and fibroblast (Paul and Sharma, 2004; Ueno *et al.*, 2001). Chitosan has higher wound break strength and collagenases activity as compared to chitin as those with higher deacetylation degree has more activated fibroblast that would promote wound healing (Minagawa *et al.*, 2007). Antimicrobial effects of chitosan with molecular weight below 300 kDa contribute to

wound healing by inhibiting the growth of *Staphylococcus aureus* on the skin (Zheng and Zhu, 2003). In addition, chitosan with antacid and anti-ulcerative properties could prevent drug irritation in the stomach (Gupta and Kumar, 2000). On the other hand, carrageenan has antiviral effects on various types of enveloped viruses. This is owing to the presence of sulphated group in carrageenan which interferes the interaction of virus glycoprotein with the cell (Pujol *et al.*, 2002). Apart from that, carrageenan also possesses anticoagulant and antioxidant properties (de Araújo *et al.*, 2013; Yermak *et al.*, 2012).

The polysaccharides are capable for active ingredient's encapsulation and delivery depending on bioactive molecule-biopolymer binding, protein-polysaccharide interactions, pH dependent solubility differences, self-assembling, crosslinking and hydrophobic modification (Bilensoy *et al.*, 2009; Nagpal *et al.*, 2010; Patel and Velikov, 2011). Chitosan nanoparticles loaded with insulin for lung delivery showed high protein loading capacity by reaching a maximum of 80% and showing fast release of insulin from the microspheres (Grenha *et al.*, 2005). Depending on the molecular weight and degree of deacetylation, chitosan which successfully binds with oppositely charged DNA are capable for gene transfection in the HEK 293 cell (Lavertu *et al.*, 2006). Cross-linking of carrageenan and epichlorohydrin was shown to have controlled release properties as it affects the particles' swelling ratio (Keppeler *et al.*, 2009).

In mucosal delivery, the physical barrier made up of epithelium greatly reduces the permeability of active ingredients. This problem can be overcome by bioadhesive features possessed by chitosan (Pan *et al.*, 2002). Positively charged chitosan can easily adhere to negatively charged mucosal surface and transiently opens the tight junction between epithelial cells. This significantly prolongs the residence time of chitosan

nanoparticles and enhances the absorption of active ingredients across epithelium (Bravo-Osuna *et al.*, 2007; Dudhani and Kosaraju, 2010; Martinac *et al.*, 2005). Nanoparticles synthesized by complexation of chitosan and DNA are shown to be a promising vehicle for oral gene delivery due to its mucoadhesive properties (Plapied *et al.*, 2010). Besides that, in a comparison between both chitosan and Carbopol hydrogels to act as wound dressing, chitosan hydrogel has twice the retention of active ingredients on the skin as compared to Carbopol hydrogel, hence suggesting that the chitosan formulation has better bioadhesive properties (Hurler and Škalko-Basnet, 2012).

κ -carrageenan-chitosan nanoparticles have high potential to be exploited specific site targeting through EPR effects. The biocompatible nanoparticle with suitable particle size can pass through the blood vessel and accumulate at the tumor with ease. Cisplatin-loaded glycol chitosan nanoparticle showed antitumor efficacy in tumor-bearing mice (Kim *et al.*, 2008), revealing the possibilities of κ -carrageenan-chitosan nanoparticles towards the treatment of tumor. Apart from EPR effect, we can also make the most out of tumor and inflammatory cell which has lower endosomal pH and slightly higher temperature as compared to normal cell. Acidic or hyperthermic condition induced disassembly of stimuli sensitive nanoparticle, thus enhanced the release of entrapped active ingredients. This is a result of protonation of amine group or changes in lowering critical solution temperature (LCST) of nanoparticles (Fan *et al.*, 2008; Jin *et al.*, 2012; Nogueira *et al.*, 2013; Wang and Zhang, 2012). Paclitaxel loaded pH sensitive nanoparticle has enhanced cytotoxicity in tumor-bearing mice as compared to those cells in normal pH (Li *et al.*, 2009). On top of that, doxorubicin hydrogel containing chitosan-doxorubicin conjugates and Pluronic with physical gelation above LCST, has better *in vivo* therapeutic effect on solid tumor as compared to free doxorubicin (Cho *et al.*, 2009). Targeted delivery can be achieved through specific targeting receptor and

ligand-bearing nanoparticles or degradation by specific microorganisms (Park *et al.*, 2010). Folate receptor which is mostly absent in normal cell was being found plentifully in malignant tumors, especially ovarian carcinoma (Zhao and Lee, 2004). This special characteristic promotes folic acid to bind specifically on the receptor for higher active ingredients' delivery (Mansouri *et al.*, 2006). On the other hand, microflora which are found abundantly in intestine can specifically breakdown the glycosidic bond of polysaccharides for colon-specific targeted delivery (Gupta *et al.*, 2012; Hejazi and Amiji, 2003).

CHAPTER 3: MATERIALS AND METHODS

Lipid nanoparticle, liposome, water-in-oil microemulsion and κ -carrageenan-chitosan nanoparticle with its own special features, could aid in the dissolution and permeation of active ingredients via improved encapsulation and controlled release. Thus, each system was individually prepared, optimized and characterized for its physicochemical properties. Depending on the system, the characterizations might include particle size, zeta potential, morphology, thermal properties, pH, electrical conductivity, viscosity and/or infrared spectrophotometry. From the obtained results of characterization, the most suitable formulation for each system was being encapsulated with active ingredients of different solubility in water and evaluated for their release profile.

3.1 Materials

Arachidic acid, linoleic acid, linolenic acid, oleic acid, polyoxyethylene sorbitan monopalmitate (Tween 40), polyoxyethylene sorbitan monostearate (Tween 60), polyoxyethylene sorbitan monooleate (Tween 80), polyoxyethylene sorbitan trioleate (Tween 85), sorbitan monooleate (Span 80), L-ascorbic acid, caffeine, lidocaine, phosphate buffered tablet, sodium hydroxide pellet, boric acid, sodium tetraborate, and phosphotungstic acid were purchased from Sigma-Aldrich, USA. Erucic acid, sorbitan monopalmitate (Span 40) and κ -carrageenan were obtained from Fluka, Switzerland. Chitosan was from Acros, Belgium. Glacial acetic acid, hydrochloric acid and sodium acetate trihydrate were from Merck, USA. Extra virgin olive oil was purchased from Laleli, Turkey. All materials were used without any further purification.

Deionized water with resistivity of 18.2 mS cm^{-1} was dispensed from Barnstead NANOpure[®] Diamond[™] (Thermo Scientific, USA). U-shaped clear capillary cell was from Malvern, UK. Quartz clear cell was from Thermoscientific, USA. DSC hermetic

pan was from TA instruments, USA. The dialysis membrane was from DIANORM GmbH, Germany. Last but not least, the 400 mesh TEM copper grid was from Electron Microscopy Sciences, USA.

3.2 Preparation of delivery carriers

3.2.1 Preparation of NLC

For the preparation of NLC, arachidic acid and erucic acid were both selected as solid lipid, oleic acid as liquid lipid while Span 40 as emulsifier. Fatty acids were being selected as the lipid components, owing to the fact that they can be metabolized by the body and thus being served as energy resources. Apart from that, it is cost effective, biocompatible and can be found abundantly either in natural or synthetic forms. On the other hand, Span 40 is non-toxic and biocompatible.

NLC was prepared by employment of hot homogenization technique. Mixture of fatty acids, being listed as in Table 3.1 and Span 40 was weighed at ratio 8:2 (w/w) and melted at 90 °C. Deionized water (2 ml) of same temperature was then added into the mixture and homogenized using T25 basic homogenizer (IKA, Germany) for 10 minutes with the speed of 15000 rpm. Lastly, the homogenized sample was immediately poured into ice cooled deionized water to form NLC.

Table 3.1: Compositions of lipid components for the preparation of NLC

Sample	Fatty Acids (weight percentage)		
	Arachidic acid	Oleic acid	Erucic acid
NLC 1	80	10	10
NLC 2	70	20	10
NLC 3	60	30	10
NLC 4	50	40	10
NLC 5	40	50	10

3.2.2 Preparation of liposome

The C18 unsaturated fatty acid liposome with a final concentration of 10 mM was prepared via thin film hydration method. Depending on their respective molecular weight of unsaturated fatty acids, oleic acid (13.9 mg), linoleic acid (14.0 mg) and linolenic acid (14.1 mg) were all weighed and dissolved in 1 ml of chloroform. The solvent was then evaporated by using a rotary evaporator (Rotavapor[®] R-114, BÜCHI[®], Switzerland) at 45.0 °C to form a thin layer of lipid film on the wall of round bottom flask. The lipid thin film was rehydrated with 2 ml of 50 mM borate buffer pH 8.6 and dispersed using a bath sonicator (JEIO Tech, Korea) for a minute to form liposome. The pH of the liposomal solution was being adjusted to pH 8.6 by using 50 mM sodium hydroxide or hydrochloric acid, then topped up to a final volume of 5 ml in a volumetric flask.

3.2.3 Preparation of water-in-oil microemulsion

The preparation of water-in-oil microemulsion was done by mixing a specific amount of deionized water, olive oil and surfactant with mild agitation. In our case, Span 80 was mixed individually at a ratio of 1:1 with various types of Tween surfactants, namely Tween 40, 60, 80 and 85. The mixed surfactant was then added with olive oil and deionized water. The mixture was agitated using a small orbital shaker (MS1 shaker, IKA[®], Germany) at 1000 rpm for a minute.

In order to identify the region of microemulsion formation, ternary phase diagram was constructed. With a total weight of 2 g (w/w), 5% of it was contributed by mixed surfactant while the remaining 95% was added with olive oil and deionized water. As an example, when 5% of mixed surfactant was present in the formulation, it was topped up with 1% of deionized water and 94% of olive oil (w/w), followed by agitation. In a

similar amount of surfactant, the procedure was repeated with an increased amount of deionized water and a decreased amount of olive oil proportionally, at a 1% difference to make up a total of 100% (w/w). The process was then repeated by varying the amount of the mixed surfactant with a 5% increment until the surfactant amount finally reached 95%. Visual observation of a single phase clear solution indicated the microemulsion phase and was marked on the ternary phase diagram. The prepared microemulsion was being labelled according to the mixed surfactant that presents in the formulation, i.e. Span 80 and Tween 40 was identified as ST40, Span 80 and Tween 60 as ST60, Span 80 and Tween 80 as ST80, as well as Span 80 and Tween 85 as ST85.

3.2.4 Preparation of κ -carrageenan-chitosan nanoparticle

κ -carrageenan-chitosan nanoparticle was prepared by formation of polyelectrolyte complex (PEC) of two oppositely charged polymer. With this, 100 mg of chitosan and 100 mg of κ -carrageenan were dispersed individually and being stirred overnight in sodium acetate buffer which ranged from pH 3 to pH 6 for a final concentration of 1 mg ml⁻¹ (w/v) in both solutions. For the κ -carrageenan solution, it was heated at 60 °C for 10 minutes before being stirred overnight. Then, the solutions with same pH were mixed at a speed of 1000 rpm for 30 minutes by using MR Hei-Standard magnetic stirrer (Heidolph, Schwabach, Germany) in various ratios of 1:5, 2:4, 3:3, 4:2, and 5:1 (v/v) respectively to form κ -carrageenan-chitosan nanoparticle to a final volume of 30 ml. The mixture was centrifuged at 14,000 rpm for an hour by using centrifuge (Velocity 18R Refrigerated Centrifuge, Dynamica Scientific Ltd., United Kingdom) to collect the κ -carrageenan-chitosan nanoparticle and subsequently, the pellet was dried in vacuum oven (SHEL LAB vacuum oven, Sheldon Manufacturing Inc., USA) with a vacuum control of 25 inch Hg. The yield of each combination was then weighed.

3.3 Principle and characterization of delivery carriers

3.3.1 Particle size and zeta potential

The Malvern Zetasizer Nano Series performs size measurement by using the technique known as dynamic light scattering (DLS). DLS measures Brownian motion and relates it to the size of particle. It was done by illuminating the particles with a laser and analyzing the intensity fluctuations in the scattered light. When the particle was illuminated, it will show bright and dark area. The bright area appears when the light passes through unscattered, whereas the dark area appears when the light was scattered and detected by the detector. The relationship between the size of a particle and its speed which due to Brownian motion, is defined in the Stroke-Einstein equation as in Eq. 1,

$$D_t = \frac{kT}{6\pi\eta R_h} \quad \text{Eq. 1}$$

where D_t is the translational diffusion constant ($\text{m}^2 \text{s}^{-1}$), k is the Boltzmann constant ($1.3806 \times 10^{-23} \text{ m}^2 \text{ kg s}^{-2} \text{ K}^{-1}$), T is the absolute temperature (K), π is the ratio of a circle's circumference to its diameter of approximately 3.1416, η is the viscosity of the solution ($\text{kg m}^{-1} \text{s}^{-1}$), and R_h is the hydrodynamic radius of particle (m).

Thus, if a large particle is being measured, it moves slowly and the intensity of scattered light fluctuates slowly. On the contrary, a smaller particle will have a faster motion whereby the intensity of scattered light will fluctuate more vigorously. Other than the size of the measured particle, changes in the viscosity or temperature could also affect the frequency of collision and as a result, it affects the coalescent. At higher viscosity or lower temperature, frequency of collision will be lower, thus coalescent will be relatively lower for a stable formulation.

In the measurement of zeta potential, firstly we need to determine the electrophoretic mobility of a sample by performing an electrophoresis to evaluate the velocity of the particle using laser Doppler velocimetry (LDV). Then, the zeta potential was calculated by substitution of the obtained electrophoretic mobility in the Henry equation (Eq. 2),

$$U_E = \frac{2\varepsilon\zeta f(\kappa a)}{3\eta} \quad \text{Eq. 2}$$

where U_E is the electrophoretic mobility ($\text{m}^2 \text{s}^{-1} \text{V}^{-1}$), ε is the dielectric constant, ζ is the zeta potential (mV), η is the viscosity of the solution ($\text{kg m}^{-1} \text{s}^{-1}$), and $f(\kappa a)$ is Henry's function with a value of 1.5 for polar solvent as Smoluchowski approximation or 1.0 for non-polar solvent as Huckel approximation.

The magnitude of zeta potential gives an indication of the potential stability of a colloidal system. If the particles in suspension have a large negative or positive zeta potential, they will tend to repel each other and have lesser tendency to flocculate. On the other hand, if the particles have low zeta potential values, it is easier for the particle to come together and flocculate. In most cases, particles with a zeta potential which is either more positive than +30 mV or more negative than -30 mV are considered stable.

In the experiment, the mean z-average, size distribution, zeta potential and the standard deviation of the sample were obtained using the Malvern Zetasizer Nano Series (Nano ZS, Malvern Instruments, UK) performed at 25.0 °C. The sample was loaded in a quartz clear cell with a 1 cm path length for measurement of particle size and particle size distribution while U-shaped gold pleated folded capillary cell was used for zeta potential determination. The particle size was measured in triplicates whereby each measurement consists of 12 runs on the sample and the average particle size was obtained. All prepared delivery carriers were determined for their particle size, particle

distribution and zeta potential except for water-in-oil microemulsion which was evaluated only for particle size and particle distribution. The dispersing medium for NLC, liposome and κ -carrageenan-chitosan nanoparticle is water while for water-in-oil microemulsion is olive oil.

3.3.2 Transmission electron microscopy (TEM)

In TEM, the source of illumination is a beam of high velocity electrons accelerated under vacuum, focused by condenser lens onto the specimen. The loss and scattering of electrons by the individual part of the structure, formed the image seen on the micrograph after passed through several objective lenses until they reached the fluorescence screen. The wavelength of the propagating electrons at a given accelerating voltage can be determined by an equation derived from the deBroglie equation that shown as *Eq. 3*,

$$\lambda = \frac{h}{\sqrt{2mqV}} \quad \text{Eq. 3}$$

where λ is the wavelength of an electron (m), h is the Planck's constant of 6.6261×10^{-34} J s, m is the electron mass with 9.1094×10^{-31} kg, q is the electron charge of 1.6022×10^{-19} C, V is the accelerating voltage (eV). From calculation, TEM with accelerating voltage of 120 kV and 200 kV, have electrons' wavelength of 3.54 pm and 2.74 pm respectively. Hence, the resolution of the image increases when the accelerating voltage of the electron beam increases.

The morphology of prepared delivery carrier via negative-staining method, was observed under a TEM (Carl Zeiss LIBRA[®] 120, Germany or JOEL JEM-2100F, Japan), conducted at the School of Biological Sciences, University Sains Malaysia (USM, Malaysia) or Physics Department, University Malaya (UM, Malaysia) respectively. A

drop of sample solution was positioned on a 400 mesh carbon coated copper grid and left for a timeframe between 30 seconds to 3 minutes. The excess sample solution was removed by using filter paper and being air-dried for a minute. The sample on the grid was then added with one drop of 1% phosphotungstic acid solution and left for few minutes to stain the sample. Any excess solution was dabbed with filter paper and air-dried prior to being visualized under the TEM. The acceleration voltage was applied at 120 kV for Carl Zeiss LIBRA[®] 120 and 200 kV for JOEL JEM-2100F.

3.3.3 Differential scanning calorimetry (DSC)

DSC monitors heat effects which associated with phase transitions and chemical reactions as a function of temperature. It records the difference in heat flow to the sample and reference at the same temperature. Since the DSC was performed at constant pressure, the heat flow is equivalent to enthalpy changes. The heat flow difference between the sample and reference was shown as *Eq. 4* below,

$$\Delta \frac{dH}{dt} = \left(\frac{dH}{dt} \right)_{sample} - \left(\frac{dH}{dt} \right)_{reference} \quad \text{Eq. 4}$$

where Δ is the change of any changeable quantity, $\frac{dH}{dt}$ is the heat flow (mW) of amount of heat supplied at given time.

The heat flow difference can be either positive or negative. In an endothermic process such as dehydration, reduction and some decomposition of sample, heat is being absorbed thus the heat flow difference is positive. On the other hand, in an exothermic process such as crystallization, oxidation and some decomposition of sample, heat is being released thus the heat flow difference is negative. From the thermogram of heat

flow, the thermal profile such as onset temperature, peak temperature and melting enthalpy of samples can be analyzed and calculated.

The thermal profile of samples was monitored by DSC Q20 (TA instruments, USA). 2 to 3 mg of lipid nanoparticle was weighed in a 40 µl hermetic aluminium pan. The DSC analysis was performed with a scan rate of 5 °C per minute within a temperature range from 20 to 300 °C depending on the sample. An empty pan was used as the reference. The analysts were being repeated for 3 cycles.

3.3.4 Critical vesicular concentration (CVC)

The measurement of CVC depends on the effect of solute or monomer on the surface tension as stated in Gibbs adsorption isotherm, which was shown in *Eq. 5*,

$$\Gamma = \frac{I}{nRT} \left(\frac{\delta\gamma}{\delta \ln C} \right) \quad \text{Eq. 5}$$

where Γ is the surface concentration (mol m⁻²), n is the number of mole (mol) which implies the mass of a substance to its relative mass, R is the gas constant of 8.3145 m³ Pa K⁻¹ mol⁻¹, T is the absolute temperature (K), δ is the changes of any changeable quantity, γ is the surface tension (N m⁻¹), and $\ln C$ is the natural logarithm for concentration of substance in bulk phase (mol m⁻³).

Surface tension changes drastically with proportional to the changes of monomer when the concentration is prior to reach CVC. Despite that, after reaching CVC, the surface tension varies slightly towards the changes of monomer concentration or remains relatively constant. The point of inflection indicates the CVC of the solution.

In the experiment, the CVC of liposome was determined using tensiometer (K100, KRÜSS-GmbH, Germany) by measuring a series of liposomal solution ranged from 0.017 to 6.74 mM. The solution was poured into a vessel and five measurements were taken using tensiometer by employing du Noüy ring method at 30.0 °C (Teo *et al.*, 2012). The mean surface tension of the solution was plotted against ln [fatty acid]. The minimum concentration required for the vesicle formation could be estimated from the inflection point obtained from the graph.

3.3.5 FTIR

The operation of FTIR is based on Michelson Interferometer whereby the light directed to beam splitter was half reflected while the other half was transmitted. The two beams with different optical paths will then reflected back to the beam splitter which causes constructive or destructive of particular frequency and transferred into signal which known as interferogram. Thus, FTIR operates based on the principle called Fourier transform with a mathematical expression as *Eq. 6* whereby the interferogram was converted into a spectrum.

$$F(\omega) = \int_{-\infty}^{+\infty} f(x) e^{i\omega x} dx \quad \text{Eq. 6}$$

where $F(\omega)$ is the spectrum, $f(x)$ is the interferogram, ω is the angular frequency, and dx is the optical path difference. Since Fourier transform is a density function, the spectrum is obtained by integrating the interferogram.

An infrared spectrum represents a fingerprint of a sample with absorption peaks which corresponds to the frequencies of vibrations between the bonds of the atoms which make up the material. For example, the absorption band of around $1680 - 1620 \text{ cm}^{-1}$ and

3550 – 3200 cm⁻¹ represents alkenyl C=C and phenol O-H stretch respectively. This showed that the infrared spectrum for each material is different from each other because of the uniqueness in the combination of atoms. Hence, FTIR is usually applied in qualitative analysis to identify the functional group that presents in a material. This method is quick, time saving, suitable for many types of sample and no external calibration required.

The functional group of chitosan powder, κ -carrageenan powder, the mixture of chitosan with κ -carrageenan powder as well as dried κ -carrageenan-chitosan nanoparticle, all were being determined using FTIR (Perkin Elmer, USA). The FTIR spectra were recorded in the range of 4000 – 450 cm⁻¹ with 16 scans at spectral resolution of 4 cm⁻¹ (Rajaram and Natham, 2013). The spectrum of κ -carrageenan - chitosan nanoparticle was compared with the spectrums of chitosan powder and κ -carrageenan powder to identify the formation of new bonding in κ -carrageenan-chitosan nanoparticle.

3.3.6 Swelling percentage

The dried κ -carrageenan-chitosan nanoparticle was weighed and added with 5 ml of pH 7.4 phosphate buffer. Then, at the time interval of 15 minutes, 30 minutes, 1 hour, 2 hours, 4 hours, 6 hours, 12 hours and 24 hours, the swelled κ -carrageenan-chitosan nanoparticle was being weighed accordingly. The maximum swelling percentage of κ -carrageenan-chitosan nanoparticle after 24 hours was calculated as Eq. 7,

$$SP = \frac{a - b}{b} \times 100\% \quad \text{Eq. 7}$$

where SP is the swelling percentage whereby the swelling properties of a particle is measured, a is the weight of swelled κ -carrageenan-chitosan nanoparticle (g), b is the weight of dried κ -carrageenan-chitosan nanoparticle (g).

3.3.7 pH

The pH of a solution measures the degree of acidity or alkalinity relative to the ionization of water. It involves comparison of the potential of solutions with unknown $[H^+]$ to a known reference potential. pH meter converts the voltage ratio between a reference half-cell and a sensing half-cell to pH values. The changes in potential and detection of $[H^+]$ were represented by Nernst equation (Eq. 8),

$$E = E_r + \left(\frac{2.303RT}{zF} \right) \log \left(\frac{[H^+]_u}{[H^+]_i} \right) \quad \text{Eq. 8}$$

where E is the total potential difference (V), E_r is the standard cell potential (V), R is the gas constant of $8.3145 \text{ J K}^{-1} \text{ mol}^{-1}$, T is the absolute temperature (K), z is the valence or charge of the ion, F is the Faraday's constant of $9.65 \times 10^4 \text{ C mol}^{-1}$, $[H^+]_u$ is the hydrogen ion concentration of measured sample (mol m^{-3}), $[H^+]_i$ is the hydrogen ion concentration of internal reference (mol m^{-3}).

The pH of prepared water-in-oil microemulsion, liposome, and buffer solution was measured using the S47-K SevenMulti™ dual meter pH/conductivity (Mettler Toledo, Switzerland). The pH probe is InLab® Expert Pro electrode with a solid polymeric electrolyte. The measurement was carried out in three replicates.

3.3.8 Conductivity

Conductivity is the measurement of the ability of an electrolyte solution to conduct electricity. The principle of conductivity measurement determines the resistance of the

solution between two electrodes that separated by a fixed distance. Resistance is determined according to Ohm's Law (Eq. 9) through the ratio of voltage to current of an object while the conductance is the reciprocal of resistance.

$$G = \frac{I}{R} = \frac{I}{V} \quad \text{Eq. 9}$$

where G is the conductance ($\text{kg}^{-1} \text{m}^{-2} \text{s}^3 \text{A}^2$ or Ω^{-1}), R is the resistant ($\text{kg m}^2 \text{s}^{-3} \text{A}^{-2}$ or Ω), I is the current (A), V is the voltage ($\text{kg m}^2 \text{s}^{-3} \text{A}^{-1}$ or V). The standardized conductivity (S m^{-1}) is obtained by multiplying the conductance with cell constant, whereby cell constant is the ratio of the distance between the electrodes to the area of the electrodes.

Conductivity measurement is useful in the determination of the continuous phase of the prepared microemulsion. When aqueous solution is the continuous phase, the conductivity will be very much higher than that of water-in-oil microemulsion. This is due to the fact that aqueous is a better conductor than oil (Anjali *et al.*, 2010).

The conductivity of water-in-oil microemulsion was measured by using S47-K SevenMulti dual meter pH/conductivity (Mettler Toledo, Switzerland). The measurement was determined using InLab[®] 731 with four-graphite poles of a cell constant 0.57 cm^{-1} . The measurement was carried out in three replicates.

3.3.9 Viscosity

Viscosity measures the flow ability of a material moving through surfaces. Fluids resist relative motion of layers with differing velocities within them, opposing changes in the initial formation, hence generating internal resistance to flow. A fluid showing high resistance to opposing flow is said to be thick or viscous while those having small

resistance to flow are thin or runny. The viscosity of a sample is defined by shear stress over shear rate as *Eq. 10* below,

$$\eta = \frac{\tau}{\dot{\gamma}} \quad \text{Eq. 10}$$

where η is the viscosity of the sample (Pa s), τ denotes the shear stress where amount of force applied to sample per unit area (Pa), and $\dot{\gamma}$ signifies the shear rate where velocity per unit height (s^{-1}).

Newtonian fluid is independent on the shear rate whereby the shear stress is proportional to shear strain rate. For non-Newtonian fluid, the viscosity is affected by the shear rate which causes the sample to be shear thickening or shear thinning.

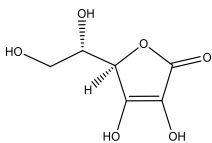
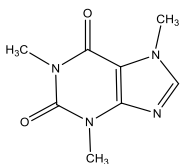
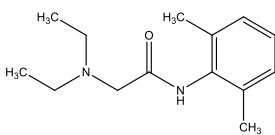
Viscosity of the prepared water-in-oil microemulsion was determined using a Bohlin Instruments Gemini advanced rheometer (Malvern, UK). The method used was from Basheer *et al.* (2013) with some modification. The measurement was performed at a controlled temperature of 25.0 ± 0.1 °C, using a 1°/60 mm cone and plate geometry with a gap of 30 μm in a shear range of 0.1 - 100 s^{-1} . The apparent viscosity of sample was recorded at a shear rate of 50 s^{-1} .

3.4 Loading efficiency, encapsulation efficiency and release profile of nanocarrier

Based on the physicochemical characterization of prepared nanocarriers, formulation with the most desired properties was selected from each system for encapsulation or solubilisation of active ingredients, followed by active ingredients release using Franz diffusion cell. Depending on their solubility in water, the active ingredients selected were ascorbic acid, caffeine and lidocaine with decreasing hydrophilicity. Ascorbic acid, caffeine and lidocaine are grouped under Class I, II and III respectively under

biopharmaceutical classification system. Their chemical structure and properties were shown in Table 3.2.

Table 3.2: Chemical structure and properties of active ingredients

	Chemical structure	Solubility in water	Molecular Weight (g mol ⁻¹)	Melting Point (°C)
Ascorbic Acid		Freely	176.12	191
Caffeine		Sparingly	194.19	238
Lidocaine		Slightly	234.34	68.5

3.4.1 Loading and encapsulation of active ingredients

3.4.1.1 Preparation and evaluation of encapsulated NLC

The active ingredients encapsulated NLC was prepared using the same method as unloaded NLC. The only difference in the preparation is that active ingredients were first dissolved in the medium where it was soluble. Thus, ascorbic acid was dissolved in water while caffeine and lidocaine were dissolved in lipid phase. The prepared sample was filtered through 0.2 µm nylon filter (Sartorius Stedim, Belgium) whereby the NLC will entrapped on donor part of the membrane while NLC-free clear filtrate was measured by Cary[®] 50 UV-Vis spectrophotometer (Varians, Agilent Technologies, USA) using two clear side quartz cuvette with 1 cm path length.

3.4.1.2 Preparation and evaluation of encapsulated liposome

The loading of active ingredients into fatty acid liposomes was prepared in a similar way as NLC whereby lidocaine and caffeine were individually dissolved together with

the lipid phase before subjected to solvent evaporation while ascorbic acid was added during the rehydration process. The encapsulated liposomal sample was centrifuged through 50 kDa molecular weight cut off (MWCO) vivaspin6 column (Sartorius Stedim, Belgium) at 1500 rpm for 15 minutes whereby unencapsulated active ingredients will be separated out while the liposome will be remained in the upper part of vivaspin6 column. The unencapsulated active ingredient was measured by Cary® 50 UV-Vis spectrophotometer using two clear-sided quartz cuvette with 1 cm path length.

3.4.1.3 Preparation and evaluation of water-in-oil microemulsion

For loading of active ingredients in water-in-oil microemulsion, the active ingredients were first solubilized in deionized water before introduced in the mixture as aqueous phase. The amount of active ingredients was solubilized at optimum concentration of lidocaine in water of 3 mg ml⁻¹ to standardize their amount in the formulation.

3.4.1.4 Preparation and evaluation of encapsulated κ -carrageenan-chitosan nanoparticle

During entrapment of active ingredients, the sample was prepared as unloaded κ -carrageenan-chitosan nanoparticle except that the active ingredients were first dissolve in κ -carrageenan solution prior to mixing with chitosan solution. The mixtures were then centrifuged to collect the active ingredients loaded κ -carrageenan-chitosan nanoparticle while the supernatant was used to estimate the unloaded active ingredients by employing Cary® 50 UV-Vis spectrophotometer using two clear-sided quartz cuvette with 1 cm path length.

For all nanocarriers except water-in-oil microemulsion, the loading efficiency (*Eq. 11*) and encapsulation efficiency (*Eq. 12*) were being calculated as the equation below,

$$LE = \frac{b - c}{a} \times 100\% \quad \text{Eq. 11}$$

$$EE = \frac{b - c}{b} \times 100\% \quad \text{Eq. 12}$$

where *LE* is the loading efficiency of the active ingredients (%), *EE* is the encapsulation efficiency of the active ingredients (%), *a* is the weight of NLC/ liposome/ κ -carrageenan-chitosan nanoparticle (g), *b* is the total weight of active ingredients present in the formulation (g), *c* is the weight of unencapsulated active ingredients (g).

3.4.2 Franz diffusion cell for active ingredient's release profile

A cumulative percentage of active ingredients' release from delivery carrier was carried out at 37.0 °C for a period of 24 hours using the in-line Hanson MicroettePlus™ diffusion system (Hanson Research, USA). The diffusion system was equipped with a vertical clear glass diffusion cell of 0.9 cm orifice diameter, 1.9 ml donor volume and 4 ml receptor volume. A dialysis membrane of 5000 Da molecular weight cut-off (MWCO) was soaked in the receptor medium for at least 12 hours prior to be mounted between the donor and receptor chamber. The donor chamber consisted of 500 µg active ingredients while the receptor chamber was filled with a pH 7.4 phosphate buffer solution. At predetermined time intervals of 0.5 hour, an hour, 2 hours and subsequent 2 hours, the sample was automatically collected. The concentration of active ingredient in the collected sample was estimated by employing a Cary® 50 UV-Vis spectrophotometer, using a quartz cuvette with a 1 cm path length. The experiment was conducted for six replicates.

3.4.3 Kinetic models

The drug release model was determined by fitting the results of cumulated release of active ingredients into the zero-order model, the first-order model, the Higuchi model, the Hixson-Crowell model and the Korsmeyer-Peppas model (Dash *et al.*, 2010).

3.4.3.1 Zero-order model

Zero-order model is usually applied in describing the drug dissolution of several types of modified release pharmaceutical dosage forms in some transdermal systems. Apart from that, it is also suitable for the release of drug from matrix tablet with low soluble drugs in coated form and osmotic system. The dissolution of active ingredients can be represented by *Eq. 13*:

$$Q_0 - Q_t = K_0 t \quad \text{Eq. 13}$$

where Q_0 is the initial amount of drug in the solution (g), Q_t is the amount of drug dissolved in time t (g), K_0 is the zero order release constant, and t is the time (s). In zero-order model, the graph is plotted as cumulative percentage released against time.

3.4.3.2 First-order model

First-order model is used to describe absorption and/or elimination of drugs which contain water soluble drug in porous matrices. It is presumed that the drug diffusion is in one direction and concentration dependent. The dissolution of active ingredients can be represented by *Eq. 14*:

$$\text{Log } C = \text{Log } C_0 - \frac{Kt}{2.303} \quad \text{Eq. 14}$$

where C is the concentration of drug at designated time (g L^{-1}), C_0 is the initial concentration of drug (g L^{-1}), K is the first order rate constant, and t is the time (t). The slope is defined as $\frac{K}{2.303}$. For first-order model, the graph was plotted as log of the remaining percentage release against time.

3.4.3.3 Higuchi model

Higuchi model is valid for all the time until the drug was totally depleted from the system. In most cases, it is applied for drug dissolution from several types of modified release pharmaceutical dosage forms, transdermal system and matrix tablet with water soluble drug. In this system, it is presumed that the initial drug concentration in the matrix is much higher than drug solubility; drug diffusion takes place only in one dimension; drug particles are much smaller than system thickness; matrix swelling and dissolution are negligible; drug diffusivity is constant and perfect sink conditions are always attained in the release. The dissolution of active ingredients can be represented by Eq. 15:

$$Q = K_H \times t^{1/2} \quad \text{Eq. 15}$$

where Q is the amount of drug released in time t per unit area ($\text{g s}^{-1} \text{ m}^{-2}$), K_H is the Higuchi dissolution constant, and t is the time (s). In Higuchi model, the graph is plotted as the cumulative percentage release against the square root of time.

3.4.3.4 Hixson-Crowell model

Hixson-Crowell model fits best to pharmaceutical dosage in tablet form where the dissolution occurs in planes that are parallel to the drug surface if the tablet dimension diminishes proportionally, in such a manner that the initial geometrical form keeps constant all the time. The dissolution of active ingredients is represented by Eq. 16:

$$W_0^{1/3} - W_t^{1/3} = Kt$$

Eq. 16

where W_0 is the initial amount of drug in the pharmaceutical dosage form (g), W_t is the remaining amount of drug in pharmaceutical dosage form at time t (g), K is the constant incorporating the surface-volume relation, and t is the time (s). The graph of Hixson-Crowell model is plotted as the cube root of drug percentage remaining against time.

3.4.3.5 Korsmeyer-Peppas model

Korsmeyer-Peppas model is applied to understand the release of drug from a polymeric system. The mechanisms considered in this model include diffusion of solvent into the polymeric system, swelling of polymeric system, formation of gel, diffusion of active ingredients out of the polymeric system and dissolution of the polymeric system's matrix. The dissolution of active ingredients is represented by Eq. 17:

$$\frac{M_t}{M_\infty} = Kt^n$$

Eq. 17

Where t is the time (s), $\frac{M_t}{M_\infty}$ is the fraction of drug released at time t , K is the release rate constant, n is the release exponent. In Korsmeyer-Peppas model, the graph is plotted as the log cumulative percentage release against log time. In spite of that, the mechanism is limited to the first 60% of drug release from the system.

CHAPTER 4: RESULTS AND DISCUSSION

4.1 Physical characterization of delivery carriers

Depending on the characteristics of the carrier system, the prepared samples were characterized to select the more suitable formulation from each system for active ingredients' encapsulation and release. For NLC, particle size, zeta potential, morphology and thermal profile were evaluated. For liposome, particle size, zeta potential, morphology, CVC were determined. For water-in-oil microemulsion, particle size, morphology, viscosity, pH and conductivity were assessed. For κ -carrageenan-chitosan nanoparticle, particle size, zeta potential, morphology, FTIR and swelling percentage were measured.

4.1.1 Characterization of NLC

The NLCs prepared by Span 40 and mixed fatty acids of arachidic acid, erucic acid and oleic acid, were evaluated for their particle size, zeta potential, thermal profile and morphology. In the formulations, erucic acid and Span 40 were unvaried ingredients while percentages of arachidic acid and oleic acid in mixed fatty acids were both decreased and increased by 10% respectively for each formulation. Thus, the evaluation of prepared NLC was being focused on the effect of varied ratio of solid and liquid lipids towards the stability of the formulations. The formulation which consists 80% of arachidic acid and 10% of oleic acid in the mixed fatty acids was named as NLC 1. The mixture was gradually varied until NLC 5 which consists 40% of arachidic acid and 50% of oleic acid in the mixed fatty acids.

The particle size analysis of prepared NLC was shown to be affected by the amount of oleic acid presents in the formulation. From Figure 4.1, a gradual increase of oleic acid by 10% weight percentage of the lipid mixture in the formulation caused an apparent

increase in the particle size of the NLC when the formulation was evaluated on the first day. The changes in the particle size were observed for all NLC formulations when the stability of the NLC prepared was evaluated. It was shown that beyond Day 14th, the changes of the particle size reached maximum particle stability whereby there is none or minimum changes in particle size for the formulation prepared. In addition, the polydispersity index of the NLC which has a value of 0.22 for all NLC indicates that the formulation has a high tendency to be an unimodal distribution. The increase in particle size with respect to a higher amount of oleic acid in the formulation can be explained from the nature of oleic acid, which has an unsaturated double bond at C9-C10, formed a kink in the structure. As a result, it prevents the formation of compact and rigid NLC with smaller particle size. In addition, higher amount of liquid lipid in the formulation might also attribute to a more disordered crystalline structure which affects the particle size of the NLC (Sangsen *et al.*, 2015).

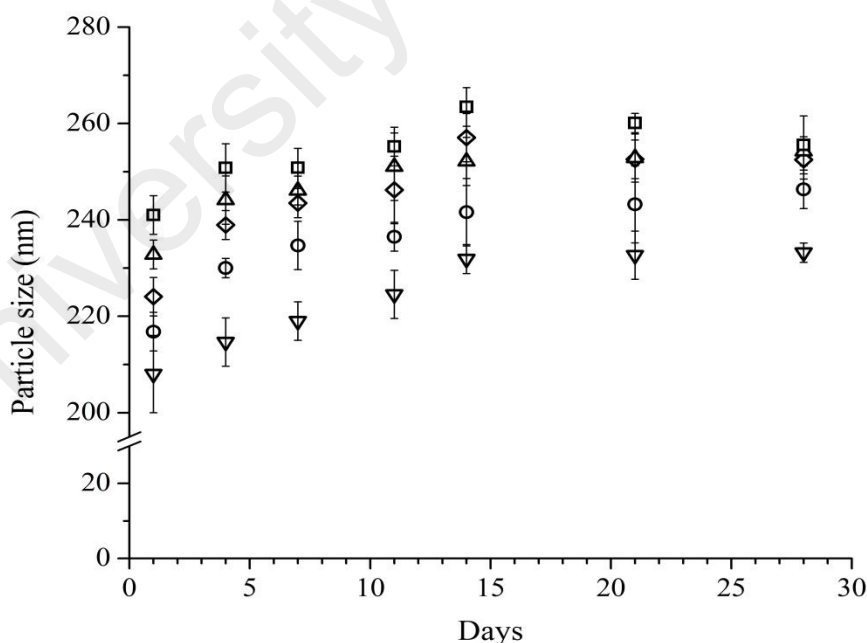


Figure 4.1: Changes in particle size of NLC samples prepared by using different fatty acid compositions for a storage period of 28 days at 30 °C. The symbols ▽ = NLC 1, ○ = NLC 2, ◇ = NLC 3, △ = NLC 4, □ = NLC 5.

Besides particle size, on the first day after preparing the NLC, the zeta potential which fluctuate within -52 ± 3 mV for all NLC formulations showed no significant difference in the zeta potential (Figure 4.2). Nevertheless, the changes in zeta potential of the NLC has a similar pattern with the particle size, whereby it showed an overall a slight increase of zeta potential followed by stable zeta potential around -47 mV after Day 10th. The sample is defined as a stable dispersion if the measured zeta potential has a magnitude of more than positive or less than negative 30 mV. The stability of NLC is enhanced by the degree of electrostatic repulsion between the adjacent NLC particles with similar charged in the solution, thereby preventing the NLC particles from aggregation.

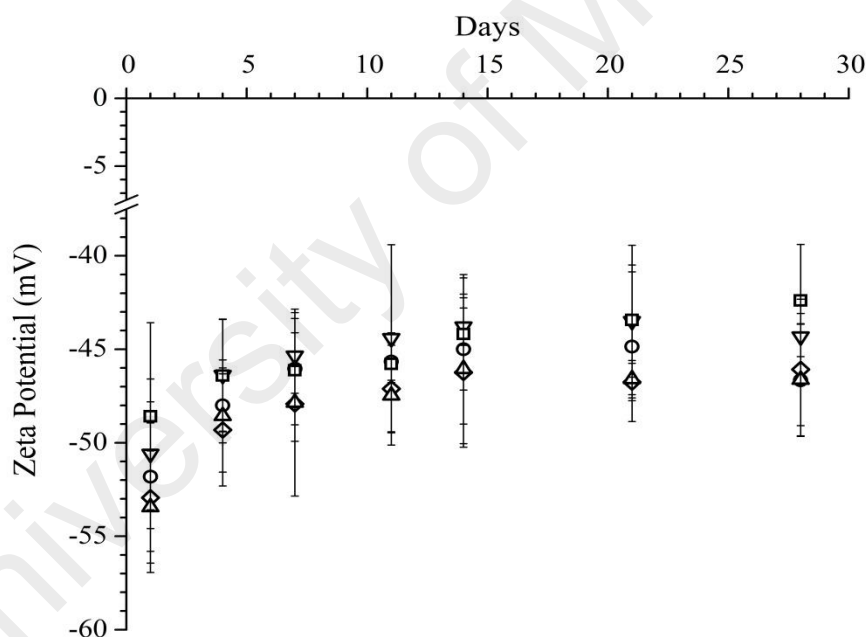


Figure 4.2: Changes in zeta potential of NLC aqueous suspension with varied fatty acid compositions as a function storage time of 28 days at 30 °C. The symbols ▽ = NLC 1, ○ = NLC 2, ◇ = NLC 3, △ = NLC 4, □ = NLC 5.

In addition, DSC analysis was performed on NLC sample in order to determine the heat gain or heat loss for a certain mass of sample with respect to time. The results may be affected by the physical or chemical changes of the sample. Thus, from the thermal parameters of onset temperature, peak temperature and melting enthalpy which obtained

from DSC curve, the structure of the sample can be predicted. The onset temperature is known as the melting point, peak temperature is the temperature at which maximum reaction rate occurs while melting enthalpy is calculated by the integration of the area above or below the baseline. These three parameters are highly affected by the compositions which present in the NLC. As a consequence, those with more liquid lipid have a lower onset temperature, peak temperature and enthalpy changes as compared to those with higher solid lipid content (Figure 4.3 and Table 4.1).

The change in the thermal parameters on the NLC prepared is affected by the amount of oleic acid which made up the particle. Oleic acid, with the melting point of 13-14 °C, tends to melt at room temperature as compared to arachidic acid and erucic acid which have a melting point above 40 °C. On that account, a mixture with less oleic acid is expected to form a more rigid solid structure with higher crystallinity. Apart from that, the peaks of melting temperature broaden while the peak height gradually decreased when the amount of oleic acid was gradually increased. This indicates the loss in the crystallinity of NLC.

Table 4.1: Thermal parameters of fatty acids based NLC

	Onset Temperature, (°C)	Peak Temperature, (°C)	Melting Enthalpy, ΔH (J g ⁻¹)
NLC 1	67.6	71.8	156.7
NLC 2	65.4	70.5	144.9
NLC 3	59.0	67.7	109.4
NLC 4	53.2	65.9	67.82
NLC 5	49.9	62.5	59.51

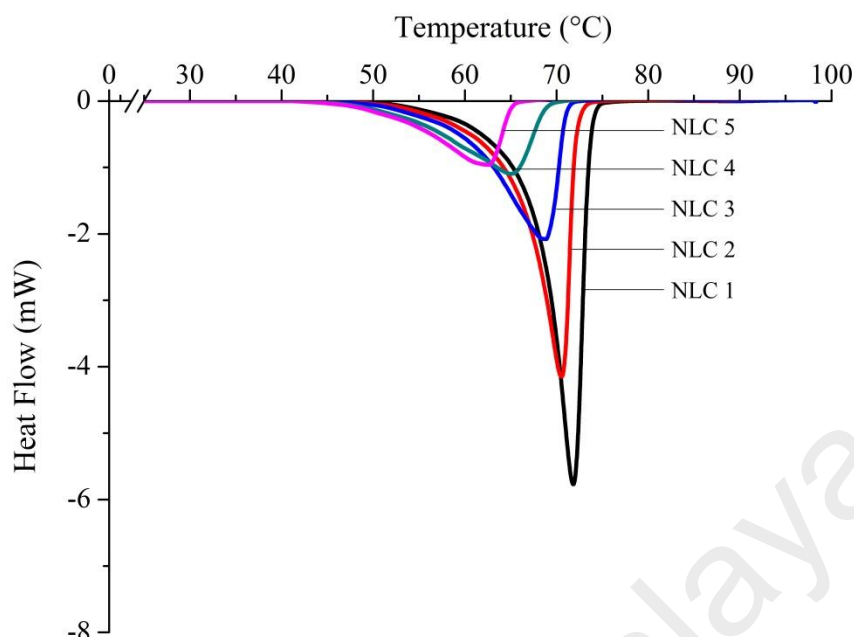


Figure 4.3: Differential scanning calorimetry thermogram of NLC. The experiment was performed from 25 °C to 100 °C at a scan rate of 5 °C per minute.

As a supplementary to the above results, three TEM micrographs as in Figure 4.4 clearly showed the morphology of the NLC prepared. NLC 1 which has the least oleic acid, had particles which were more rounded and uniform in shape as in Figure 4.4(a). However, when about 20% more oleic acid was added into the formulation as compared to NLC 1, the shape of NLC 3 turned to be more elongated in shape as shown in Figure 4.4(b). The shape of NLC 5 was further extended and the overall size is larger than those with lesser oleic acid as in Figure 4.4(c). The size result of TEM is in agreement with the particle size obtained from DLS measurement, whereby the ascending order of particle size is $\text{NLC 1} < \text{NLC 3} < \text{NLC 5}$. NLC with higher liquid lipid content might possess higher active ingredients' encapsulation efficiency. Nevertheless, from the micrographs, it gave us an idea that NLC was unsuitable to have liquid lipid more than 30% in the lipid components as the sample might form oil droplet apart from NLC.

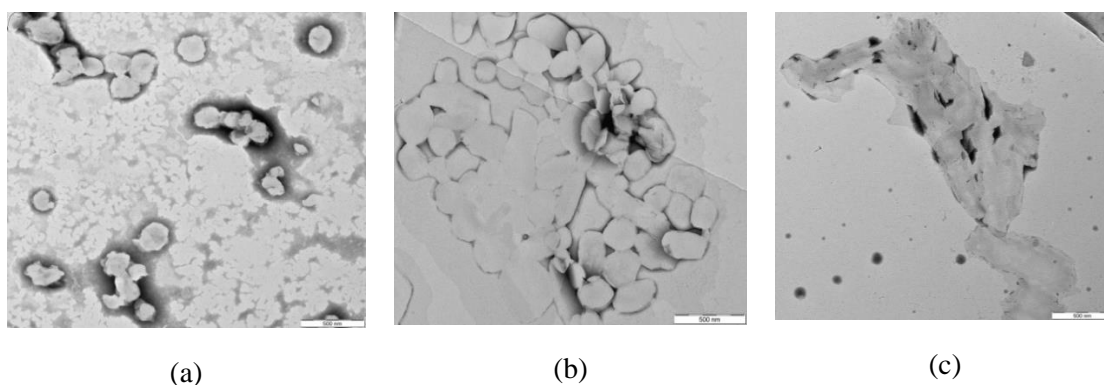


Figure 4.4: TEM micrographs of NLC where (a) is NLC 1, (b) is NLC 3, and (c) is NLC 5. All micrographs were taken at $10,000\times$ magnification using Carl Zeiss LIBRA[®] 120.

As a summary, the evaluation of physical characteristics for NLC indicated that NLC with different fatty acids as lipid phase was successfully prepared. Among the NLC, NLC 3 exhibit the most desired properties of the nanoparticle, whereby the size is around 250 nm with a zeta potential of less than -45 mV. In addition, the TEM micrographs of NLC 3 showed to have an acceptable shape with no oil droplet formed as compared to those with higher oleic acid in the compositions. Besides that, thermal profile of NLC 3 with lower onset temperature than those with higher solid lipid, indicated that NLC 3 requires lesser energy for deformation of the NLC. This could enhance the release rate of active ingredients encapsulated NLC. Hence, NLC 3 was being selected for the encapsulation of active ingredients and prediction of release profile.

4.1.2 Characterization of Liposome

Liposomes prepared by using different types of C18 unsaturated fatty acids, namely oleic acid (C18:1), linoleic acid (C18:2), and linolenic acid (C18:3), were evaluated for their physical characteristics which include CVC by employing surface tensiometer, particle size and zeta potential by using zetasizer, followed by morphology with the use of TEM.

The CVC is the minimum concentration where vesicles formed. The surface tension of the solution was shown to decrease linearly as a function of fatty acid concentration until it reached the inflection point, followed by a plateau, even when the concentration of fatty acid was increased (Figure 4.5). This phenomenon can be explained by the Gibbs adsorption isotherm of the monolayer at the air-water interface. When the adsorption of free fatty acids at the air-water interface gradually increased, a dramatic reduction in surface tension was observed with small changes in the bulk phase concentration. At the point near the CVC, the interface was at its maximum surface coverage, thus promoting aggregation of the fatty acids in the solution to form vesicles in order to reduce the high free energy. This was followed by a plateau in the surface tension when the surface access concentration was at its optimum (Eastoe, 2005; Treiner, 2006).

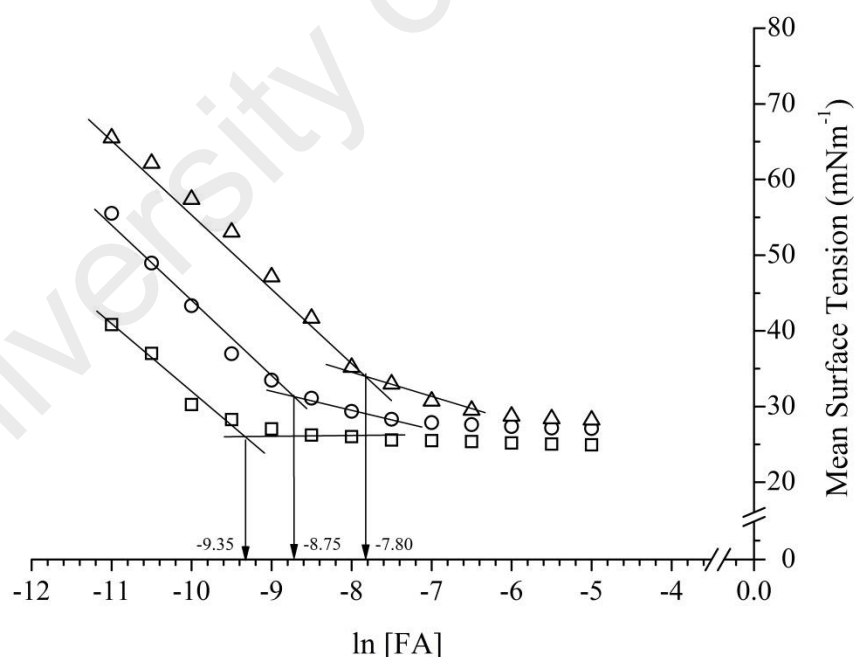


Figure 4.5: Surface tension of fatty acids liposome solution with different concentrations evaluated at pH 8.6 with a temperature of 30 °C. \square = oleic acid, \circ = linoleic acid, Δ = linolenic acid. The arrow indicates the critical vesicular concentration of fatty acid liposomes.

From the CVC value estimated from the surface tension profile, it was observed that the prepared fatty acid liposomes had an increasing trend in their CVC values with respect to the degree of unsaturation in the fatty acids. Oleic acid, with only one double bond, had a CVC of 0.09 mM. Linoleic acid and linolenic acid, with additional one and two double bonds as compared to oleic acids, had CVC values that increased nearly twice and four folds to 0.16 mM and 0.41 mM respectively. This can be explained by the degree of unsaturation in the hydrocarbon chain of the fatty acid, which affects the polarity of the fatty acids. The effect of unsaturation towards the polarity of the hydrocarbon chain of fatty acids was shown by Nikolova-Damyanova (2009), whereby those with a higher degree of unsaturation were eluted at an earlier retention time in silver ion high performance liquid chromatography (HPLC). The increase in the polarity of the unsaturated hydrocarbon chain was due to the delocalization of π -electrons (Folmer, 2003). By reason of that, oleic acid, which has the least degree of unsaturation, is more hydrophobic as compared to linoleic acid and linolenic acid, thereby favouring the formation of vesicles through hydrophobic interaction, thus lowering the CVC value. A similar trend was also reported previously (Teo *et al.*, 2011), which showed that the CVC value of a fatty acid is bond unsaturation-dependent. Despite that, the CVC values at pH 8.6 showed a lower CVC value compared to pH 9. The phenomenon is explained through the relationship between the pKa of the material and the pH of the prepared solution. Oleic acid, linoleic acid and linolenic acid have pKa of 9.85, 9.24 and 8.28 respectively (Kanicky and Shah, 2002). At these pKa values, half of the fatty acid is in ionized form, while the other half is in unionized form. Hence at a pH that is higher than the pKa value, most of the fatty acids tend to be in ionized form as compared to those with a lower pH. That being the case, at pH 8.6, the amount of unionized fatty acid is higher as compared to those at pH 9.0, thereby favours the formation of vesicles due to

the ionic pair interaction between the ionized and non-ionized forms of fatty acids via lateral hydrogen bonding at lower pH (Apel *et al.*, 2002; Fameau *et al.*, 2014).

Aside from CVC, particle size and zeta potential are also important parameters to evaluate the prepared liposome. The particle size of liposomes has been shown to be influenced by the degree of unsaturation of fatty acids, whereby those with more double bonds have a smaller particle size, as tabulated in Table 4.2.

Table 4.2: Particle size, polydispersity index and zeta potential of fatty acid liposome and their stability for two weeks at 30 °C

Time (Day)	Particle Size (nm)			Polydispersity Index			Zeta Potential (mV)		
	1 st	7 th	14 th	1 st	7 th	14 th	1 st	7 th	14 th
Oleic acid	101.4	102.7	102.8	0.28	0.28	0.30	-104	-101	-105
	(1.2)	(1.8)	(2.6)	(0.02)	(0.03)	(0.02)	(3.5)	(2.5)	(3.8)
Linoleic acid	87.15	97.3	104.7	0.31	0.32	0.27	-101	-98.2	-94.7
	(3.1)	(2.5)	(1.7)	(0.03)	(0.03)	(0.02)	(2.8)	(3.5)	(2.1)
Linolenic acid	77.28	100.6	109.4	0.42	0.37	0.30	-99	-102	-97.5
	(2.3)	(2.8)	(2.1)	(0.03)	(0.02)	(0.02)	(4.3)	(2.6)	(3.2)

The particle size, polydispersity index and zeta potential of fatty acid liposome is depending on their degree of unsaturation. Oleic acid liposome has a better stability as compared to linoleic and linolenic acid liposome. Upon two weeks storage, all the liposome has almost the same physical properties. The numbers in bracket indicate the standard deviation of the measurement obtained.

This phenomenon is due to the fluidity of the fatty acid molecules in the presence of the double bonds. Linolenic acid, with three double bonds, has a higher bending flexibility could form a smaller liposome as compared to the other two fatty acids (Ishii and Nii, 2014). However, oleic acid liposome was shown to be more stable as compared to the other fatty acids as there is apparently no change in the particle size and zeta potential whereas linoleic and linolenic acid liposomes have shown an increase in particle size which come to marginal change after Day 7th due to the destabilization of high fluidity membrane. The hydrodynamic radius of the particles increased as a result of flocculation of the liposome particles. The polydispersity index of all the liposomes was shown to be between 0.25 and 0.45, indicating a broad range of particle distribution

among the vesicles. In addition, there is no drastic change in zeta potential of all the fatty acid liposomes after two weeks of storage. This was attributed by buffering effect between the buffer and electrolytes present in the solution, which might minimize the fluctuation of the zeta potential changes.

The morphology of prepared liposome appeared to be rounded in shape but polydispersed in size when observed under TEM. On average, the diameter of the observed micrographs is slightly larger than DLS measurements, indicating that there might be structural collapse of the sample at a pressure of 3×10^{-5} Pa in the TEM chamber. Among the three samples, sample prepared by using oleic acid as in Figure 4.6(a), showed to be rounded in shape with well-defined boundary than those prepared by linoleic acid and linolenic acid which presented in Figure 4.6(b) and Figure 4.6(c) respectively. Additionally, more unsaturation on the fatty acid chain gave a broader greyish shadow at the edge of the prepared samples. This suggested that oleic acid which presumably with better rigidity could stay intact as compared to the other two samples which smeared when exposed to vacuum pressure in TEM. Nevertheless, no aggregation was observed in this system.

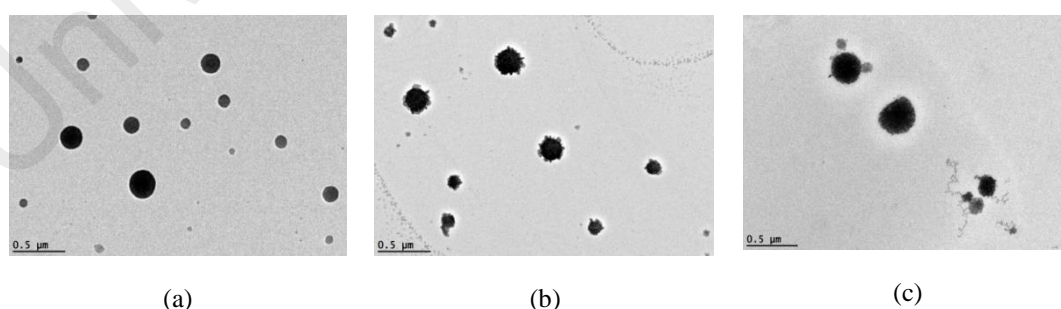


Figure 4.6: TEM micrographs of liposome where (a) represents oleic acid, (b) represents linoleic acid, and (c) represents linolenic acid liposome. For those micrographs, all were taken at $8,000 \times$ magnification by using JOEL JEM-2100F.

As a summary, the physical characteristics of oleic acid liposome was shown to be superior than the other two types of fatty acid liposomes by having a particle size around 100 nm and high magnitude of zeta potential. Additionally, the TEM micrographs further confirmed that oleic acid liposomes are more rounded in shape. In addition to that, oleic acid which has lower CVC value, would ease the assembly and formation of vesicle in the bulk phase. Thus, oleic acid liposome was selected for the encapsulation of active ingredients and the release profile was determined.

4.1.3 Characterization of water-in-oil microemulsion

Water-in-oil microemulsion was prepared by mixing different compositions of water, olive oil, and mixed surfactants. At the initial stage, phase diagram was plotted to determine the region where the microemulsion could be found, followed by physical properties evaluations which included pH, conductivity, particle size, viscosity and morphology.

The ternary phase diagram showed that the prepared water-in-oil microemulsion, formed a region at low water content in the presence of surfactant ranging between 20% and 90% (w/w) as shown in Figure 4.7. When the samples were prepared using Span 80 with Tween 85 mixed surfactant, the microemulsion phase was found within a narrower region between 20% and 50% as shown in Figure 4.7(d). The region was found broader and ranging between 30% and 90% when mixed surfactant of Span 80 and Tween 40, 60 or 80 were used as shown in Figure 4.7(a), Figure 4.7(b) and Figure 4.7(c) respectively. The result was found similar to the work done by Syed and Peh (2014) whereby microemulsion forms at higher surfactant region. This is probably due to the effect of hydrophilic and lipophilic properties of the surfactant. Despite the fact that the Tween surfactants have a similar headgroup, Tween 85 is more hydrophobic than the

other three Tween surfactants. This is attributed by the presence of three lipophilic tails in Tween 85 compared to the other three Tween surfactants which has only one lipophilic tail. Thus, the microemulsion stabilized by Span 80 and Tween 85 surfactants is restricted to a smaller region as compared to the other microemulsions. As a result, surfactant range between 30% and 50% for mixed surfactant compositions is the most suitable composition range that appears to fit all the surfactant combinations. In order to accommodate a higher amount of water solubilised active ingredients, a higher water phase is crucial when selecting the formulation. For that reason, a mixture of 40% surfactant, 56% olive oil and 4% deionized water was selected for further characterization and discussion.

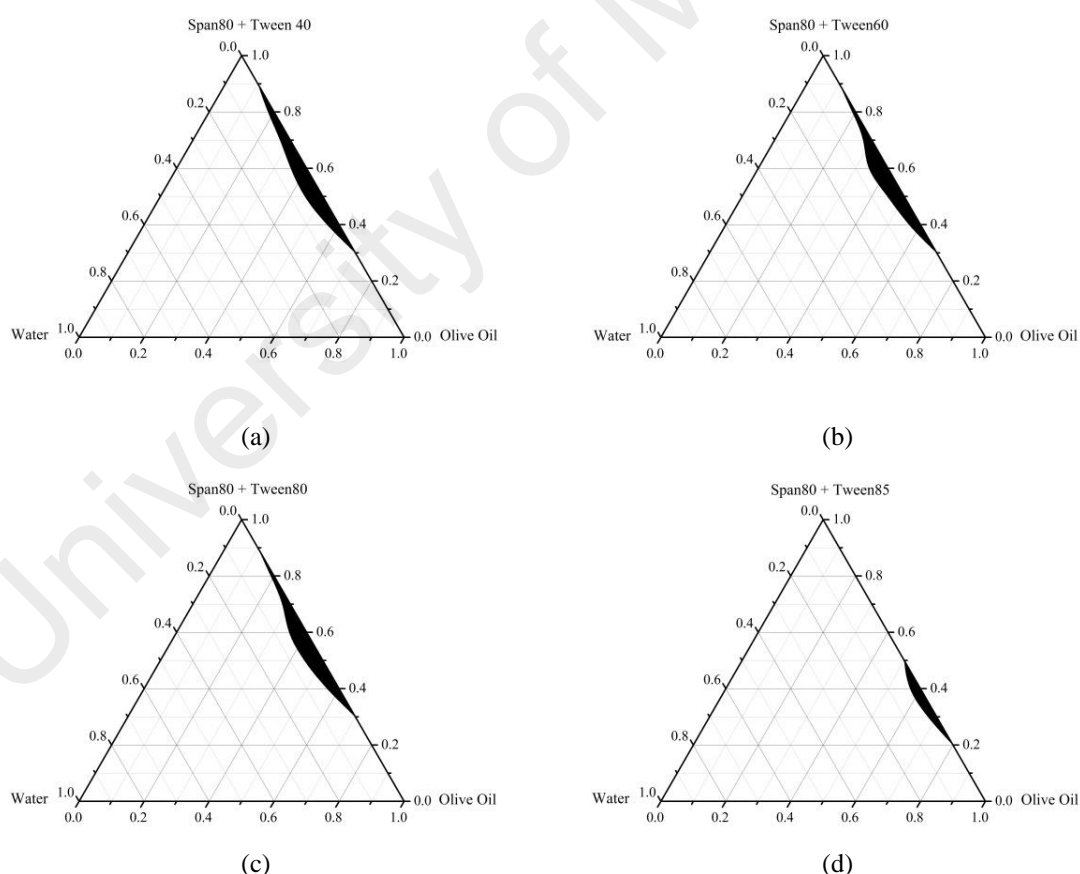


Figure 4.7: Ternary phase diagram of microemulsion prepared by olive oil, water and mixed surfactants of Span 80 with various types of Tween surfactants, namely (a) Tween 40, (b) Tween 60, (c) Tween 80 and (d) Tween 85. The shadowed region indicates the presence of microemulsion.

A formulation with a suitable pH range is crucial as it will affect the efficacy of active ingredients' delivery and might cause irritation to the skin if the pH is unsuitable. In this perspective, the most preferred condition for topical applications would be a neutral pH. The results showed that ST85 and ST80 have the lowest and highest pH of 6.25 and 7.36 respectively among those microemulsions while both ST40 and ST60 have a pH close to 7 (Table 4.3). The variation in pH obtained is plausibly attributed to the hydroxyl ions adsorption at the non-ionic polar headgroup of the surfactants, which arisen from the interaction of hydrogen bond at the ether-oxygen of the polyoxyethylene chain, hence resulting in an overall negatively charged surface (Liu *et al.*, 2006; Marinova *et al.*, 1996). Tween 85 which has three lipophilic tails is more hydrophobic attributed by the shielding of the polyoxyethylene chain. Thenceforth the adsorption of hydroxyl ions on Tween 85 is less preferable (Hsu and Nacu, 2003) as compared to the other three Tween surfactants. As a consequence, the magnitude of pH reduction in ST85 is comparatively higher as compared to the other three microemulsions. Additionally, Tween 40, Tween 60 and Tween 80, which all consist of single aliphatic tail, have hydroxyl value around 90-105, 81-96 and 65-80, respectively, indicate the amount of free sorbitol-derived cyclic ethers present in the surfactants. If the hydroxyl value of the sample is higher, the acid value is also comparatively higher. This is in agreement with the results, whereby the pH is in the order of ST40 < ST60 < ST80 (Rowe *et al.*, 2009; Wakita *et al.*, 2014). Hence, ST40, ST60 and ST80 are more preferable for topical applications. The results from the conductivity analysis of the microemulsions showed that conductivity values are mostly less than 0.05 mS cm^{-1} , which indicate that the microemulsions formed are all water-in-oil microemulsions. The microemulsion that stabilized by a non-ionic surfactant, has a negligible charge, thus prevents or slows down the migration of droplets, which results in low conductivity (Bumajdad and Eastoe, 2004). In addition, it has also been reported that a formulation

which is made up of deionized water and olive oil, other than the non-ionic surfactant, also resisted the electrical conductivity (Anjali *et al.*, 2010).

Table 4.3: Physical properties of water-in-oil microemulsions prepared with different types of Tween surfactants measured at 30 °C

	pH	Conductivity (mS cm ⁻¹)	Particle Size (nm)
ST40	6.81 ± 0.05	< 0.05	29.98 ± 1.0
ST60	6.99 ± 0.03	< 0.05	30.81 ± 1.8
ST80	7.36 ± 0.06	< 0.05	22.42 ± 0.9
ST85	6.25 ± 0.06	<< 0.05	16.86 ± 0.7

The particle size of the water-in-oil microemulsion is directly determined by the packing parameter of the surfactants. Since all four microemulsions were being selected at certain compositions, they have similar compositions in their formulations, except for Tween surfactants. Therefore, the Tween series is the main contributor for a different packing parameter, which will be further discussed on their effect towards the changes of the particle size. Tween surfactants consist of hydrophilic polyethoxylated sorbitan headgroups, will orientate inwards to the aqueous phase, and hydrophobic fatty acid tail facing outwards to the oil phase during the formation of the water-in-oil microemulsion. Since all Tween surfactants have a similar headgroup but a different aliphatic hydrocarbon tail, the particle size of the microemulsion depended on the packing parameter of the surfactant's aliphatic hydrocarbon tail. ST40 (C16:0) and ST60 (C18:0) which have saturated fatty acid tails, give a marginal increase in particle size when the hydrocarbon chain length increases. When unsaturated Tween 80 (ST80, C18:1) was introduced into the system, the particle size was reduced to around 23 nm, as compared to ST60 which has a particle size around 31 nm. ST80 has the same hydrocarbon chain length as ST60 but it is different in the degree of saturation, whereby the former has one double bond at C9-C10. The double bond in Tween 80 gives a certain degree of bending on the aliphatic hydrocarbon tail, thus changes the packing parameter of the surfactant

from a cone shape to rod shape. The rod shape surfactant favours the water-in-oil microemulsion as compared to the cone shape. When the aliphatic hydrocarbon tail was increased to three unsaturated tails (ST85, C₁₈:1), the particle size was further reduced to around 17 nm. The reduction in particle size is attributed to those three unsaturated hydrocarbon tails of Tween 85, aids the formation of inverted cone shape which is the most preferable shape for water-in-oil microemulsion. Apart from the aliphatic hydrocarbon tails, HLB value of surfactants would also affect the particle size of microemulsion. The surfactant with a lower HLB (ST85) value tends to possess a less hydrated headgroup as compared to the one with a higher HLB value. The headgroup which does not swell significantly can produce a more compact arrangement and gives a smaller particle size. Besides that, the particle size result is in correlation with viscosity, whereby those with small particle sizes have low viscosity. This is true as smaller particles will flow much easier as compared to those larger particles when shearing is applied. Microemulsions with polydispersity index around 0.15 suggest that the microemulsion is uniform in size.

On the other hand, the viscosity of a microemulsion is being affected by the types and concentrations of surfactants, oils, water, co-solvents, ionic strength, pH and temperature of the formulation (Lawrence and Rees, 2000). In general application, microemulsion with low viscosity is easy to apply on the skin. Nevertheless, its high fluidity makes it difficult to be controlled during application. Microemulsion with a higher viscosity is the most preferred condition for application in this system. Most microemulsion's studies exhibited Newtonian fluid because a change in the shear rate has none or minimal effects on their viscosity and shear stress (Figure 4.8). ST85 has the lowest apparent viscosity of 146.2 mPa s as compared to the other three microemulsions which have the apparent viscosity of around 200 mPa s at a shearing

rate of 50 s^{-1} . This is due to the transition of the packing parameters of the surfactant, which favours the formation of water-in-oil microemulsions in ST85 as compared to the other surfactants (Mishra *et al.*, 2000), thus ST85 has a lower viscosity.

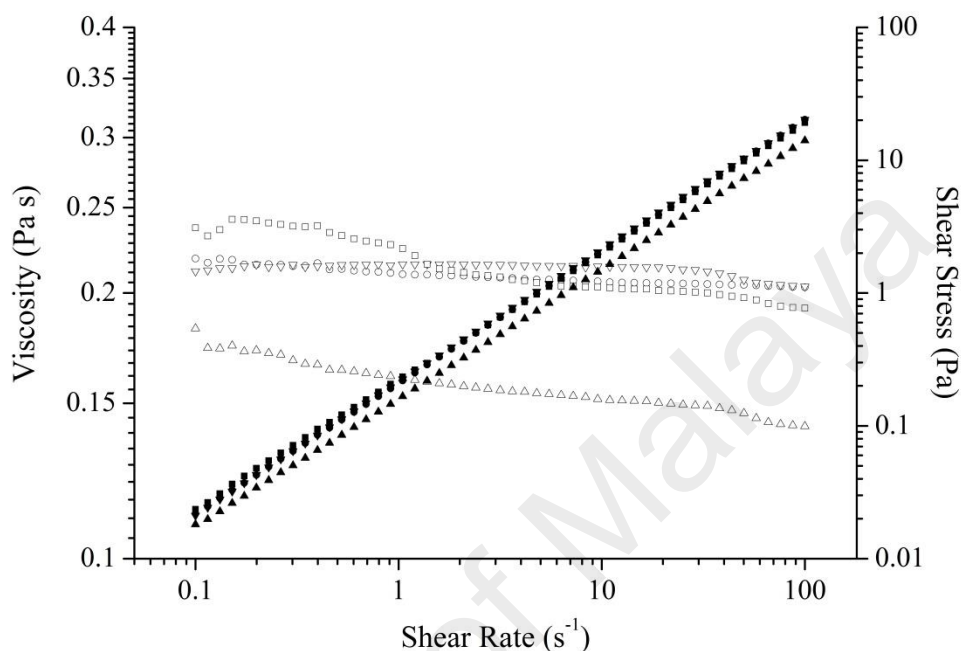


Figure 4.8: Rheological behaviour of microemulsions prepared with different types of Tween surfactants in a shear rate of $0.1 - 100 \text{ s}^{-1}$. The symbols \square = ST40, \circ = ST60, ∇ = ST80, and \triangle = ST85 where opened symbols represent viscosity while solid symbols represent shear stress.

The observation of TEM micrographs with $10,000 \times$ and $20,000 \times$ magnifications showed that microemulsion appeared to be rounded in shape and small in particle size as in Figure 4.9(a) and Figure 4.9(b) respectively. From the analysis, the averaged particle size of the sample, i.e. around 30 nm, is in agreement with the results obtained from the DLS. In spite of that, the micrographs of the TEM showed that the particles are polydispersed as there are a few particles which have a larger droplet size of nearly 60 nm. This could be attributed to the fusion of oil droplet during the drying process or as a consequence of the droplet collapsing at a very low pressure of 10^{-8} mbar in the TEM chamber. Nevertheless, no particle flocculation was being observed in this system.

From the results attained, ST80 will be a more suitable candidate to encapsulate active ingredients as compared to other prepared microemulsions. This is because it has a better pH and viscosity than ST85 and smaller particle size than ST40 and ST60. That being so, active ingredients encapsulated ST80 was subjected to a further analysis for stability evaluation and *in vitro* release of active ingredients from ST80.

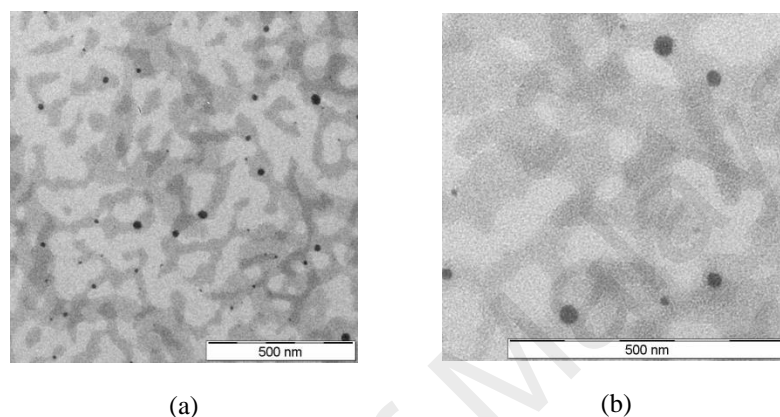


Figure 4.9: TEM micrographs of ST80 microemulsion taken at different magnifications of (a) 10,000 \times and (b) 20,000 \times magnification. In this visualization, Carl Zeiss LIBRA[®] 120 is being employed.

4.1.4 Characterization of κ -carrageenan-chitosan nanoparticle

The κ -carrageenan-chitosan nanoparticle was synthesized by polyelectrolyte complexation using different ratio of 1% chitosan and 1% κ -carrageenan (v/v) to produce κ -carrageenan-chitosan nanoparticle. The polyelectrolyte complexation is achieved by electrostatic interaction between positively charged chitosan amino groups and negatively charged κ -carrageenan sulphate groups that present in the solution. The κ -carrageenan-chitosan nanoparticle was determined for its size, zeta potential and morphology in aqueous suspension whereas the yield, swelling percentage, and FTIR spectrum was being evaluated in the dried form.

The particle size analysis showed that the κ -carrageenan-chitosan nanoparticle synthesized is pH dependent as presented in Figure 4.10. Regardless of the pH during preparation, the κ -carrageenan-chitosan nanoparticle was shown to have the smallest average particle size around 400 nm when the mass ratio of κ -carrageenan:chitosan is in 1:1. Additionally, when the amount of κ -carrageenan in the mixture was gradually increased, the particle size will decrease until it reached the equal mass ratio and subsequently followed by an increase in particle size.

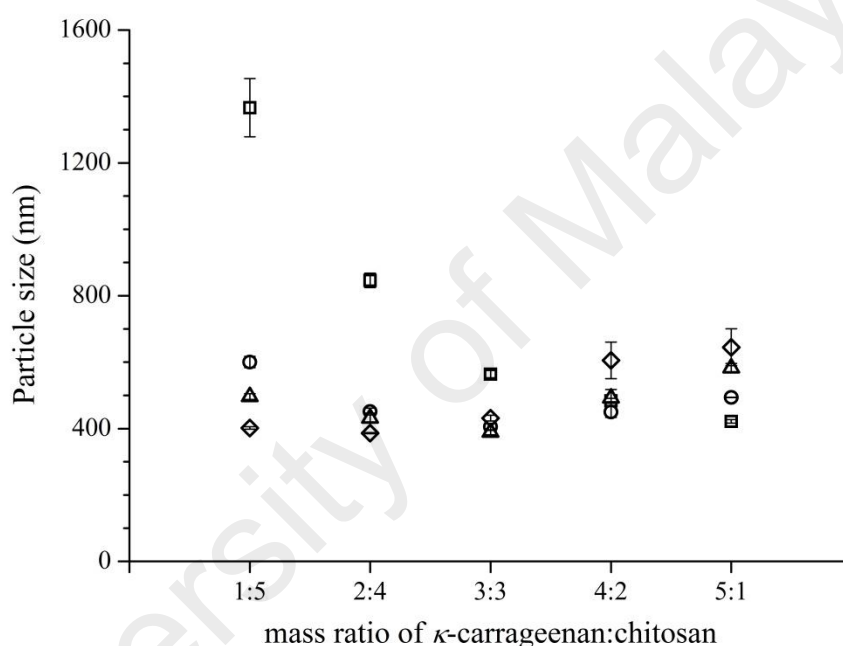


Figure 4.10: Particle size of κ -carrageenan-chitosan nanoparticle prepared at 30 °C using pre-dissolved 1% κ -carrageenan and 1% chitosan at different mass ratios in a pH ranged from 3 to 6. The symbols \square = pH 3, \circ = pH 4, \triangle = pH 5, \diamond = pH 6.

This phenomenon occurs as we presumed that κ -carrageenan and chitosan were in 1:1 stoichiometry charge ratio. As a consequence, one sulphate group from the κ -carrageenan will be ionically complexed with amino group from the chitosan (Figure 4.11).

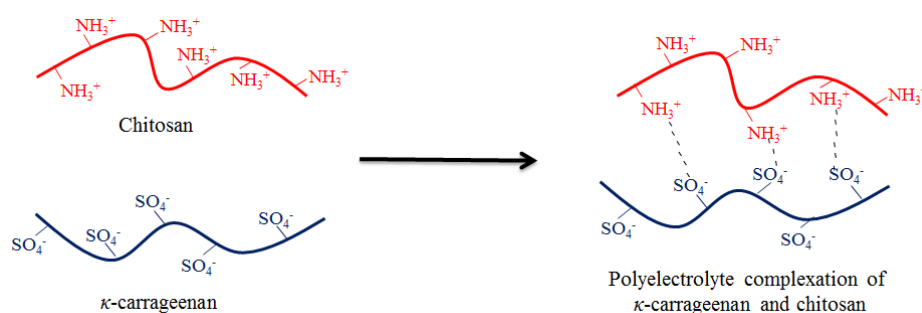


Figure 4.11: Schematic diagram of polyelectrolyte complexation for κ -carrageenan and chitosan. The positively charged amino group (red) of chitosan will react with negatively charged sulphate group (blue) of κ -carrageenan.

When the amount of κ -carrageenan in the formulation was gradually increased with a decreased in the amount of chitosan, κ -carrageenan could further react with positively charged chitosan, to form a more compact structure with smaller particle size. Further increase in the amount of κ -carrageenan after the maximum complexation with chitosan was achieved, would reverse the scenario due to the presence of excess anionic charges in the solution. The negative charge will neutralize the positive charge of the chitosan, thus opposite charged interaction will eliminate the electrostatic repulsion and lead to precipitation of the κ -carrageenan-chitosan nanoparticle (Long *et al.*, 2015). This was supported by the zeta potential measurement of the κ -carrageenan-chitosan nanoparticle, whereby an increase in κ -carrageenan in the solution would cause a decrease in the net zeta potential of the formulation (Figure 4.12).

As a consequence, in the mixture where κ -carrageenan is in highly excess, the net charge becomes negative, indicates that κ -carrageenan dominate in the solution (Rodrigues *et al.*, 2012). Apart from the properties of materials, the changes in pH would also affect the zeta potential of the prepared κ -carrageenan-chitosan nanoparticle. When the pH was being increased from pH 3 to pH 6, there is a drop in the zeta potential to a more negative magnitude. This is attributed by the present of more

alkalinity in the solution when the pH is increasing from pH 3 to pH 6, the particles tend to acquire more negative charge.

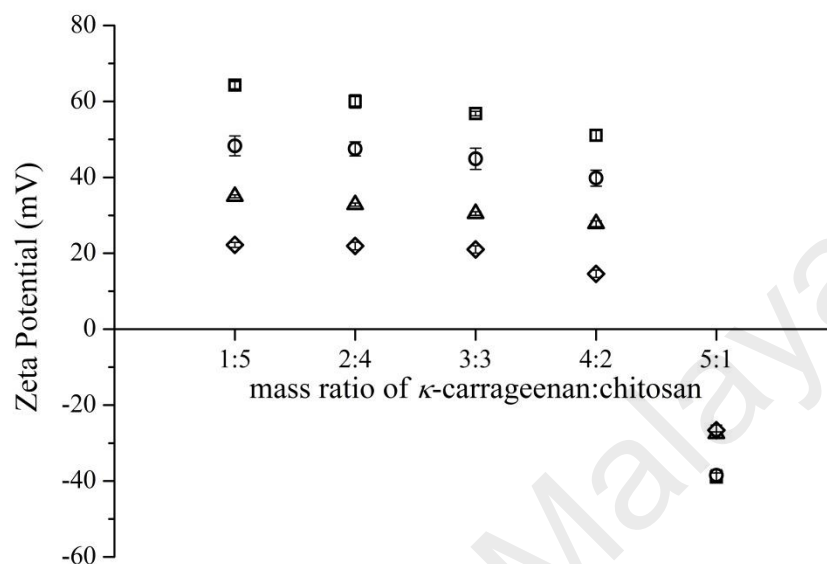


Figure 4.12: Zeta potential of κ -carrageenan-chitosan nanoparticle prepared at 30 °C using pre-dissolved 1% κ -carrageenan and 1% chitosan at different mass ratios in a pH ranged from 3 to 6. The symbols \square = pH 3, \circ = pH 4, Δ = pH 5, \diamond = pH 6.

After the particle size and zeta potential evaluation, the κ -carrageenan-chitosan nanoparticle prepared was centrifuged and dried under vacuum oven to produce thin film for the evaluation of percentage yield, swelling percentage and FTIR analysis.

The percentage yield of the κ -carrageenan-chitosan nanoparticle was highly depending on the mass ratio of κ -carrageenan:chitosan present in the solution (Table 4.4). Changes in pH do significantly affect the percentage yield for those dissolved in pH 3 to pH 5. Nevertheless, pH 6 showed a large magnitude of yield's increment, which is attributed to the precipitation of undissolved chitosan in the solution during centrifugation.

Table 4.4: Percentage yield of dried κ -carrageenan-chitosan nanoparticle prepared at different pH

κ -carrageenan:chitosan	Yield of dried κ -carrageenan-chitosan nanoparticle (%)			
	pH 3	pH 4	pH 5	pH 6
1:5	8.61 \pm 1.0	8.23 \pm 0.8	8.08 \pm 0.7	37.67 \pm 0.8
2:4	21.68 \pm 1.1	20.22 \pm 1.4	21.02 \pm 2.0	45.02 \pm 1.4
3:3	33.30 \pm 1.7	35.30 \pm 1.3	37.30 \pm 2.0	65.34 \pm 1.3
4:2	70.59 \pm 1.9	78.23 \pm 1.0	80.23 \pm 1.6	82.63 \pm 1.0
5:1	49.67 \pm 1.4	53.95 \pm 1.6	55.95 \pm 1.8	54.65 \pm 2.0

In the range of pH from 3 to 5 compared to pH 6, the percentage yield of the κ -carrageenan-chitosan nanoparticle was increased by nearly two folds whenever the ratio of κ -carrageenan:chitosan was varied from 1:5 to 4:2. Further increase of κ -carrageenan causes the decrease in the percentage yield of κ -carrageenan-chitosan nanoparticle. The plausible explanation of this is that when the mass ratio of the κ -carrageenan was gradually increased, there were more κ -carrageenan which can complex with the chitosan presents in the solution until it reaches the maximum complexation at the ratio of 4:2. Nevertheless, when the ratio was further varied to 5:1, κ -carrageenan dominates the solution. The yield was decreased by the fact that there were not enough of chitosan which can complex with the κ -carrageenan present (Grenha *et al.*, 2010).

On the other hand, when the dried κ -carrageenan-chitosan nanoparticle was swelled in pH 7.4 phosphate buffer solution, it was observed that the swelling of the κ -carrageenan-chitosan nanoparticle is pH dependent (Table 4.5). κ -carrageenan-chitosan nanoparticle swelled nearly 120% to 200%, depending on the mass ratio of κ -carrageenan:chitosan. The κ -carrageenan-chitosan nanoparticle has a higher magnitude of swelling when it was initially prepared at a lower pH. This is attributed by the huge different in pH of the prepared κ -carrageenan-chitosan nanoparticle and phosphate buffer. This will further dissociate the interaction of amino group and sulphate group, which leads to greater swelling at a lower pH (Carneiro *et al.*, 2013; Mahdavinia *et al.*,

2015). Other than that, κ -carrageenan which has greater swelling ability than chitosan in aqueous, gives rise to the highest swelling percentage at κ -carrageenan:chitosan mass ratio of 5:1.

Table 4.5: Swelling percentage of dried κ -carrageenan-chitosan nanoparticle in pH 7.4 phosphate buffer solution

κ -carrageenan:chitosan	Swelling percentage (%)			
	pH 3	pH 4	pH 5	pH 6
1:5	163.63 \pm 7.4	151.80 \pm 3.6	140.08 \pm 8.2	122.12 \pm 2.4
2:4	170.34 \pm 4.3	149.65 \pm 4.4	141.02 \pm 9.4	127.40 \pm 4.7
3:3	174.32 \pm 3.2	152.34 \pm 3.6	144.30 \pm 6.5	126.53 \pm 3.1
4:2	183.65 \pm 5.7	165.56 \pm 8.9	157.23 \pm 6.5	137.81 \pm 8.1
5:1	191.12 \pm 5.4	200.49 \pm 5.9	195.69 \pm 5.2	190.65 \pm 4.9

The FTIR analysis is used to identify the presence or absence of functional group in a sample when two or more substances are being complexed or dissociated. In order to present the complexation of κ -carrageenan-chitosan nanoparticle, FTIR spectra was scanned within the wavelength of 4000-450 cm^{-1} for κ -carrageenan, chitosan, mixture of κ -carrageenan with chitosan powder and dried κ -carrageenan-chitosan nanoparticle were displayed as in Figure 4.13.

The FTIR spectrum of chitosan powder as in Figure 4.13(a) showed three typical peaks at 1650 cm^{-1} , 1593 cm^{-1} and 1062 cm^{-1} , which indicate the presence of amide I, amide II and glycosidic bond respectively. Amide I band is due to C=O stretching and vibration while amide II is due to the stretching vibration in combination with N-H bending. On the other hand, the FTIR spectrum of κ -carrageenan powder as in Figure 4.13(b) with four important peaks at 1229 cm^{-1} , 1064 cm^{-1} , 921 cm^{-1} and 845 cm^{-1} , respectively indicate sulphate group, glycosidic bond, 3,6-anhydrogalactose and galactose-4-sulfate. In order to prove that both chitosan and κ -carrageenan were required to be in ionized solution form for complexation, the chitosan powder and κ -carrageenan powder were

mixed together at 1:1 mass ratio to identify the FTIR spectrum as in Figure 4.13(c). As a result, the FTIR spectrum showed a similar pattern with κ -carrageenan, indicating no complexation occurs. A new absorption band at 1548 cm^{-1} indicating the presence of NH_3^+ group and slight shift of the spectrum as in Figure 4.13(d), showed a possible formation of nanoparticle as a result of protonation and hydrogen bonding (Grenha *et al.*, 2010; Li *et al.*, 2013).

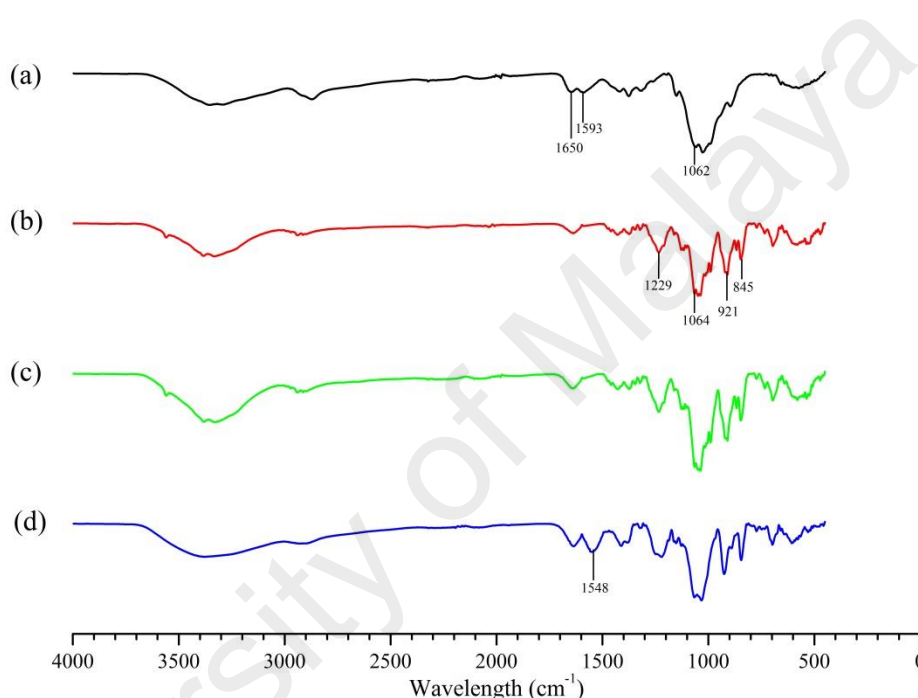


Figure 4.13: FTIR spectrum of (a) chitosan powder, (b) κ -carrageenan powder, (c) mixture of 1:1 κ -carrageenan with chitosan powder and (d) κ -carrageenan-chitosan nanoparticle at a wavelength of $4000\text{--}450\text{ cm}^{-1}$.

As a supplement, the morphology of the prepared κ -carrageenan-chitosan nanoparticle with $30,000\times$ and $120,000\times$ magnifications were shown to have a solid and compact structure which is rounded to irregular in shape as in Figure 4.14 (a) and Figure 4.14(b) respectively. The particle size of the sample was shown to be very much smaller than the DLS measurements as a result of an average value was obtained based on the intensity of particle. Large particles give higher intensity even though they have the same amount of particles as the small particles. In DLS measurement, when the measurement was as the number of particles calculated, the distribution of κ -

carrageenan-chitosan nanoparticle majorly falls below 100 nm. This corresponds to the result of TEM and where the size of particle is less than 50 nm.

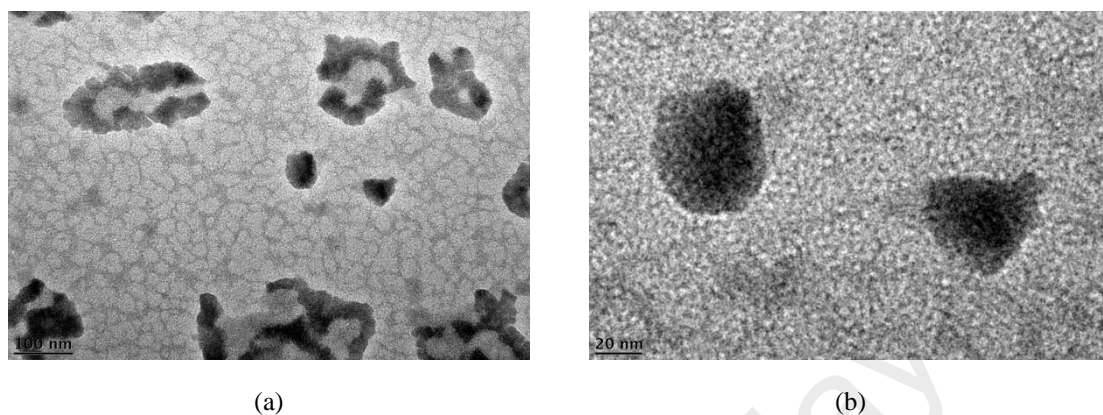


Figure 4.14: Morphology of κ -carrageenan-chitosan nanoparticle prepared at 1:1 mass ratio of κ -carrageenan and chitosan. The micrographs were taken at (a) 30,000 \times and (b) 120,000 \times magnification by using JOEL JEM-2100F.

The physical evaluation revealed that κ -carrageenan-chitosan nanoparticle was successfully produced by having a new absorption band at 1548 cm^{-1} . Among the prepared combinations in pH 3 to 6, all κ -carrageenan and chitosan with a mass ratio of 1:1 has the smallest particle size. Despite that, κ -carrageenan-chitosan nanoparticle prepared in pH 4 was being selected. This was because the κ -carrageenan-chitosan nanoparticle has a similar particle size of pH 5 of around 400 nm yet it has higher magnitude of zeta potential and better swelling percentage as compared to the one in pH 5.

4.2 Loading and encapsulation efficiency of active ingredients

For each type of delivery carrier, formulation with the most desired physicochemical properties was selected for encapsulation or solubilisation of active ingredients. Both the loading efficiency and encapsulation efficiency of active ingredients with varied water solubility in delivery carrier were assessed. The changes in the physicochemical properties of active ingredients encapsulated delivery carrier were further discussed.

4.2.1 Encapsulated NLC

The loading efficiency of active ingredients in NLC corresponds to the increment of the amount of active ingredient until it reaches the optimum loading amount (Figure 4.15). Lidocaine, which is slightly soluble in water has the highest loading efficiency in NLC as compared to caffeine and ascorbic acid which is sparingly soluble and very soluble in water respectively. The loading efficiency of lidocaine in NLC is at least four times higher than that of both ascorbic acid and caffeine. This is owing to the lipophilic properties of lidocaine, whereby it can easily incorporate into the lipid matrix of NLC than the other two active ingredients.

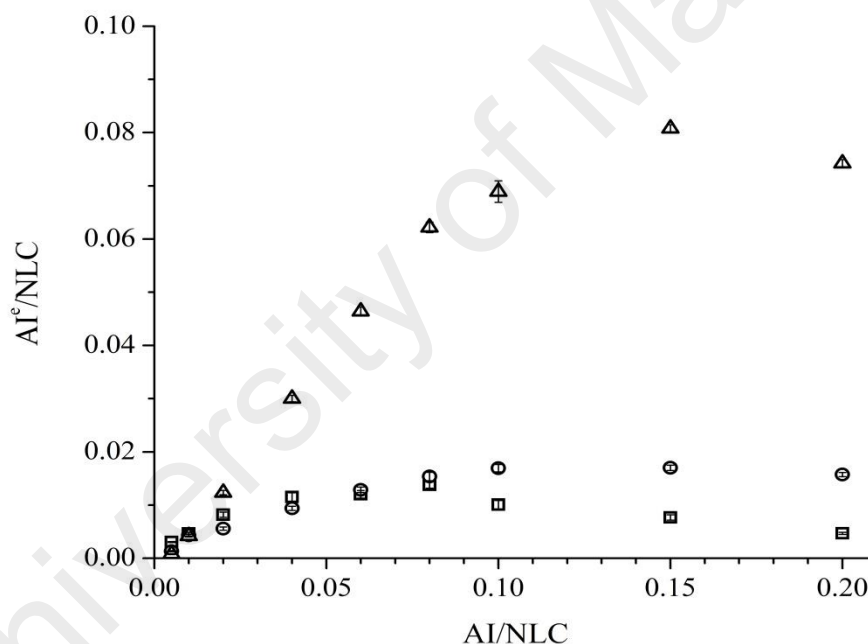


Figure 4.15: Active ingredients loaded NLC at different weight ratios of active ingredients to NLC. Where symbol □ = ascorbic acid, ○ = caffeine, △ = lidocaine while AI = active ingredients, AI^e = loaded active ingredients.

On the other hand, encapsulation efficiency of active ingredients showed that the encapsulation efficiency will increase gradually until it reaches its optimum encapsulation percentage, followed by a decrease in the encapsulation efficiency even though the loading efficiency is still increasing (Figure 4.16). Lidocaine, which is slightly soluble in water has the highest encapsulation efficiency of around 78% as

compared to caffeine of around 43%. Surprisingly, ascorbic acid which is very soluble in water, theoretically should have lower encapsulation efficiency than caffeine and lidocaine, anyhow gave a high encapsulation efficiency when the ratio of active ingredients to NLC is less than 0.05. This might be attributed to the adsorption of positively charged ascorbic acid on the surface of the NLC.

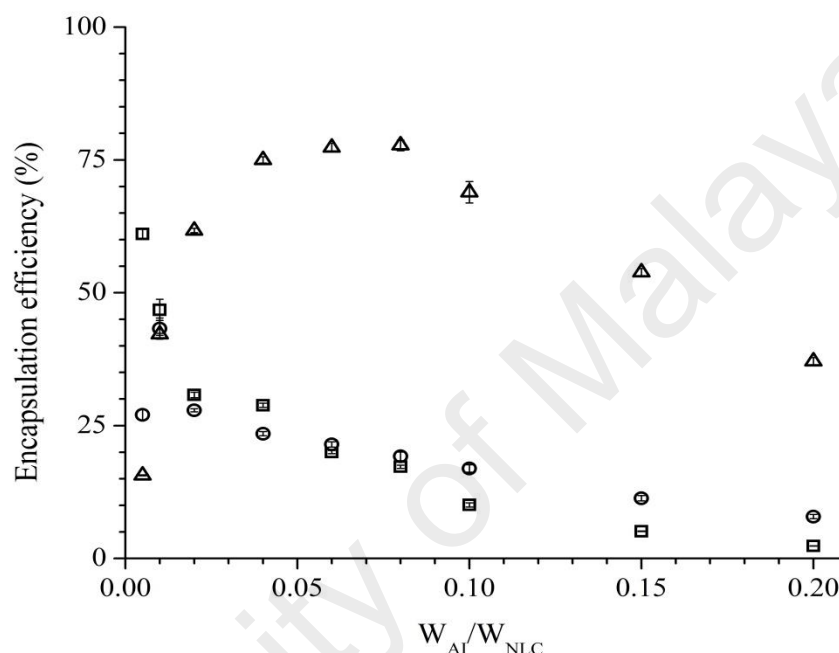


Figure 4.16: Encapsulation efficiency of active ingredients in varied weight ratios of active ingredients to NLC. Where symbol \square = ascorbic acid, \circ = caffeine, Δ = lidocaine while W= weight, AI= active ingredients.

The active ingredients encapsulated NLC were evaluated for their particle size and zeta potential. The encapsulation of caffeine and lidocaine in NLC, do not show any significant changes in their particle sizes. But, ascorbic acid encapsulated NLC showed a drastic change in particle size by two folds as compared to unencapsulated NLC (Figure 4.17). This is plausibly because the changes in the pH of the aqueous phase after addition of ascorbic acid induce aggregation to the NLC. Nevertheless, all samples showed only a slight increase in particle size over time. This indicates that despite there are changes in the particle size, the active ingredients encapsulated NLC still being remained as a stable formulation.

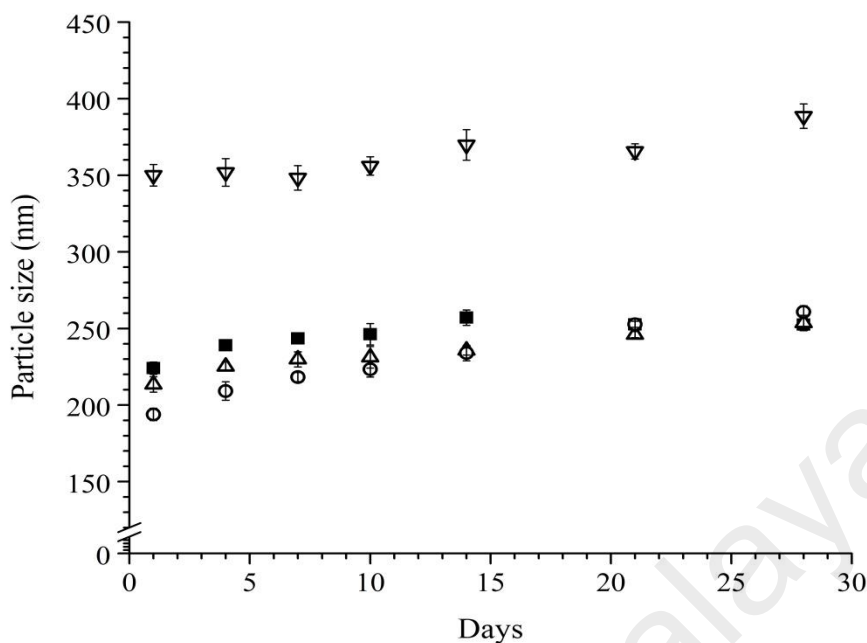


Figure 4.17: Effect of active ingredients towards the stability of NLC with respect to storage time at 30 °C. Where symbols ■ = unloaded NLC, ▽ = ascorbic acid, Δ = caffeine, ○ = lidocaine.

The zeta potential of active ingredients encapsulated NLC corresponds to the value of unencapsulated active ingredients' zeta potential in water. The zeta potential of ascorbic acid, caffeine and lidocaine were positively, zero and negatively charged respectively. This affects the overall charge of ascorbic acid, caffeine and lidocaine encapsulated NLC by showing an increase, no change and decrease in zeta potential correspondingly (Figure 4.18). Ascorbic acid, which is positively charged, neutralized some of the negatively charged NLC to give a more positive zeta potential. When the zeta potential was being evaluated for 4 weeks, it shows a slight increase in the zeta potential for all encapsulated or unencapsulated NLC. On top of that, the zeta potential becomes stable after Day 7th.

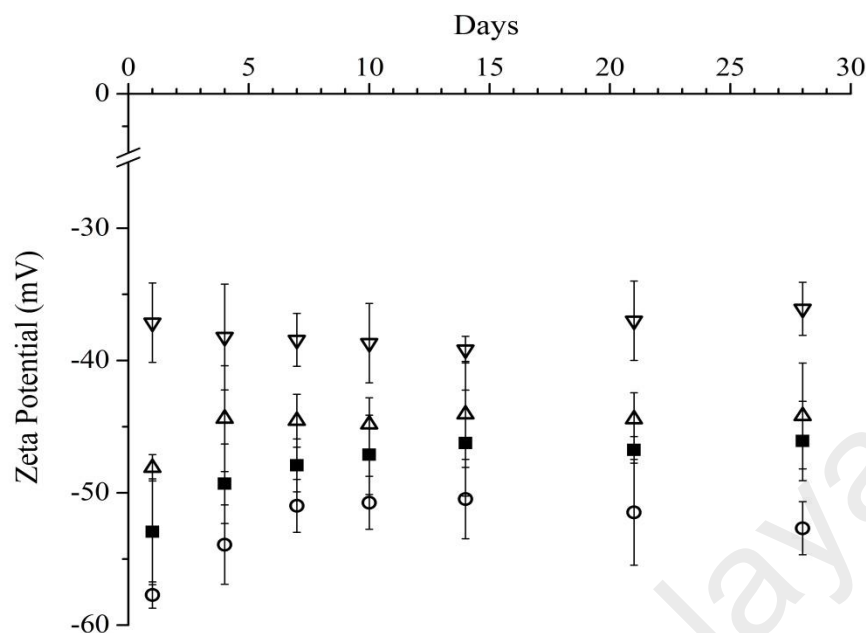


Figure 4.18: Changes in zeta potential and stability of active ingredients loaded NLC as a function of storage time at 30 °C. Where symbols ■ = unloaded NLC, ▽ = ascorbic acid, Δ = caffeine, ○ = lidocaine.

4.2.2 Encapsulated liposome

Both the loading efficiency and encapsulation efficiency of active ingredients in liposome from 0.1 to 0.5 mole ratio of active ingredients to fatty acid were tabulated in Table 4.6 and Table 4.7 respectively. When the mole ratio of active ingredients to fatty acid increased gradually from 0.1 to 0.5, the loading efficiency of active ingredients also increases for all active ingredients. The increment is owing to the presence of a higher concentration of active ingredients, hence increases the chance of active ingredients to be loaded in the liposome during the rehydration of fatty acid thin film. Apart from that, the loading and encapsulation efficiency of the liposomes are correlated with the solubility of the active ingredients in water. Lidocaine, which is slightly water soluble has the highest loading and encapsulation efficiency, followed by caffeine and ascorbic acid. Lidocaine, which is more lipid soluble has a high possibility to be embedded in the bilayer of the vesicle; caffeine, which can be soluble in both water and lipid can be

encapsulated either at the bilayer or the inner core of the vesicle while ascorbic acid, which is more water soluble is more likely to stay in the aqueous phase of liposome.

Table 4.6: Loading efficiency of oleic acid liposome prepared by using active ingredients with different water solubilities as a model to predict the capability of liposome in encapsulating active ingredients

n_{AI}/n_{FA}	Ascorbic Acid	Caffeine	Lidocaine
0.1	2.18 ± 0.10	3.31 ± 0.36	8.82 ± 0.27
0.2	3.96 ± 0.31	7.23 ± 0.19	17.07 ± 0.37
0.3	5.73 ± 0.50	10.89 ± 0.28	24.85 ± 0.85
0.4	7.71 ± 0.40	12.40 ± 0.36	32.67 ± 0.67
0.5	9.49 ± 0.56	15.88 ± 0.30	38.97 ± 0.98

n_{AI}/n_{FA} is equivalent to the mole ratio of active ingredients to oleic acid. Loading efficiency is the percentage calculated from the active ingredients loaded to a fixed amount of fatty acid. The loading efficiency increased when the active ingredients loaded increased. The active ingredient which is more hydrophobic tends to have a higher amount loaded in all the three fatty acid liposomes.

Table 4.7: Encapsulation efficiency of C18 unsaturated fatty acid liposome using three different active ingredients with varied water solubilities

n_{AI}/n_{FA}	Ascorbic Acid	Caffeine	Lidocaine
0.1	21.79 ± 1.0	32.13 ± 3.5	88.57 ± 2.7
0.2	19.79 ± 1.5	34.51 ± 0.9	84.51 ± 1.9
0.3	19.11 ± 1.7	34.86 ± 0.9	83.17 ± 2.8
0.4	19.29 ± 1.0	31.12 ± 0.9	80.87 ± 1.7
0.5	18.98 ± 1.1	31.68 ± 0.6	78.29 ± 2.0

n_{AI}/n_{FA} is equivalent to the mole ratio of active ingredients to oleic acid. Encapsulation efficiency is calculated from the amount encapsulated to initial amount loaded. The encapsulation efficiency mostly decreased when the active ingredients loaded increased. The active ingredient which is more hydrophobic tends to have a higher amount encapsulated in all the three fatty acid liposomes.

On the contrary, the encapsulation efficiency showed a decrease with an increase of active ingredients to fatty acid mole ratio. When more active ingredients are being loaded, it has higher chances to be entrapped in liposomes. Yet, the amount loaded which does not increase proportionally, will reduce the encapsulation efficiency of the oleic acid liposome. Along with the encapsulation of active ingredients, changes in particle size (Figure 4.19) and zeta potential (Figure 4.20) was also evaluated.

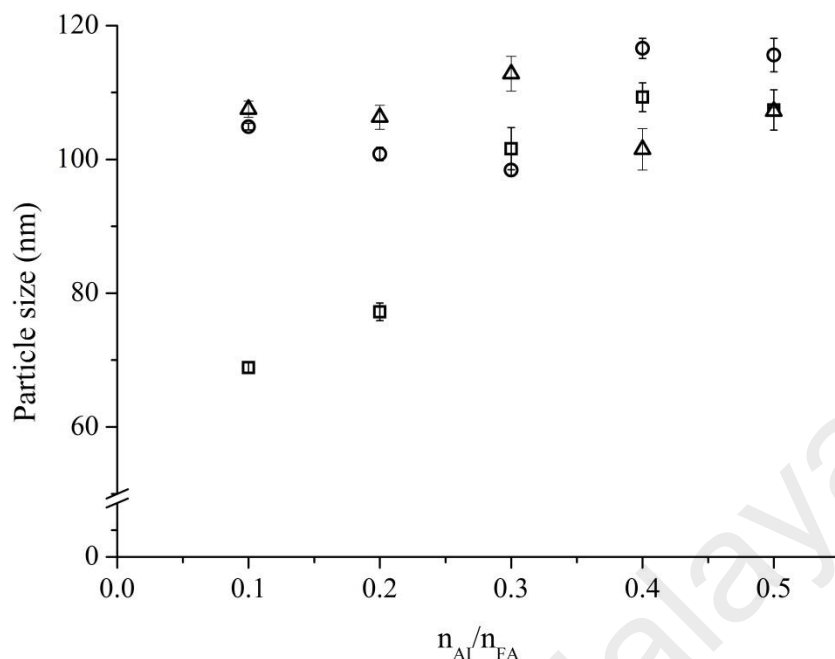


Figure 4.19: Particle size of oleic acid liposomes after loaded with different active ingredients at mole ratios of 0.1 to 0.5 active ingredients to fatty acid (n_{AI}/n_{FA}). Where symbol \square = ascorbic acid, \circ = caffeine, Δ = lidocaine.

When the active ingredients were loaded at mole ratios of 0.1 to 0.5 active ingredients to fatty acid, there were no apparent differences in the particle size and the zeta potential for both caffeine and lidocaine. Nevertheless, there was a slight difference in the particle size of ascorbic acid loaded liposome. This change was mainly caused by the acidic pH of ascorbic acid. The positive charge of ascorbic acid eased the formation of the liposome and thus produced a smaller particle size within the liposome formation range. Nevertheless, the situation was reversed when the amount of ascorbic acid added exceeded the buffering zone, which turned the liposome solution into an emulsion. As a result, the solution requires more sodium hydroxide to adjust the pH to 8.6, and the particle size gradually increased. The particle size of ascorbic acid loaded liposome corresponded to the loading efficiency, whereby those liposomes with a smaller particle size had a lower loading efficiency.

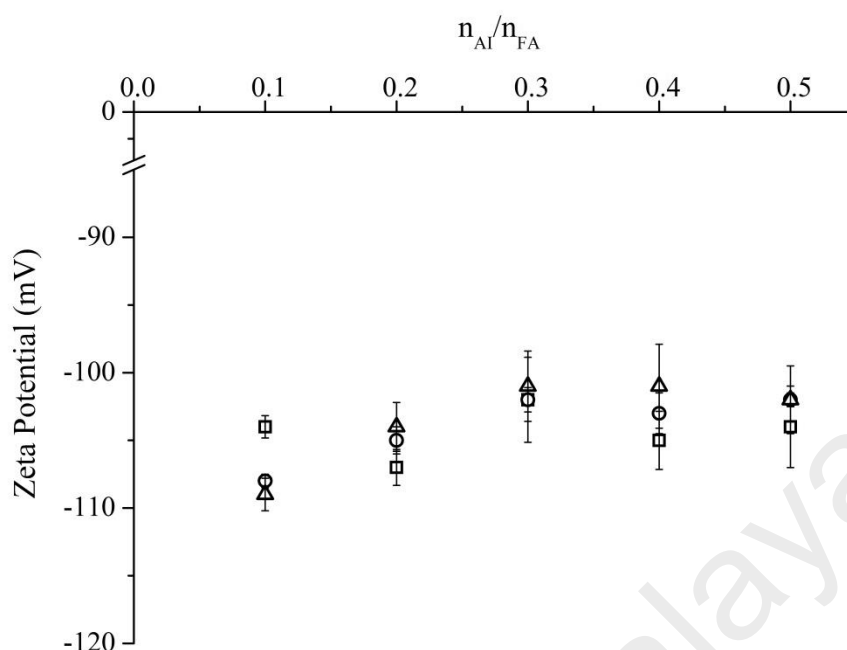


Figure 4.20: Zeta potential of oleic acid liposomes after loaded with different active ingredients at mole ratios of 0.1 to 0.5 active ingredients to fatty acid (n_{AI}/n_{FA}). Where symbol \square = ascorbic acid, \circ = caffeine, Δ = lidocaine.

When the active ingredients loaded liposome was being monitored for 14 days, we noticed that the particle size of ascorbic acid loaded liposome increased drastically with the increase in active ingredient mole ratio whereas there is no effect on both the caffeine and lidocaine loaded liposomes (Table 4.8).

Table 4.8: Changes in particle size of active ingredients loaded oleic acid liposome after 2 weeks of storage at 30 °C

n_{AI}/n_{FA}	Particle Size (nm)					
	Ascorbic acid		Caffeine		Lidocaine	
	1 st	14 th	1 st	14 th	1 st	14 th
0.1	68.86	103.3	104.9	93.05	107.5	107.3
0.2	77.22	185.1	100.8	104.6	106.3	106.4
0.3	101.6	211.8	98.42	102.3	112.8	109.5
0.4	109.3	392.6	116.6	113.4	101.5	108.0
0.5	107.4	446.0	115.6	114.3	107.2	109.0

The plausible reason is the presence of ascorbic acid in the solution which induces the aggregation of liposome. It is supported by the increase of zeta potential (Table 4.9) to a less negative value after Day 14th. This situation can be overcome by either coating the liposomes with polymer or lyophilizing the solution once it is being prepared.

Table 4.9: Changes in zeta potential of active ingredients loaded oleic acid liposome after 2 weeks of storage at 30 °C

n_{AI}/n_{FA}	Zeta Potential (mV)					
	Ascorbic acid		Caffeine		Lidocaine	
	1 st	14 th	1 st	14 th	1 st	14 th
0.1	-104	-101	-108	-104	-109	-106
0.2	-107	-99.5	-105	-107	-104	-102
0.3	-102	-98.6	-102	-102	-101	-105
0.4	-105	-62	-103	-103	-101	-100
0.5	-104	-52.3	-102	-106	-102	-101

4.2.3 Encapsulated water-in-oil microemulsion

The amount of active ingredients that could be loaded into the water-in-oil microemulsion depends on the solubility of active ingredients in water. On that account, the active ingredients were respectively dissolved in deionized water at the temperature of 30 °C with a gradual increment in the amount of 0.1 mg active ingredients. The optimum amount of which the active ingredients can be dissolved (Table 4.10) is determined when there is precipitation being observed at the bottom of the vials.

Table 4.10: Optimum weight of active ingredients solubilized in 1 ml of deionized water

Approximate amount solubilized (mg ml ⁻¹)	
Ascorbic acid	345.6
Caffeine	32.3
Lidocaine	3.1

The obtained amount of active ingredients being solubilized in deionized water is within the range when comparing with the water solubility as stated in drugbank (Law *et al.*,

2014). Water solubility of lidocaine that obtained from drugbank is around 4.1 mg ml^{-1} at 30°C , which is close to our data of 3.1 mg ml^{-1} . The variation in data might be due to the purity of the active ingredients when performing the experiments. Caffeine, on the other hand, has a water solubility of 21.6 mg ml^{-1} at 25°C whereas ascorbic acid has a higher solubility of 400 mg ml^{-1} at 40°C . In accordance to our data, the amount of active ingredients loaded in microemulsion, 3 mg ml^{-1} was selected based on the optimum concentration of lidocaine to standardize the amount of active ingredient solubilized in the aqueous phase of the prepared ST80 water-in-oil microemulsion.

Ascorbic acid, caffeine and lidocaine with different water solubilities were individually loaded in ST80. The loading of the active ingredients showed no drastic change in the particle size, pH, conductivity and viscosity of ST80 as tabulated in Table 4.11.

Table 4.11: Physical properties of active ingredients loaded ST80 microemulsions

	pH	Conductivity (mS cm^{-1})	Apparent Viscosity (mPa s)	Particle Size (nm)
Blank ST80	7.36 ± 0.06	< 0.05	207.0 ± 0.9	22.42 ± 0.94
Ascorbic Acid	7.08 ± 0.10	< 0.05	205.0 ± 0.5	22.84 ± 0.69
Caffeine	7.31 ± 0.08	< 0.05	207.2 ± 0.8	22.98 ± 0.75
Lidocaine	7.47 ± 0.07	< 0.05	205.6 ± 0.6	23.18 ± 0.82

No apparent change in physical properties of ST80 microemulsion after loading of ascorbic acid, caffeine and lidocaine at 3 mg ml^{-1} respectively.

The size of the loaded microemulsion was similar to a blank microemulsion, whereby the particle size and apparent viscosity were around 23 nm and 206 mPa s, respectively. This is attributed to the non-ionic surfactant used in the preparation, whereby the additives had a negligible impact on the physical characteristic of microemulsion (Prieto & Calvo, 2013). However, there is a slight change in the pH of the ascorbic acid loaded microemulsion. The decrease in the pH of the microemulsion from 7.36 to 7.08 might be arised from the nature of ascorbic acid, which is acidic ($\text{pK}_a = 4.10$). Nevertheless, a

slight change in the pH has no effect on the stability of the microemulsion, suggesting that ST80 is suitable for loading of a wide range of active ingredients.

4.2.4 Encapsulated κ -carrageenan-chitosan nanoparticle

The loading and encapsulation efficiency of active ingredients in κ -carrageenan-chitosan nanoparticle, which affect by the hydrophilicity of active ingredients are shown in Figure 4.21 and Figure 4.22 respectively.

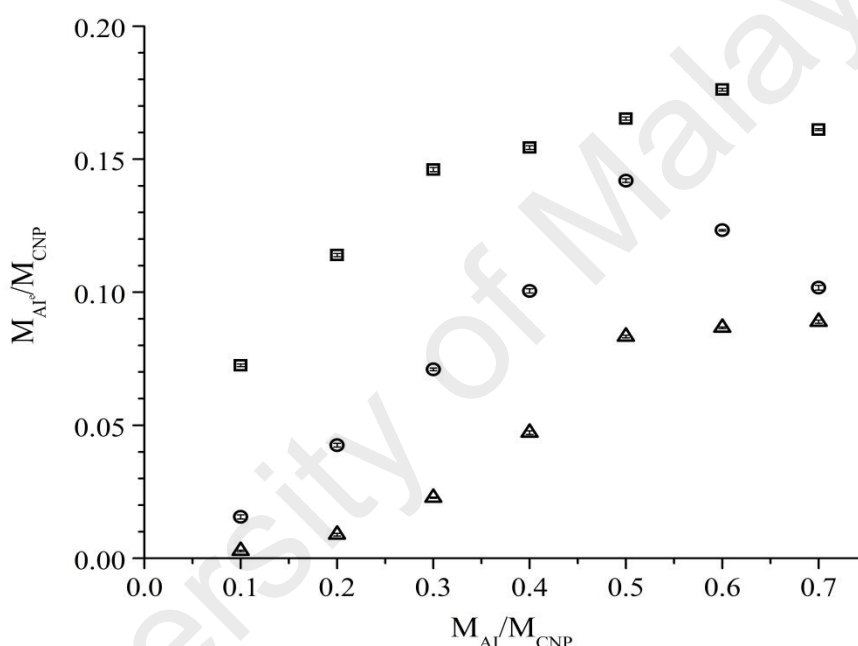


Figure 4.21: Mass ratio of active ingredients loaded into κ -carrageenan-chitosan nanoparticle. Where symbol \square = ascorbic acid, \circ = caffeine, Δ = lidocaine while M_{AI}/M_{CNP} is the mass ratio of active ingredients to the weight of κ -carrageenan and chitosan and M_{AI}^e is the mass of loaded active ingredients.

It was shown that the loading of active ingredients in the κ -carrageenan-chitosan nanoparticle will gradually increases until it reaches their optimum loading efficiency. κ -carrageenan-chitosan nanoparticle was shown to have a low loading efficiency as it only could load a maximum mass of approximately 30% of the initial amount of the active ingredients. It was being hypothesized that the loading efficiency might follow the order of solubility or the protonated forms of the active ingredients in the solution.

From the result, it was shown that the loading of active ingredients depends on their solubility in water. Ascorbic acid, which is very soluble in water has the highest loading efficiency, followed by caffeine and lidocaine. Even though the protonated and unprotonated forms of the active ingredients in acidic condition might affect its solubility, the buffering effect of the continuous phase towards the active ingredients added nullified the condition.

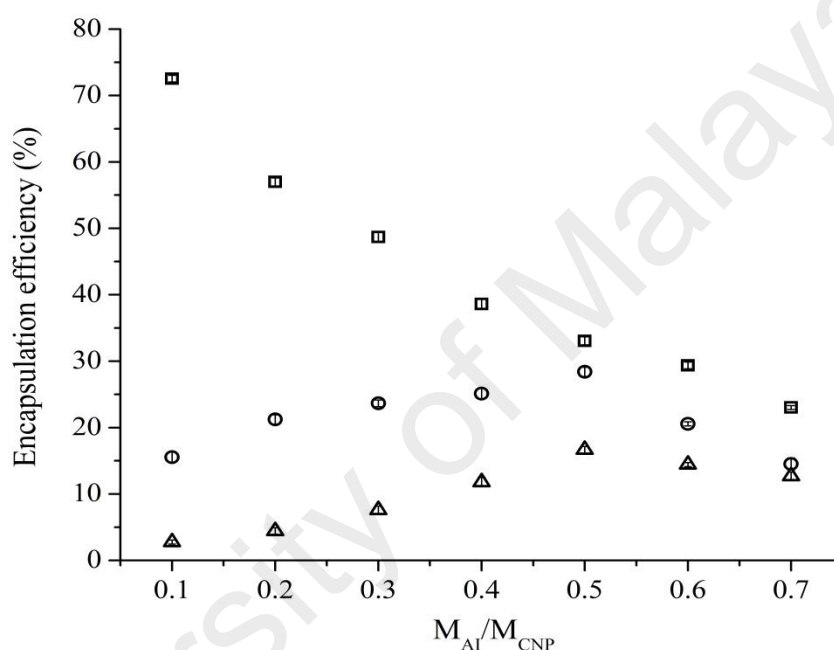


Figure 4.22: Encapsulation efficiency of active ingredients in κ -carrageenan-chitosan nanoparticle. Where symbol \square = ascorbic acid, \circ = caffeine, Δ = lidocaine while M_{AI}/M_{CNP} is the mass ratio of active ingredients to the weight of κ -carrageenan and chitosan.

Ascorbic acid has the highest encapsulation efficiency of around 72% as compared to caffeine and lidocaine which shown to be around 28% and 17% respectively. The results shown are acceptable as lidocaine, which is less water soluble tends to recede from hydrophilic κ -carrageenan-chitosan nanoparticle. The encapsulation efficiency of caffeine and lidocaine was shown to increase gradually to its optimum percentage and then decrease even though the amount of active ingredients added is still increasing and do not exceed the optimum solubility. This pattern however, was not shown in ascorbic acid encapsulated κ -carrageenan-chitosan nanoparticle. This is plausibly due to the

repulsion of charge when more active ingredients were added to the solution, thus affects the encapsulation efficiency (Boonsongrit *et al.*, 2006).

Table 4.12: Particle size and zeta potential of active ingredients loaded κ -carrageenan-chitosan nanoparticle

M_{AI}/M_{CNP}	Particle Size (nm)			Zeta Potential (mV)		
	A	B	C	A	B	C
0.1	382.9 (5.8)	399.0 (1.3)	389.5 (3.3)	45.0 (1.3)	46.2 (0.3)	45.6 (0.3)
0.2	395.2 (7.1)	382.9 (5.1)	387.3 (2.9)	45.8 (0.8)	46.5 (1.5)	44.8 (0.9)
0.3	384.4 (7.2)	387.6 (2.4)	390.1 (2.5)	46.3 (1.1)	45.2 (1.38)	43.6 (1.4)
0.4	380.8 (3.8)	398.9 (7.9)	394.1 (2.7)	45.4 (0.2)	47.1 (0.8)	42.9 (1.15)
0.5	392.6 (5.3)	413.5 (3.6)	395.6 (4.4)	45.8 (0.4)	46.1 (1.2)	42.4 (0.3)
0.6	394.3 (2.9)	398.6 (10.7)	390.5 (4.3)	46.1 (0.8)	45.6 (0.5)	42.6 (0.3)
0.7	395.7 (5.5)	391.1 (2.6)	409.2 (0.43)	46.4 (2.0)	46.4 (0.3)	41.6 (0.5)

A is ascorbic acid encapsulated κ -carrageenan-chitosan nanoparticle, B is caffeine encapsulated κ -carrageenan-chitosan nanoparticle, C is lidocaine encapsulated κ -carrageenan-chitosan nanoparticle. The numbers in bracket indicate the standard deviation of the measurements taken.

The changes in the particle size and zeta potential after loading of active ingredients in κ -carrageenan-chitosan nanoparticle were identified. The results indicate that there were no apparent change in the particle size of around 400 nm and zeta potential of 45 mV in the active ingredients loaded κ -carrageenan-chitosan nanoparticle when being prepared in 1:1 of κ -carrageenan to chitosan mass ratio at pH 4 as shown in Table 4.12.

As a summary, active ingredients with different solubility in water can be encapsulated in all of the proposed delivery vehicles. Despite that, both NLC and liposome are more suitable for the encapsulation of active ingredients that are less water soluble whereas κ -carrageenan-chitosan nanoparticle and microemulsion have preference over water

soluble active ingredients. The active ingredients' release profile from those delivery vehicles are further discussed in the following section.

4.3 Release profile of active ingredients from delivery vehicles

The release profile of both unencapsulated active ingredients and encapsulated active ingredients from different delivery vehicles were calculated and plotted as cumulative percentage release over time. Then, the plot were curve fitted into five types of kinetic models to determine the best model in order to explain the release profile of those delivery systems.

4.3.1 Release profile of unencapsulated ingredients

The release of unencapsulated active ingredients from the donor chamber to receptor chamber of Franz diffusion cell was in an ascending order of lidocaine < caffeine < ascorbic acid, as shown in Figure 4.23.

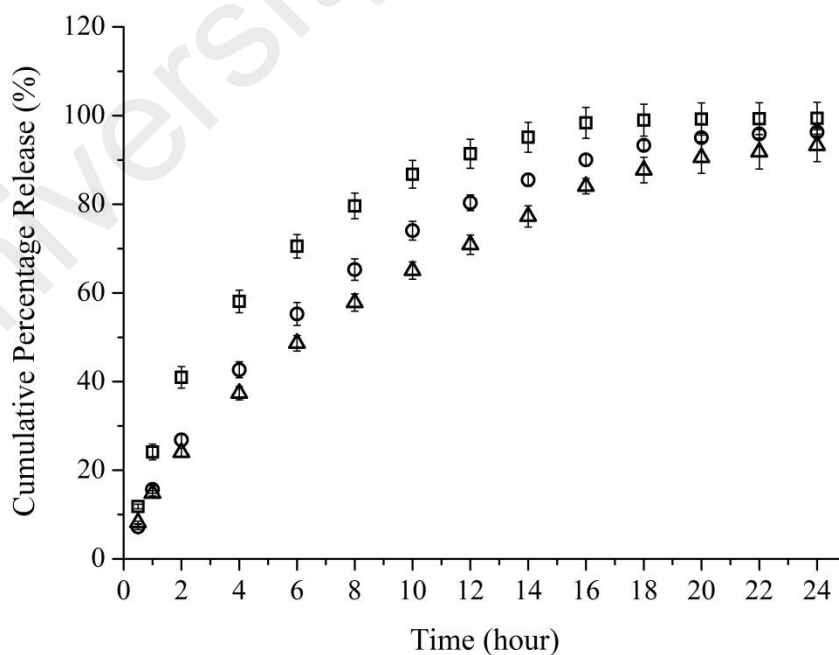


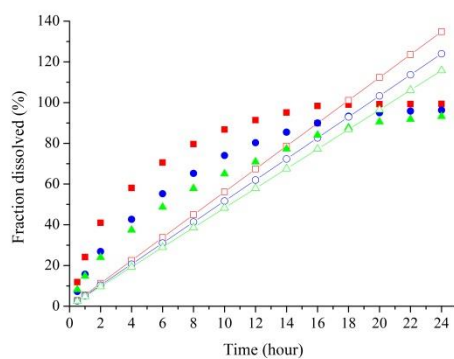
Figure 4.23: Release profile of unencapsulated active ingredients for 24 hours. Where symbol \square = ascorbic acid, \circ = caffeine, Δ = lidocaine.

The release profile was expected for the reason that diffusion of active ingredients is hydrophilicity dependent. Ascorbic acid is highly soluble in water, followed by caffeine which is sparingly soluble in water and lidocaine which is slightly soluble in water. In the presence of one layer 5000 Da dialysis membrane separating the donor and receptor chambers, eases the diffusion of the active ingredients down the gradient concentration through the membrane. Therefore, the active ingredients which are more water soluble, have a higher possibility to diffuse into the receptor chamber than those which is more hydrophobic.

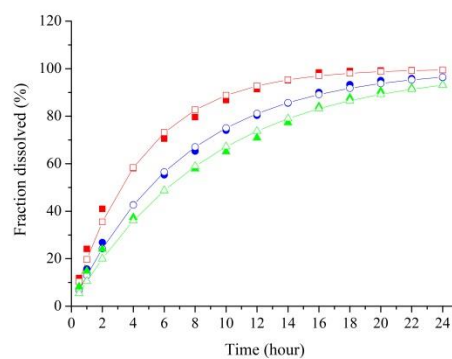
This was followed by curve fitting of the unencapsulated active ingredients' release profile into different kinetic models (Shoaib *et al.*, 2006; Dash *et al.*, 2010), to select the best model to describe the release pattern of the system. Their linear regression to the release curve and the rate constant were obtained by using DDSolver (Zhang *et al.*, 2010). The result for 24 hours curve fitting was tabulated in Table 4.13 and their plots was shown in Figure 4.24.

Table 4.13: Unencapsulated active ingredients' rate constant and the linear regression of release curve after curve fit in different kinetic models for 24 hours

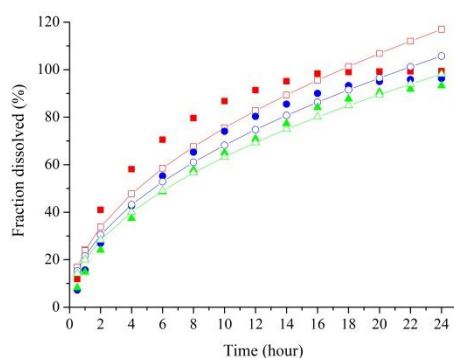
	Ascorbic acid	Caffeine	Lidocaine
Zero-order, k_0 ($\mu\text{g h}^{-1}$)	5.616 $R^2 = 0.234$	5.166 $R^2 = 0.662$	4.823 $R^2 = 0.759$
First-order, k_1 (h^{-1})	0.219 $R^2 = 0.993$	0.139 $R^2 = 0.998$	0.111 $R^2 = 0.994$
Higuchi, k_H ($\mu\text{g h}^{-1/2}$)	23.879 $R^2 = 0.894$	21.577 $R^2 = 0.972$	20.020 $R^2 = 0.987$
Hixson-Crowell, k_{HC} ($\mu\text{g h}^{-1}$)	0.056 $R^2 = 0.972$	0.037 $R^2 = 0.987$	0.030 $R^2 = 0.981$
Korsmeyer-Peppas, k_{KP} (h^{-n})	33.028 $R^2 = 0.937$	22.062 $R^2 = 0.970$	18.452 $R^2 = 0.987$



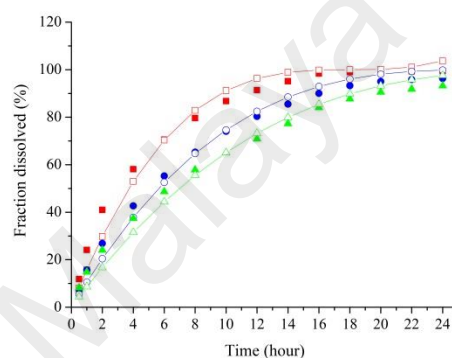
(a) Zero-order



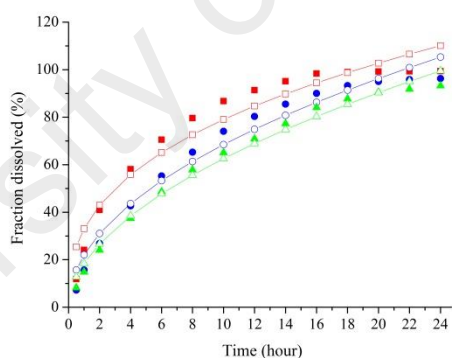
(b) First-order



(c) Higuchi



(d) Hixson-Crowell



(e) Korsmeyer-Peppas

Figure 4.24: Curve fitting of unencapsulated active ingredients release profile in different kinetic models. Where symbol \square = ascorbic acid, \circ = caffeine, Δ = lidocaine. The solid symbol represents the experimental plot while the opened symbol with line represents the predicted plot.

Apart from that, the release curve was also fitted for the first 12 hours to evaluate the possible kinetic difference in the earlier part of release. The rate constant and their linear regression were shown in Table 4.14 whereas the plot was shown in Figure 4.25.

Table 4.14: Unencapsulated active ingredients' rate constant and the linear regression of release curve after curve fit in different kinetic models for the first 12 hours

	Ascorbic acid	Caffeine	Lidocaine
Zero-order, k_0 ($\mu\text{g h}^{-1}$)	9.223 $R^2 = 0.691$	7.671 $R^2 = 0.885$	6.768 $R^2 = 0.872$
First-order, k_1 (h^{-1})	0.218 $R^2 = 0.988$	0.137 $R^2 = 0.996$	0.110 $R^2 = 0.985$
Higuchi, k_H ($\mu\text{g h}^{-1/2}$)	27.482 $R^2 = 0.982$	22.448 $R^2 = 0.968$	19.847 $R^2 = 0.976$
Hixson-Crowell, k_{HC} ($\mu\text{g h}^{-1}$)	0.058 $R^2 = 0.955$	0.038 $R^2 = 0.983$	0.032 $R^2 = 0.964$
Korsmeyer-Peppas, k_{KP} (h^{-n})	26.850 $R^2 = 0.982$	17.084 $R^2 = 0.994$	15.639 $R^2 = 0.997$

The curve fitting of release profile for the first 12 hours has shown a good linear regression towards first-order model in Figure 4.25(b) and Korsmeyer-Peppas model in Figure 4.25(e) as compared to zero-order model in Figure 4.25(a), Higuchi model in Figure 4.25(c) and Hixson-Crowell model in Figure 4.25(d). Between the two best fitted models, first-order model was still the more suitable selection to describe the release profile. In Korsmeyer-Peppas model, the mechanisms for release of active ingredients are in the order of solvent diffusion into the polymeric system, swelling of polymeric system, formation of gel, diffusion of active ingredients out of the polymeric system and dissolution of the polymeric system's matrix. Henceforth, none of the steps described in Korsmeyer-Peppas model could fit into the scenario for the unencapsulated active ingredients. As a result, first order model which focus on the diffusion of active ingredients in one direction and concentration dependent, could best describe the release profile of unencapsulated active ingredients.

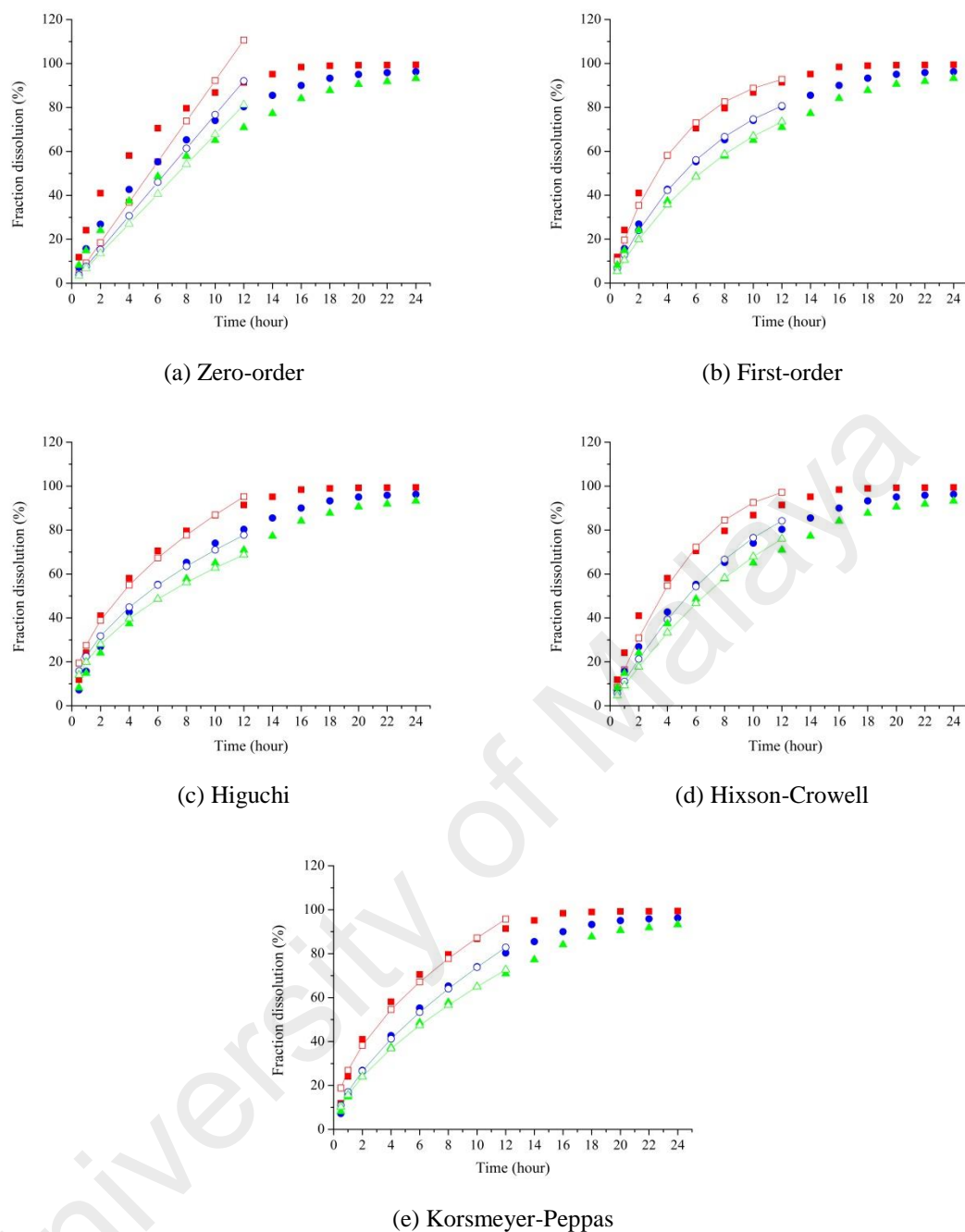


Figure 4.25: Curve fitting of unencapsulated active ingredients release profile for the first 12 hours in different kinetic models. Where symbol \square = ascorbic acid, \circ = caffeine, Δ = lidocaine. The solid symbol represents the experimental plot while the opened symbol with line represents the predicted plot.

4.3.2 Release profile of NLC

The release profile of active ingredients from NLC showed a similar pattern as that of unencapsulated active ingredients, which are in the ascending order of release lidocaine < caffeine < ascorbic acid (Figure 4.26). Nevertheless, the rate of caffeine and lidocaine

released from encapsulated NLC were much lower than that of unencapsulated active ingredients while the rate of ascorbic acid was almost similar to the unencapsulated active ingredient. This suggested that, ascorbic acid which majorly adsorbs on the surface of NLC, would detach and permeate into the receptor chamber easier when there is a drop in the chemical potential than the other two active ingredients which are embedded in the matrix core of NLC.

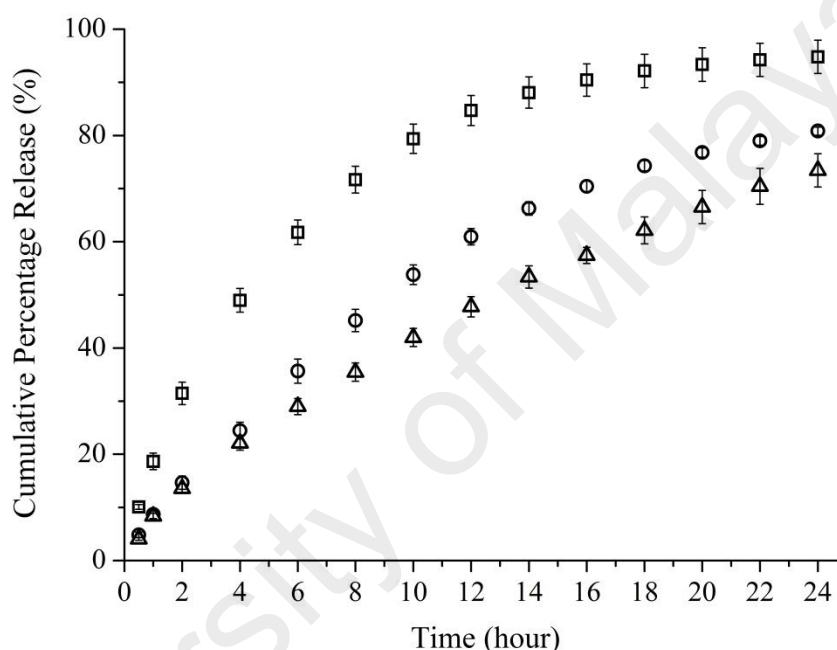


Figure 4.26: Release profile of active ingredients from NLC for 24 hours. Where symbol \square = ascorbic acid, \circ = caffeine, Δ = lidocaine.

The cumulative percentage release of active ingredients from NLC was then curve fitted into various kinetic models, to describe the release kinetic of the NLC. Their linear regression to the release curve and the rate constant were obtained by using DDSolver. The result for 24 hours curve fitting was tabulated in Table 4.15 and their curve fitting in zero-order model, first-order model, Higuchi model, Hixson-Crowell model and Korsmeyer-Peppas model were shown in Figure 4.27(a), Figure 4.27(b), Figure 4.27(c), Figure 4.27(d) and Figure 4.27(e) respectively.

Table 4.15: Active ingredients' rate constant and the linear regression of release curve from NLC after curve fit in different kinetic models for 24 hours

	Ascorbic acid	Caffeine	Lidocaine
Zero-order, k_0 ($\mu\text{g h}^{-1}$)	5.224 $R^2 = 0.454$	4.070 $R^2 = 0.870$	3.461 $R^2 = 0.927$
First-order, k_1 (h^{-1})	0.160 $R^2 = 0.993$	0.075 $R^2 = 0.998$	0.055 $R^2 = 0.996$
Higuchi, k_H ($\mu\text{g h}^{-1/2}$)	22.048 $R^2 = 0.939$	16.716 $R^2 = 0.963$	14.125 $R^2 = 0.964$
Hixson-Crowell, k_{HC} ($\mu\text{g h}^{-1}$)	0.043 $R^2 = 0.966$	0.021 $R^2 = 0.985$	0.016 $R^2 = 0.988$
Korsmeyer-Peppas, k_{KP} (h^{-n})	26.963 $R^2 = 0.950$	11.981 $R^2 = 0.982$	8.767 $R^2 = 0.999$

Curve fitting of the cumulative release profile of active ingredients from NLC showed that the release kinetic fits well in all models except the zero-order model. The remaining four kinetic models which describe the kinetics have R^2 values of at least 0.939 for all active ingredients. Among the four models, first-order model has the best linear regression towards the original plots. Additionally, in the model, it was found that the rate constant of active ingredients' release from NLC is at least 30% slower than the unencapsulated active ingredients. Hence, we hypothesized that at the initial phase of release, the active ingredients released were mostly from the continuous phase of the prepared NLC solution. This has caused a burst effect on the rate of active ingredients' release, where most of the unencapsulated active ingredients could permeate into the receptor chamber. When the chemical potential gradient decreased, the encapsulated active ingredients from NLC will gradually partition into the continuous phase. At this stage, the release rate would be much lower as more energy was required to overcome the phase barrier for it to be release to the continuous phase.

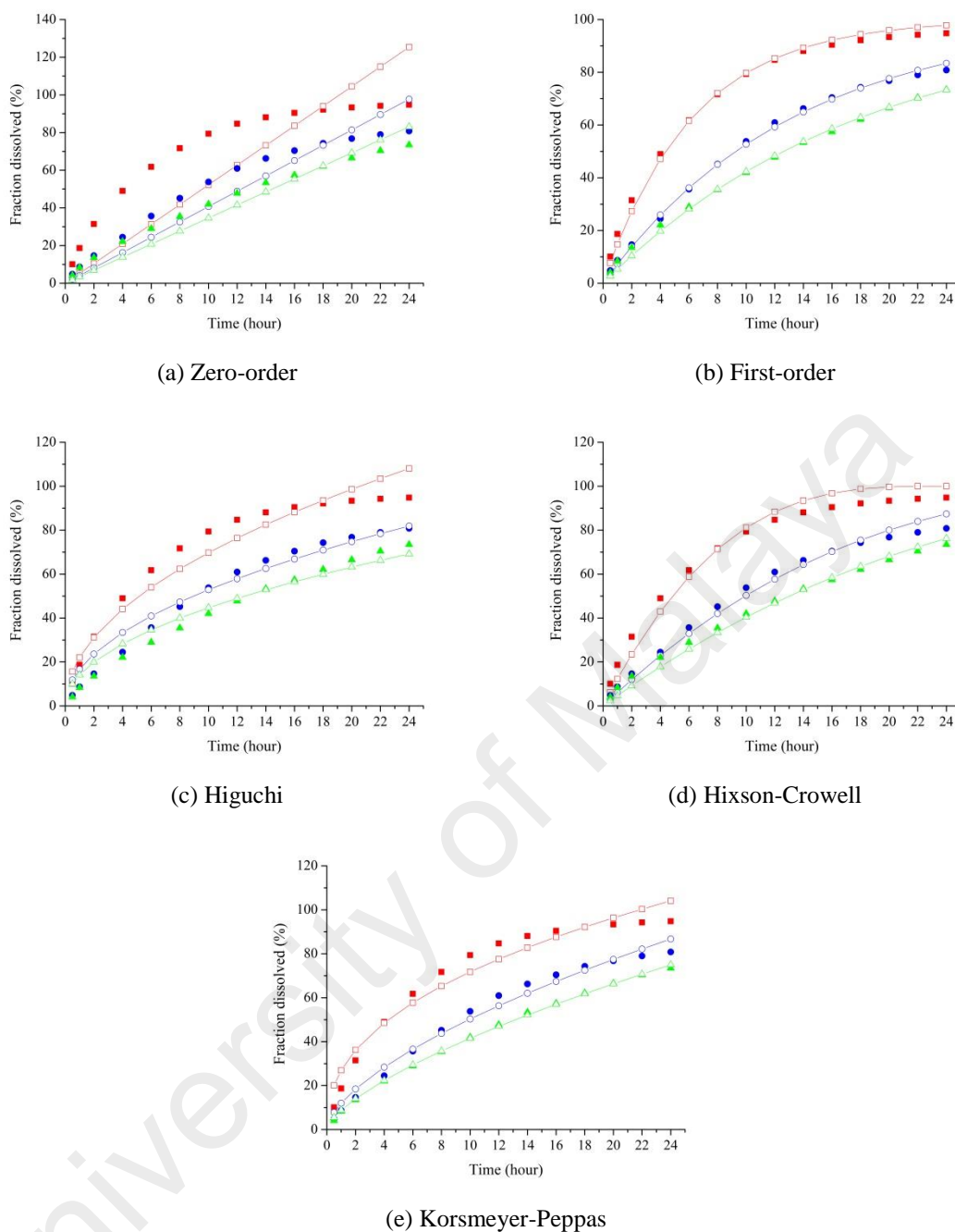


Figure 4.27: Curve fitting of active ingredients' release profile from NLC in different kinetic models for 24 hours. Where symbol \square = ascorbic acid, \circ = caffeine, Δ = lidocaine. The solid symbol represents the experimental plot while the opened symbol with line represents the predicted plot.

In order to show a more 'real-time' release kinetic, the release curve was fitted for the first 12 hours, to evaluate the possible kinetic difference in the initial part of release. The rate constant and their linear regression were tabulated in Table 4.16 whereas their curve fitting in zero-order model, first-order model, Higuchi model, Hixson-Crowell

model and Korsmeyer-Peppas model were shown in Figure 4.28(a), Figure 4.28(b), Figure 4.28(c), Figure 4.28(d) and Figure 4.28(e) respectively.

Table 4.16: Active ingredients' rate constant and the linear regression of release curve from NLC after curve fit in different kinetic models for the first 12 hours

	Ascorbic acid	Caffeine	Lidocaine
Zero-order, k_0 ($\mu\text{g h}^{-1}$)	8.314 $R^2 = 0.818$	5.429 $R^2 = 0.978$	4.316 $R^2 = 0.947$
First-order, k_1 (h^{-1})	0.165 $R^2 = 0.994$	0.076 $R^2 = 0.997$	0.056 $R^2 = 0.986$
Higuchi, k_H ($\mu\text{g h}^{-1/2}$)	24.521 $R^2 = 0.981$	15.588 $R^2 = 0.917$	12.508 $R^2 = 0.947$
Hixson-Crowell, k_{HC} ($\mu\text{g h}^{-1}$)	0.045 $R^2 = 0.971$	0.023 $R^2 = 0.997$	0.017 $R^2 = 0.977$
Korsmeyer-Peppas, k_{KP} (h^{-n})	20.942 $R^2 = 0.991$	8.406 $R^2 = 0.999$	8.091 $R^2 = 0.999$

The curve fitting of release profile for the first 12 hours has shown a good linear regression towards almost all of the kinetic models. Nevertheless, Korsmeyer-Peppas model was shown to have the nearest R^2 values to the original plot followed by first-order model. Since the release exponent of active ingredient is between the value of 0.43 and 1.00 for Korsmeyer-Peppas model, this indicated non-Fickian transport for NLC system during the first 12 hours. This demonstrated the possibility that when the NLC solution came into contact with the release medium in receptor chamber, the active ingredients close to the surface of NLC was release by diffusion. At the later time, it is plausible that the NLC undergo some structural changes either by the effects of temperature or chemical potential gradient, causing the release to be continued in a linear manner (Nagaich and Gulati, 2016; Üner *et al.*, 2014). However, the more suitable model to describe the release of active ingredients from NLC would be first-order model whereby the linear regression is considered as the best in both 12 and 24 hours.

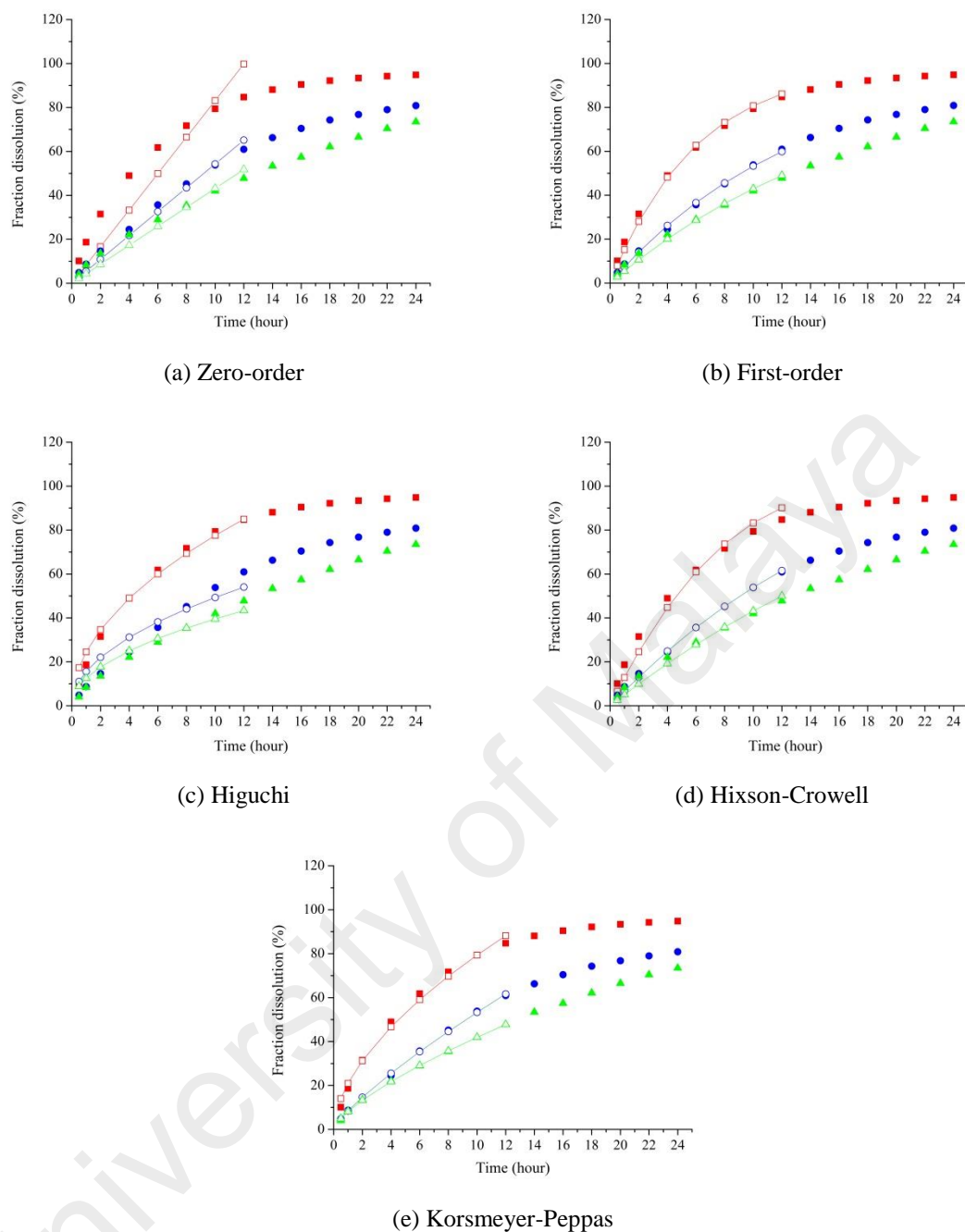


Figure 4.28: Curve fitting of active ingredients' release profile from NLC in different kinetic models for the first 12 hours. Where symbol \square = ascorbic acid, \circ = caffeine, Δ = lidocaine. The solid symbol represents the experimental plot while the opened symbol with line represents the predicted plot.

4.3.3 Release profile of liposome

The release profiles of active ingredients from oleic acid liposome are shown in an ascending order of lidocaine < caffeine < ascorbic acid (Figure 4.29). The release rate of ascorbic acid, caffeine and lidocaine from oleic acid liposome is 5%, 17% and 43%

slower than the unencapsulated active ingredients respectively. This is plausibly due to the encapsulation efficiency of those active ingredients in oleic acid liposome. The presence of unencapsulated active ingredients in the continuous phase, caused a burst effect which leads to high release rate at the initial phase of active ingredients release yet the overall release rate is slower than the free active ingredients due to encapsulation.

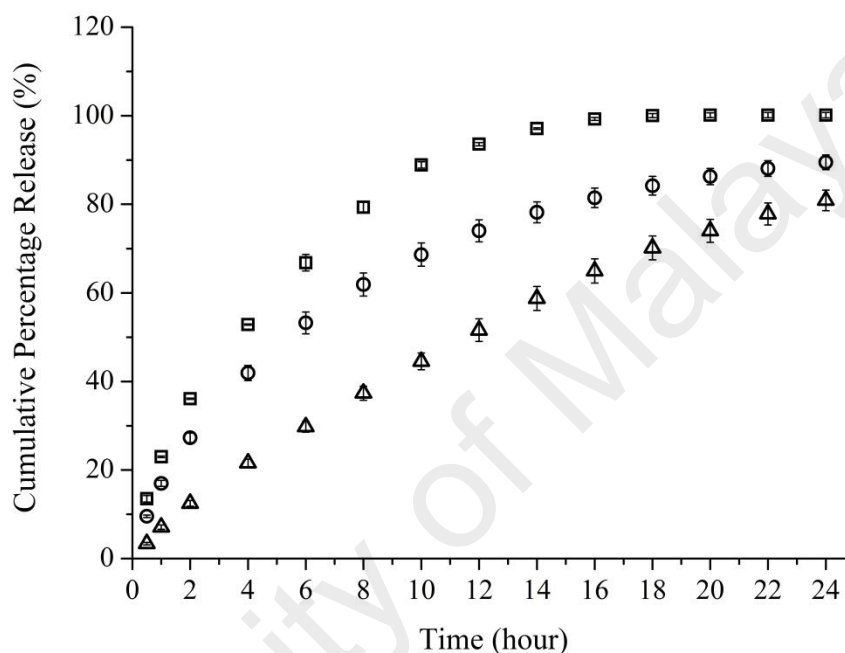


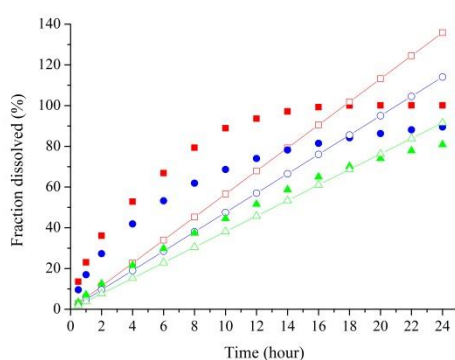
Figure 4.29: Release profile of active ingredients from liposome for 24 hours. Where symbol \square = ascorbic acid, \circ = caffeine, Δ = lidocaine.

The cumulative percentage release of active ingredients from oleic acid liposome was then curve fitted into various kinetic models, to describe the release kinetic of the liposome. Their linear regression to the release curve and the rate constant were obtained by using DDSolver. The result for 24 hours curve fitting was tabulated in Table 4.17 and their curve fitting in zero-order model, first-order model, Higuchi model, Hixson-Crowell model and Korsmeyer-Peppas model were shown in Figure 4.30(a), Figure 4.30(b), Figure 4.30(c), Figure 4.30(d) and Figure 4.30(e) respectively.

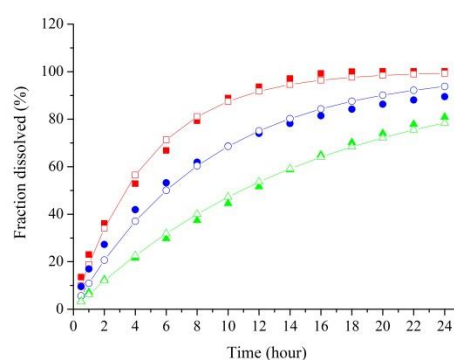
Table 4.17: Active ingredients' rate constant and the linear regression of release curve from oleic acid liposome after curve fit in different kinetic models for 24 hours

	Ascorbic acid	Caffeine	Lidocaine
Zero-order, k_0 ($\mu\text{g h}^{-1}$)	5.658 $R^2 = 0.345$	4.751 $R^2 = 0.585$	3.813 $R^2 = 0.953$
First-order, k_1 (h^{-1})	0.208 $R^2 = 0.992$	0.116 $R^2 = 0.979$	0.064 $R^2 = 0.996$
Higuchi, k_H ($\mu\text{g h}^{-1/2}$)	23.970 $R^2 = 0.914$	19.924 $R^2 = 0.974$	15.477 $R^2 = 0.943$
Hixson-Crowell, k_{HC} ($\mu\text{g h}^{-1}$)	0.054 $R^2 = 0.987$	0.031 $R^2 = 0.933$	0.018 $R^2 = 0.999$
Korsmeyer-Peppas, k_{KP} (h^{-n})	31.219 $R^2 = 0.938$	22.302 $R^2 = 0.976$	8.227 $R^2 = 0.996$

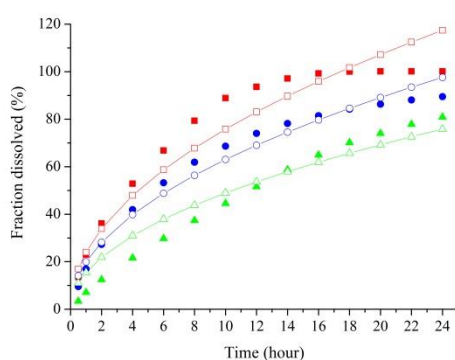
The release of active ingredients from oleic acid liposome has good linear regression towards all the kinetic models except for zero-order model. Among the kinetic models, first-order model has the closest R^2 values of at least 0.979 regardless of the active ingredients. In first-order model, the rate of active ingredient is a function of the amount of active ingredient remaining in the donor chamber. During the early stage of release, the rates of active ingredients' diffusion were high. This was due to chemical potential gradient present in the liposomal solution was abundant due to unencapsulated active ingredients as compared to the amount in receptor chamber. When the concentration of active ingredient in the donor chamber started to deplete after certain time of diffusion, the rate of active ingredients being released from the continuous phase of liposome solution also became lower. At this point, the active ingredients encapsulated in either the aqueous core or lipid bilayer of liposome, will start to diffuse out slowly to the environment through osmosis. As a result, the rate of diffusion slowed down until it reached plateau, whereby all the active ingredients were diffused to the receptor part. Additionally, the release rate of active ingredients from liposome is slightly faster than NLC. This is possibly attributed by the particle size of liposome which is smaller than NLC, ease the energy barrier for active ingredients release from liposome as compared to NLC.



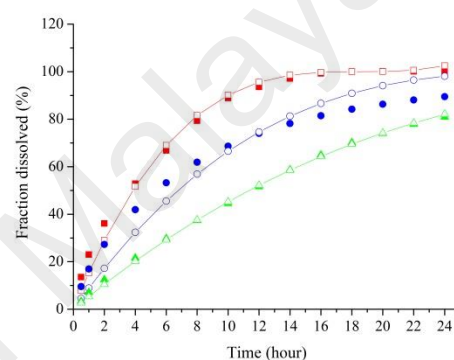
(a) Zero-order



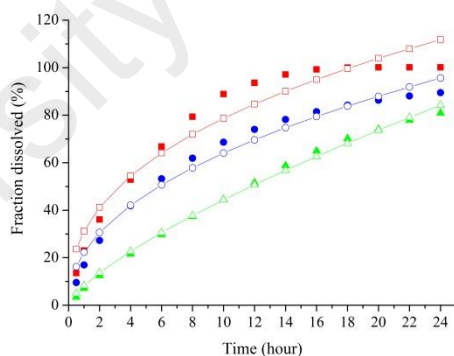
(b) First-order



(c) Higuchi



(d) Hixson-Crowell



(e) Korsmeyer-Peppas

Figure 4.30: Curve fitting of active ingredients' release profile from oleic acid liposome in different kinetic models for 24 hours. Where symbol \square = ascorbic acid, \circ = caffeine, Δ = lidocaine. The solid symbol represents the experimental plot while the opened symbol with line represents the predicted plot.

Apart from that, the release curve was fitted for the first 12 hours of release, to evaluate the possible kinetic difference in the initial part of release. The rate constant and their linear regression were tabulated in Table 4.18 whereas the curve fit in zero-order model,

first-order model, Higuchi model, Hixson-Crowell model and Korsmeyer-Peppas model were shown in Figure 4.31(a), Figure 4.31(b), Figure 4.31(c), Figure 4.31(d) and Figure 4.31(e) respectively.

Table 4.18: Active ingredients' rate constant and the linear regression of release curve from oleic acid liposome after curve fit in different kinetic models for the first 12 hours

	Ascorbic acid	Caffeine	Lidocaine
Zero-order, k_0 ($\mu\text{g h}^{-1}$)	9.202 $R^2 = 0.798$	7.209 $R^2 = 0.817$	4.549 $R^2 = 0.979$
First-order, k_1 (h^{-1})	0.204 $R^2 = 0.988$	0.125 $R^2 = 0.977$	0.060 $R^2 = 0.998$
Higuchi, k_H ($\mu\text{g h}^{-1/2}$)	27.188 $R^2 = 0.989$	21.264 $R^2 = 0.985$	13.063 $R^2 = 0.918$
Hixson-Crowell, k_{HC} ($\mu\text{g h}^{-1}$)	0.055 $R^2 = 0.976$	0.035 $R^2 = 0.947$	0.018 $R^2 = 0.995$
Korsmeyer-Peppas, k_{KP} (h^{-n})	24.034 $R^2 = 0.996$	18.277 $R^2 = 0.995$	7.078 $R^2 = 0.999$

The release profile for the first 12 hours has shown to be similar to 24 hours curve fitting, whereby the plots have good linear regression towards all of the kinetic models except zero-order model. Nevertheless, unlike 24 hours curve fitting, 12 hours curve fitting has the closest R^2 value towards Korsmeyer-Peppas model instead of first-order model. This suggested that the release of active ingredients from liposome is in biphasic, whereby the active ingredients in the continuous phase will diffuse into the receptor chamber in a faster rate due to burst release. When the amount of active ingredient in donor chamber gradually depleted, chemical potential difference between donor and receptor chamber also decreased. This has led to a change in release rate to be more linear. Additionally, the active ingredients' release exponent which falls between the value of 0.43 and 1.00 for Korsmeyer-Peppas model, indicated non-Fickian transport for oleic acid liposome during the first 12 hours. In spite of that, the more suitable model to describe the release of active ingredients from liposome would be first-order model whereby the linear regression is more similar for 12 and 24 hours.

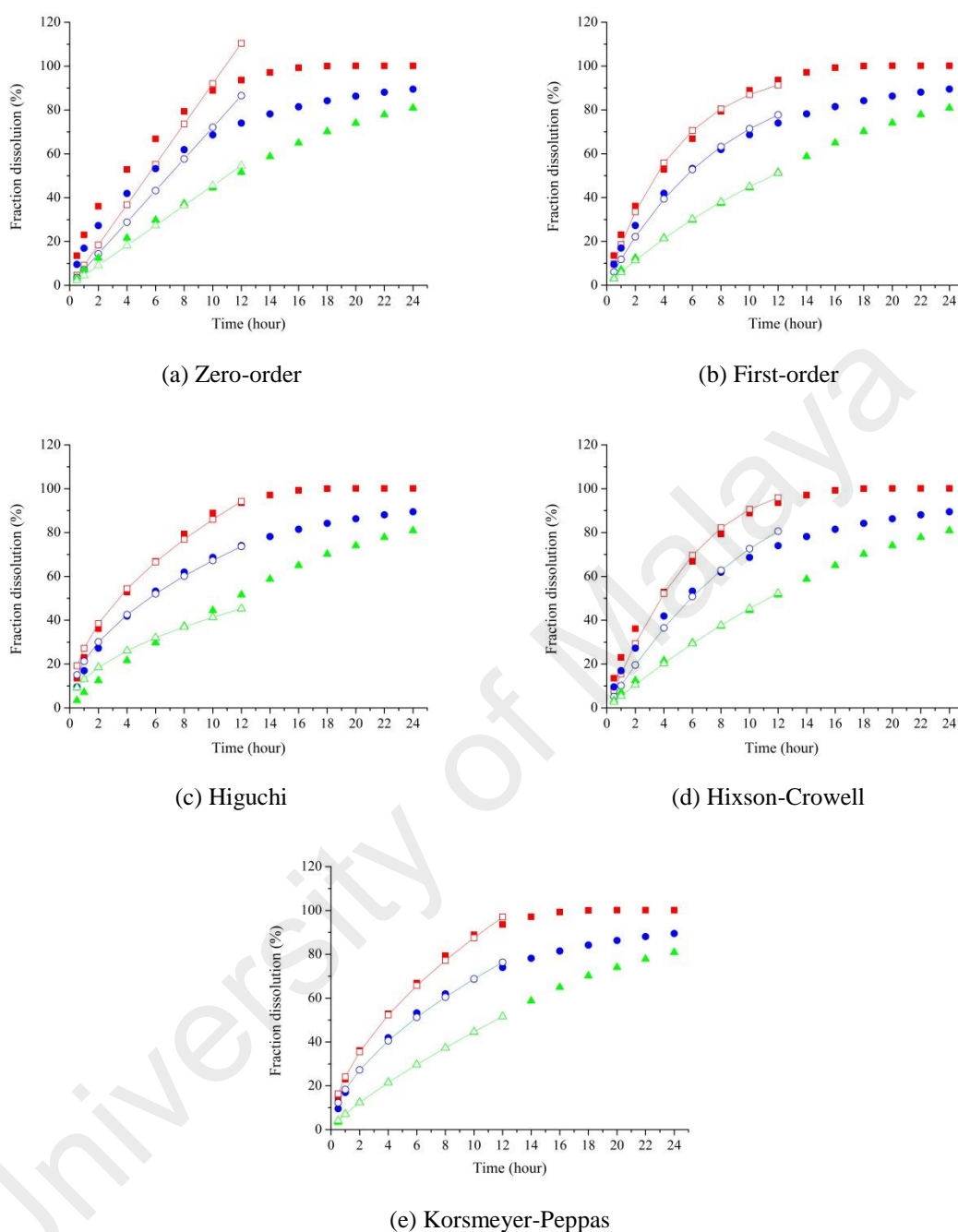


Figure 4.31: Curve fitting of active ingredients' release profile from liposome in different kinetic models for the first 12 hours. Where symbol \square = ascorbic acid, \circ = caffeine, Δ = lidocaine. The solid symbol represents the experimental plot while the opened symbol with line represents the predicted plot.

4.3.4 Release profile of water-in-oil microemulsion

The release profile of active ingredients from microemulsion can evidently represent the ability of the active ingredients to be soluble in the oil phase. The cumulative

percentage release of active ingredient is in an ascending order of ascorbic acid < caffeine < lidocaine (Figure 4.32).

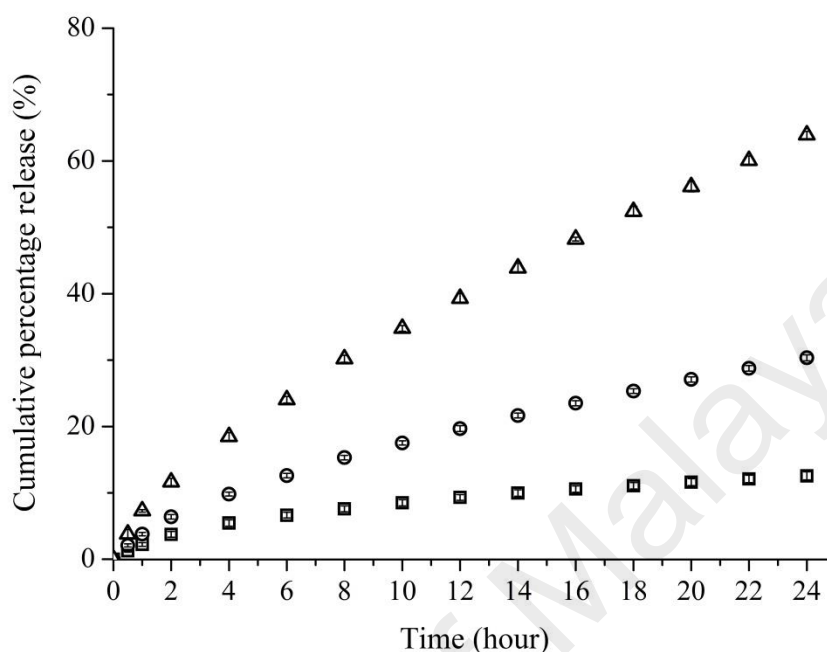


Figure 4.32: Release profile of active ingredients from water-in-oil microemulsion for 24 hours. Where symbol \square = ascorbic acid, \circ = caffeine, Δ = lidocaine.

ST80 microemulsion exhibits slow release behavior as the cumulative percentage release of active ingredients reached at most 64 % after 24 hours. The release of active ingredients from water-in-oil microemulsion depends on the partition coefficient of the active ingredients to the oil phase. Lidocaine, which is more hydrophobic than caffeine and ascorbic acid, solubilized freely in oil. Hence, lidocaine can be partition easily into the oil phase for release compared to caffeine and ascorbic acid. As a consequence, the release of lidocaine from ST80 was shown to be two folds and four folds faster than caffeine and ascorbic acid.

In addition, the release profile was fitted into various kinetic models to describe the possible mechanism of active ingredients' release from ST80. Their linear regression to the release curve and the rate constant were obtained by using DDSolver. The result for

24 hours curve fitting was tabulated in Table 4.19 and their curve fitting in zero-order model, first-order model, Higuchi model, Hixson-Crowell model and Korsmeyer-Peppas model were shown in Figure 4.33(a), Figure 4.33(b), Figure 4.33(c), Figure 4.33(d) and Figure 4.33(e) respectively.

Table 4.19: Active ingredients' rate constant and the linear regression of release curve from microemulsion after curve fit in different kinetic models for 24 hours

	Ascorbic acid	Caffeine	Lidocaine
Zero-order, k_0 ($\mu\text{g h}^{-1}$)	0.630 $R^2 = 0.701$	1.424 $R^2 = 0.901$	2.928 $R^2 = 0.939$
First-order, k_1 (h^{-1})	0.007 $R^2 = 0.739$	0.017 $R^2 = 0.943$	0.042 $R^2 = 0.992$
Higuchi, k_H ($\mu\text{g h}^{-1/2}$)	2.623 $R^2 = 0.995$	5.834 $R^2 = 0.976$	11.929 $R^2 = 0.960$
Hixson-Crowell, k_{HC} ($\mu\text{g h}^{-1}$)	0.002 $R^2 = 0.727$	0.005 $R^2 = 0.931$	0.013 $R^2 = 0.983$
Korsmeyer-Peppas, k_{KP} (h^{-n})	2.656 $R^2 = 0.995$	4.035 $R^2 = 0.999$	7.045 $R^2 = 0.999$

Among all of the kinetic models, release of active ingredients from water-in-oil microemulsion has the closest linear regression to both the Higuchi and Korsmeyer-Peppas models. In Higuchi model, it is being presumed that the initial drug concentration in the matrix is much higher than drug solubility; drug diffusion takes place only in one dimension; drug particles are much smaller than system thickness; matrix swelling and dissolution are negligible; drug diffusivity is constant and perfect sink conditions are always attained in the release environment. Whereas, in Korsmeyer-Peppas model, the mechanisms for release of active ingredients are in the order of solvent diffusion into the polymeric system, swelling of polymeric system, formation of gel, diffusion of active ingredients out of the polymeric system and dissolution of the polymeric system's matrix. Between the two models, Higuchi model would be a more appropriate model to describe the release of active ingredients from ST80 because swelling and dissolution of ST80 is negligible in this system.

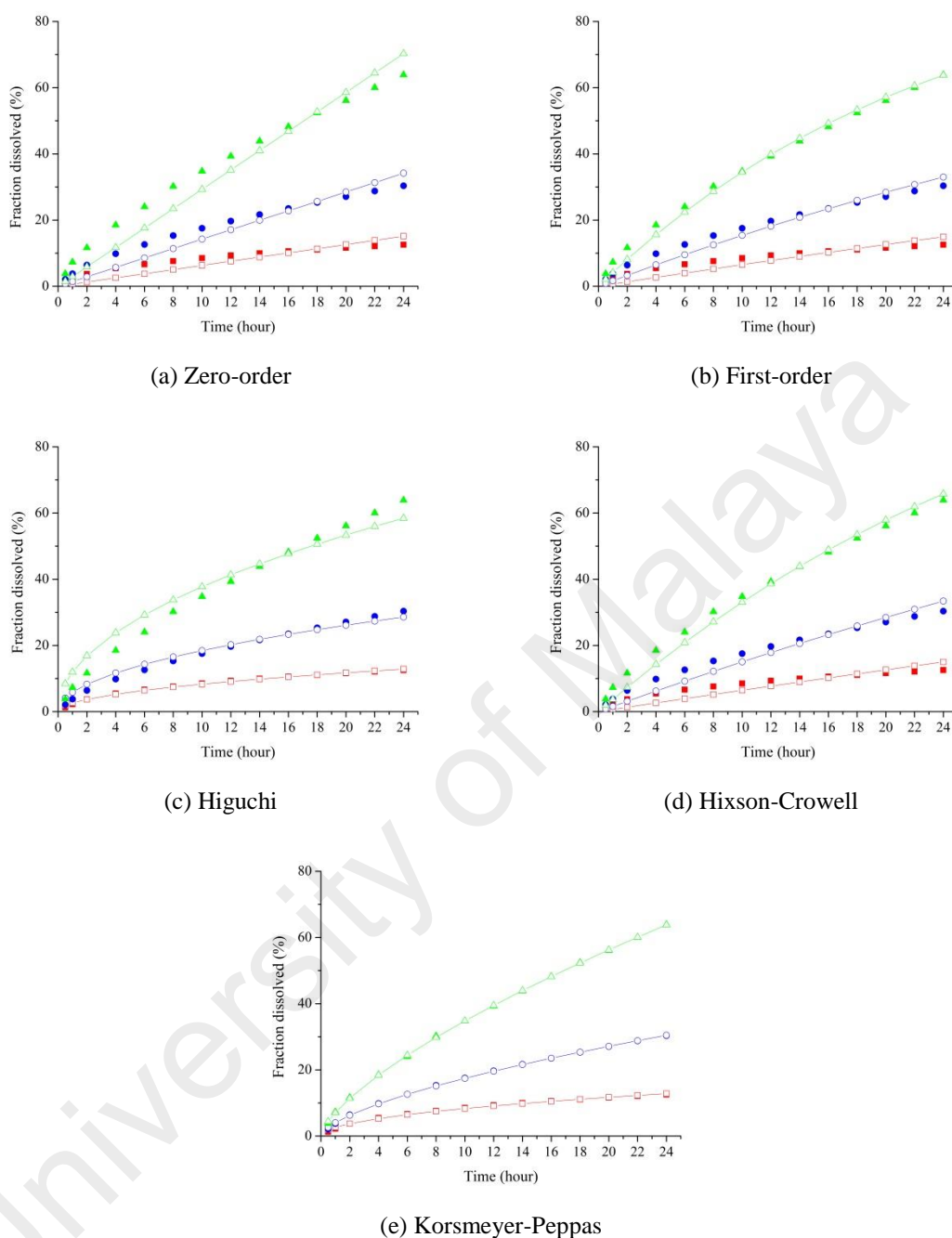


Figure 4.33: Curve fitting of active ingredients' release profile from water-in-oil microemulsion in different kinetic models for 24 hours. Where symbol \square = ascorbic acid, \circ = caffeine, Δ = lidocaine. The solid symbol represents the experimental plot while the opened symbol with line represents the predicted plot.

In order to further evaluate the mechanism, the first 12 hours of release profile was curve fitted into various kinetic models. The rate constant and their linear regression was tabulated in Table 4.20 whereas their curve fitting plot in zero-order model, first-order model, Higuchi model, Hixson-Crowell model and Korsmeyer-Peppas model

were shown in Figure 4.34(a), Figure 4.34(b), Figure 4.34(c), Figure 4.34(d) and Figure 4.34(e) respectively.

Table 4.20: Active ingredients' rate constant and the linear regression of release curve from microemulsion after curve fit in different kinetic models for first 12 hours

	Ascorbic acid	Caffeine	Lidocaine
Zero-order, k_0 ($\mu\text{g h}^{-1}$)	0.902 $R^2 = 0.773$	1.824 $R^2 = 0.905$	3.591 $R^2 = 0.934$
First-order, k_1 (h^{-1})	0.009 $R^2 = 0.795$	0.020 $R^2 = 0.932$	0.044 $R^2 = 0.974$
Higuchi, k_H ($\mu\text{g h}^{-1/2}$)	2.671 $R^2 = 0.990$	5.326 $R^2 = 0.968$	10.431 $R^2 = 0.955$
Hixson-Crowell, k_{HC} ($\mu\text{g h}^{-1}$)	0.003 $R^2 = 0.788$	0.007 $R^2 = 0.923$	0.014 $R^2 = 0.963$
Korsmeyer-Peppas, k_{KP} (h^{-n})	2.434 $R^2 = 0.994$	3.924 $R^2 = 0.999$	7.062 $R^2 = 0.999$

Similar to curve fitting of 24 hours, the first 12 hours of active ingredients release from ST80 falls into either Higuchi model or Korsmeyer-Peppas model. Even though the active ingredients' release profile has a closer linear regression to Korsmeyer-Peppas model, Higuchi model is the more suitable model to describe the release of active ingredients from ST80. The pathway taken is first the partition of the active ingredients from aqueous disperse phase into oil continuous phase. This depends on the partition coefficient of the active ingredients into olive oil. Lidocaine which is the most soluble active ingredients in olive oil, ease the partition of lidocaine into the oil phase compared to the other two active ingredients. The active ingredients which gradually increased their concentration in continuous phase through partition, creates a chemical potential in the donor chamber. This chemical potential gradient enabled the active ingredients to be diffused through the separation membrane into the receptor chamber.

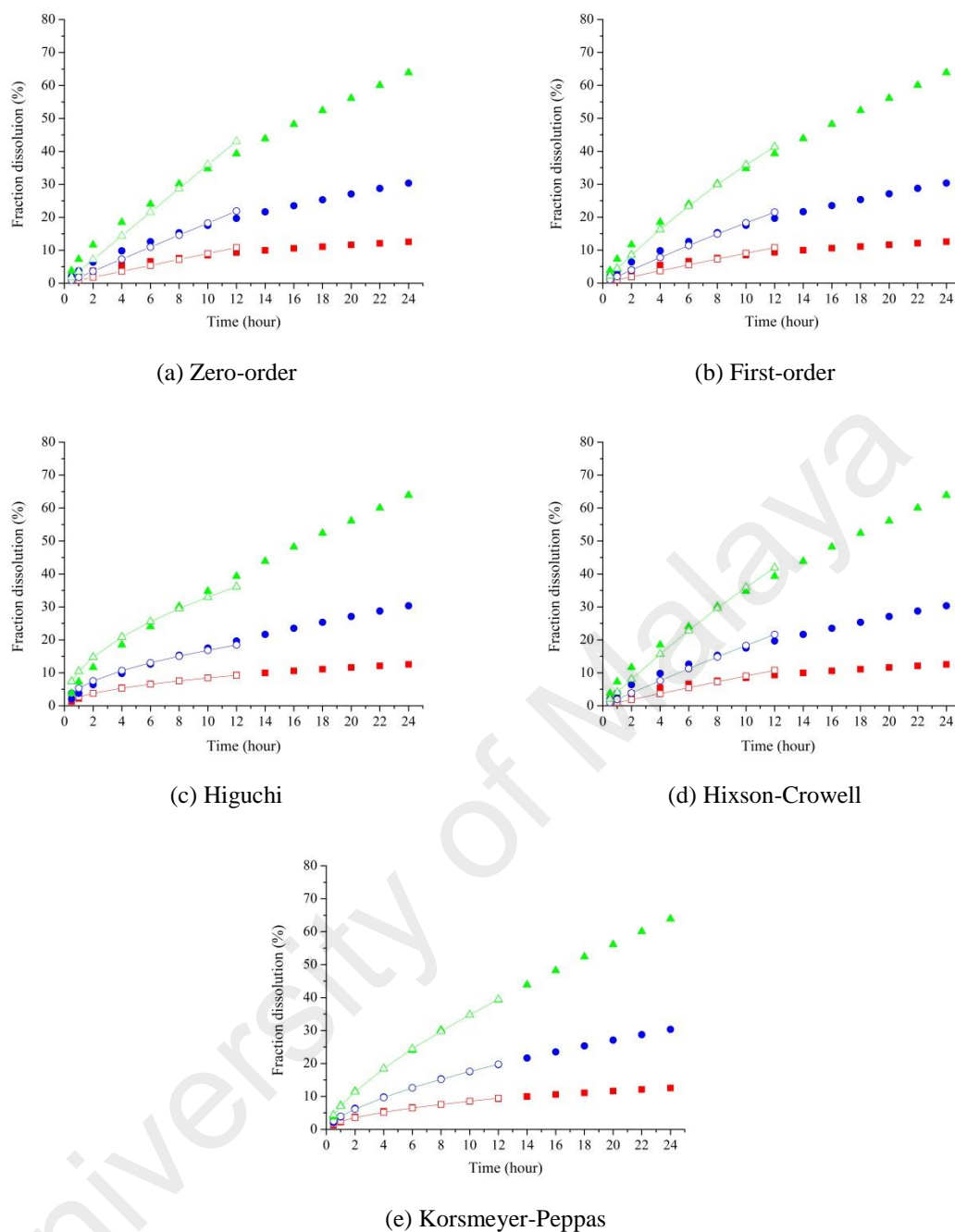


Figure 4.34: Curve fitting of active ingredients' release profile from microemulsion in different kinetic models for the first 12 hours. Where symbol □ = ascorbic acid, ○ = caffeine, Δ = lidocaine. The solid symbol represents the experimental plot while the opened symbol with line represents the predicted plot.

4.3.5 Release profile of κ -carrageenan-chitosan nanoparticle

The cumulative percentage release of active ingredients from the κ -carrageenan-chitosan nanoparticle was shown to be very low (Figure 4.35) as compared to the other three systems being described previously. The release profile of active ingredients from

κ -carrageenan-chitosan nanoparticle is in the ascending order of ascorbic acid < caffeine < lidocaine. It was unexpected that the ascorbic acid and caffeine which is freely soluble in water and sparingly soluble in water respectively, had a lower release rate than lidocaine which is slightly soluble in water. This might deduce that ascorbic acid, which was ionized at pH 7.4 would take a longer time to overcome the ionic forces before it could be released to the continuous phase. Lidocaine, which is more hydrophobic could repulse more easily to the continuous phase, thereby a higher amount of release could be attained (Boonsongrit *et al.*, 2006). Sudden increased in release of lidocaine after 14 hours could be attributed to the compactness of dried κ -carrageenan-chitosan nanoparticle, where more energy is required to overcome the barrier for release.

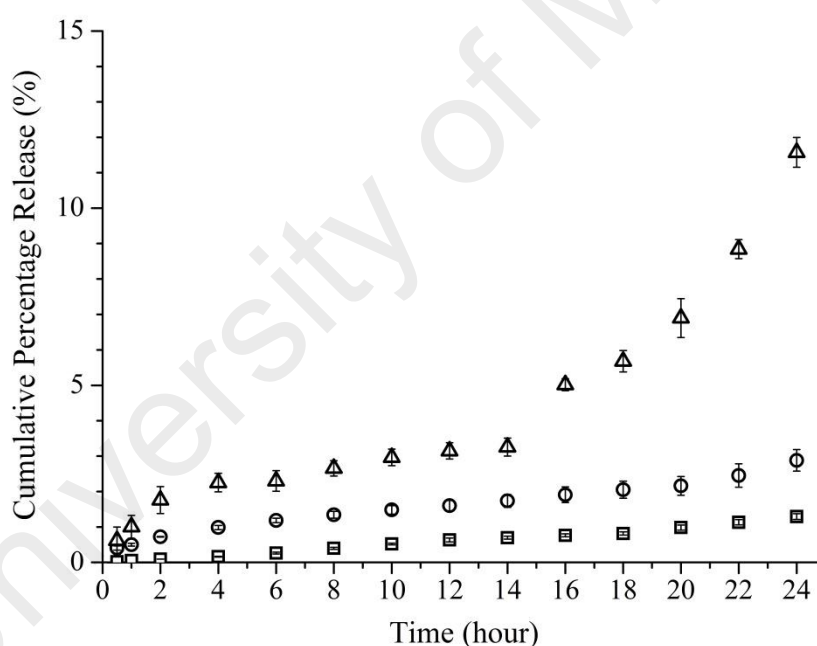


Figure 4.35: Release profile of active ingredients from κ -carrageenan-chitosan nanoparticle for 24 hours. Where symbol \square = ascorbic acid, \circ = caffeine, Δ = lidocaine.

The κ -carrageenan-chitosan nanoparticle, which has a low cumulative percentage release of active ingredients were fitted into different kinetic models. Their linear regression to the release curve and the rate constant were obtained by using DDSolver. The result for 24 hours curve fitting was tabulated in Table 4.21 and their curve fitting

in zero-order model, first-order model, Higuchi model, Hixson-Crowell model and Korsmeyer-Peppas model were shown in Figure 4.36(a), Figure 4.36(b), Figure 4.36(c), Figure 4.36(d) and Figure 4.36(e) respectively.

Table 4.21: Active ingredients' rate constant and the linear regression of release curve from κ -carrageenan-chitosan nanoparticle after curve fit in different kinetic models for 24 hours

	Ascorbic acid	Caffeine	Lidocaine
Zero-order, k_0 ($\mu\text{g h}^{-1}$)	0.050 $R^2 = 0.989$	0.122 $R^2 = 0.811$	0.367 $R^2 = 0.860$
First-order, k_1 (h^{-1})	0.001 $R^2 = 0.990$	0.001 $R^2 = 0.815$	0.004 $R^2 = 0.853$
Higuchi, k_H ($\mu\text{g h}^{-1/2}$)	0.199 $R^2 = 0.832$	0.501 $R^2 = 0.961$	1.443 $R^2 = 0.684$
Hixson-Crowell, k_{HC} ($\mu\text{g h}^{-1}$)	0.000 $R^2 = 0.990$	0.000 $R^2 = 0.813$	0.001 $R^2 = 0.855$
Korsmeyer-Peppas, k_{KP} (h^{-n})	0.041 $R^2 = 0.991$	0.421 $R^2 = 0.965$	0.078 $R^2 = 0.890$

It was found that Korsmeyer-Peppas model was the best to describe the release profile of κ -carrageenan-chitosan nanoparticle. The curve fitting into Korsmeyer-Peppas model was anticipated as the model was usually applied on polymeric system. In Korsmeyer-Peppas model, the mechanisms for release of active ingredients are in the steps of solvent diffusion into the polymeric system, swelling of polymeric system, formation of gel, diffusion of active ingredients out of the polymeric system and dissolution of the polymeric system's matrix. It was believed that active ingredients encapsulated in κ -carrageenan-chitosan nanoparticle was being released by repulsion and diffusion because there was no significant loss in mass of the κ -carrageenan-chitosan nanoparticle after a long period swelling in the pH 7.4 phosphate buffer solution.

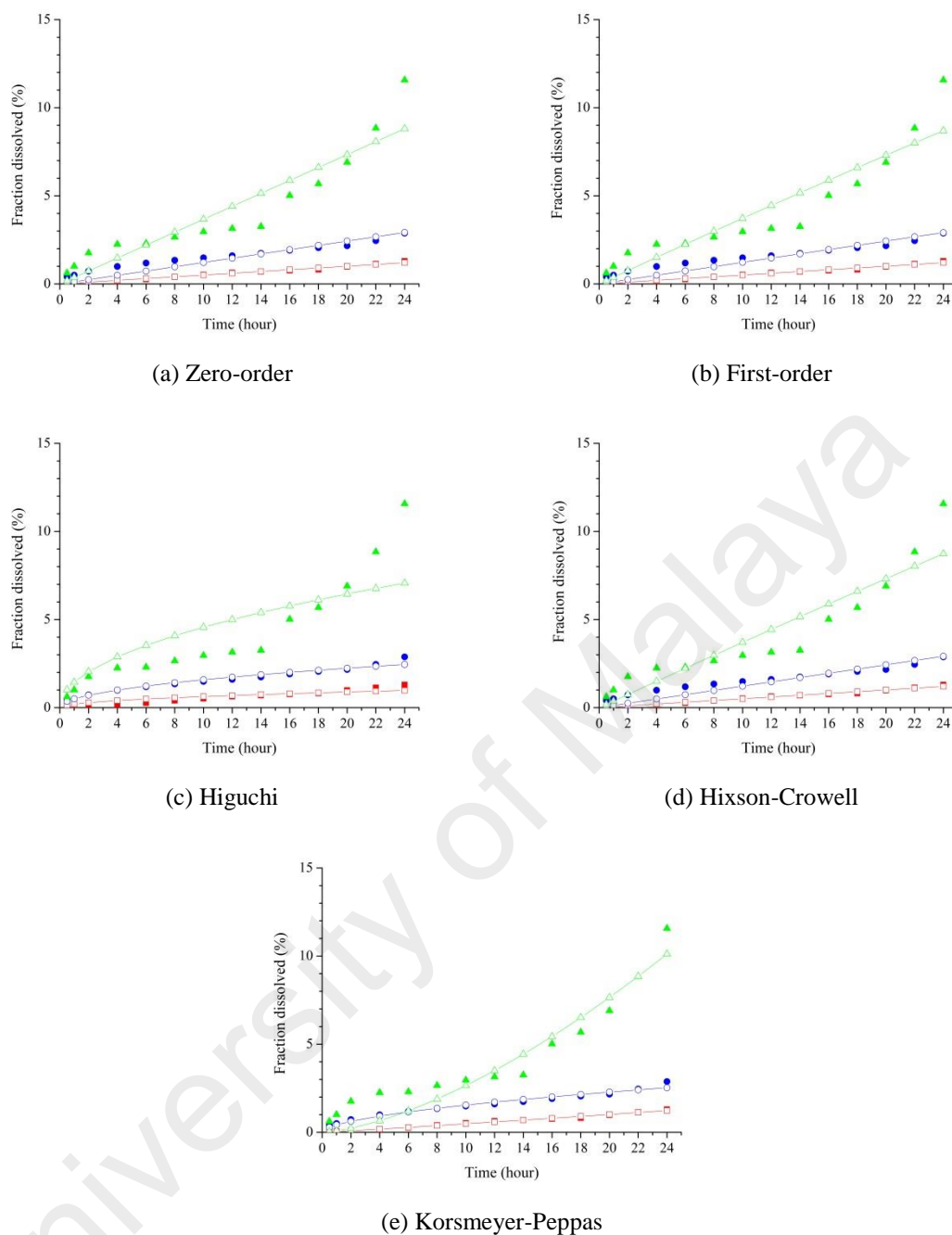


Figure 4.36: Curve fitting of active ingredients' release profile from κ -carrageenan-chitosan nanoparticle in different kinetic models for 24 hours. Where symbol \square = ascorbic acid, \circ = caffeine, Δ = lidocaine. The solid symbol represents the experimental plot while the opened symbol with line represents the predicted plot.

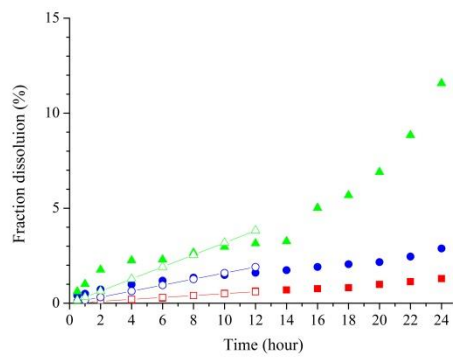
Despite that the Korsmeyer-Peppas model was shown to have the closest linear regression to the original plot of active ingredient release, the R^2 value was still far from expectation. For that reason, the first 12 hours of active ingredients release profile was curve fitted into various kinetic models to further evaluate the possible mechanism. The

rate constant and their linear regression were tabulated in Table 4.22 whereas curve fitting of plot in zero-order model, first-order model, Higuchi model, Hixson-Crowell model and Korsmeyer-Peppas model were shown in Figure 4.37(a), Figure 4.37(b), Figure 4.37(c), Figure 4.37(d) and Figure 4.37(e) respectively.

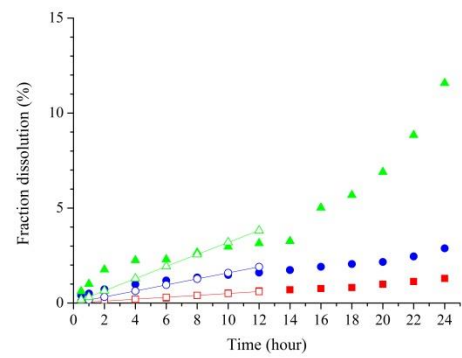
Table 4.22: Active ingredients' rate of release from κ -carrageenan-chitosan nanoparticle after curve fitting in different kinetic models for the first 12 hours

	Ascorbic acid	Caffeine	Lidocaine
Zero-order, k_0 ($\mu\text{g h}^{-1}$)	0.051 $R^2 = 0.988$	0.159 $R^2 = 0.528$	0.318 $R^2 = 0.379$
First-order, k_1 (h^{-1})	0.001 $R^2 = 0.988$	0.002 $R^2 = 0.533$	0.003 $R^2 = 0.392$
Higuchi, k_H ($\mu\text{g h}^{-1/2}$)	0.141 $R^2 = 0.798$	0.476 $R^2 = 0.992$	0.962 $R^2 = 0.944$
Hixson-Crowell, k_{HC} ($\mu\text{g h}^{-1}$)	0.000 $R^2 = 0.988$	0.001 $R^2 = 0.532$	0.001 $R^2 = 0.388$
Korsmeyer-Peppas, k_{KP} (h^{-n})	0.034 $R^2 = 0.997$	0.528 $R^2 = 0.999$	1.132 $R^2 = 0.966$

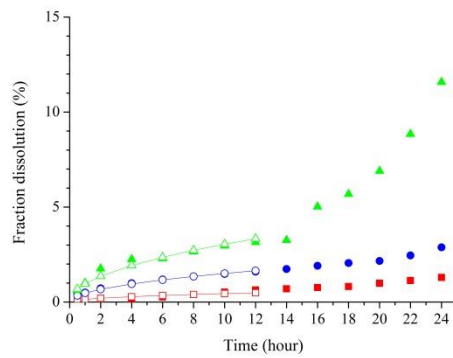
From the result, it can be clearly seen that Korsmeyer-Peppas model is the best to describe the release of active ingredients from κ -carrageenan-chitosan nanoparticle for the first 12 hours. Regardless to the type of active ingredients, the R^2 values were the closest to the active ingredients cumulative plots with the minimum value of 0.966. The n value for ascorbic acid release which was higher than 1.00 indicated super case II transport. The other two active ingredients, caffeine and lidocaine had n values which were lesser than 0.50 indicated Fickian diffusion. For super case II transport, it suggested that the release of active ingredients from κ -carrageenan-chitosan nanoparticle involved swelling and relaxation of the polymer whereas for Fickian diffusion, the mechanisms involved polymer relaxation followed by diffusion of active ingredients (Sahoo *et al.*, 2012).



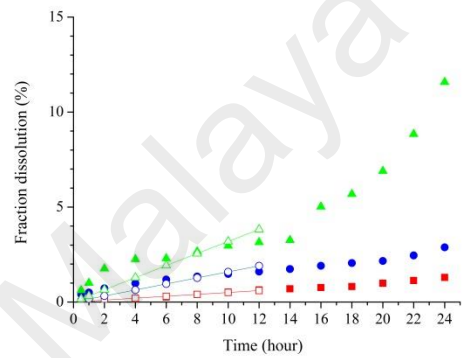
(a) Zero-order



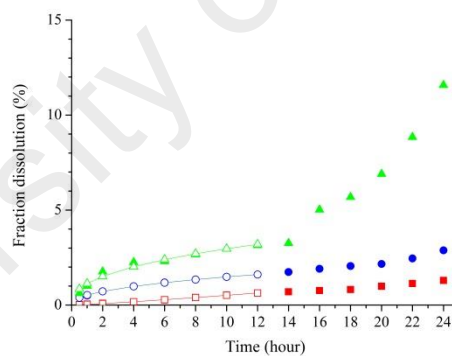
(b) First-order



(c) Higuchi



(d) Hixson-Crowell



(e) Korsmeyer-Peppas

Figure 4.37: Curve fitting of active ingredients' release profile from κ -carrageenan-chitosan nanoparticle in different kinetic models for the first 12 hours. Where symbol \square = ascorbic acid, \circ = caffeine, Δ = lidocaine. The solid symbol represents the experimental plot while the opened symbol with line represents the predicted plot.

CHAPTER 5: CONCLUSION

5.1 Summary

As a summary, each of the system has been characterized to select the best formulation for the encapsulation and release of active ingredients with varied solubility in water, namely ascorbic acid which is soluble in water, caffeine which is sparingly soluble in water and lidocaine which is slightly soluble in water. A short summary on each systems were described.

NLC is a lipid nanoparticle dispersed in aqueous continuous phase. Among the five NLC formulations prepared by using fatty acid mixture and Span 40, NLC 3 showed to be the most suitable formulation. NLC 3 exhibit high stability in continuous particle size and zeta potential measurements, good thermal profile in DSC evaluation, and with acceptable morphology when visualized under TEM. NLC is efficient in encapsulating lidocaine followed by caffeine and ascorbic acid. Nevertheless, the zeta potential of the active ingredients will affect the physical properties of the NLC. As a result, this will caused adsorption of active ingredients on the NLC and further induced aggregation of the NLC. The release of active ingredients from NLC was slower than the unencapsulated active ingredients, indicated the possibility of NLC as a slow release delivery carrier. In addition, the release has a good linear regression towards first-order model suggest that the release is concentration dependent.

Fatty acid liposome is a lipid bilayer with an aqueous core suspend in aqueous continuous phase. It is a pH sensitive liposome whereby it changes its phases according to the changes of pH. Among the three fatty acid liposomes, the oleic acid liposome displayed the best physical properties as it had the lowest critical vesicle concentration of 0.09 mM, a stable particle size of approximately 100 nm, and the highest loading

capacity compared to linoleic acid and linolenic acid liposomes. The loading efficiencies of the active ingredients in the liposomes were correlated to the degree of unsaturation of the fatty acids, whereby those with more unsaturated double bonds had lower encapsulation efficiencies. Liposome is expedient in encapsulating different types of active ingredients, particularly those with high hydrophobicity. The release profile of active ingredients from the oleic acid liposome which is slightly slower than unencapsulated active ingredients suggested that the release could be fast burst from the continuous phase followed by slow release when the concentration was depleted. Additionally, this release kinetic follows first-order release which is depends on chemical potential gradient.

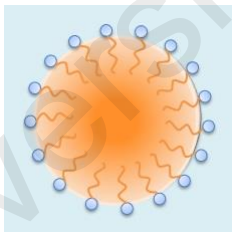
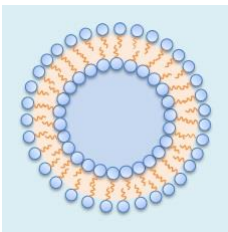
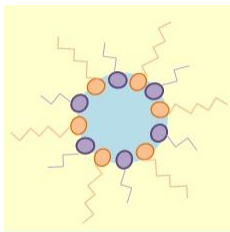
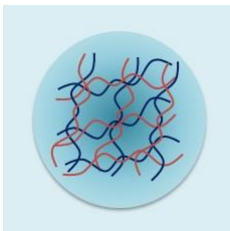
A stable water-in-oil microemulsion has been successfully prepared by a mild agitation of olive oil, water and non-ionic mixed surfactant. Among the microemulsions prepared, ST80 is more suitable for topical application as it has a better pH and higher viscosity as compared to ST85, and it is smaller in size as compared to ST40 and ST60 due to its critical packing parameters of surfactants. ST80 is also suitable as a model for the loading of many types of active ingredients. Results obtained from the active ingredients' release study show that the release profile is hydrophobicity dependent. Lidocaine, which is more hydrophobic, has a higher release rate from the microemulsion to the receptor chamber as compared to slightly soluble in water caffeine and very soluble in water ascorbic acid. The slow constant release rate of the active ingredients suggests sustained release properties of the ST80 microemulsion. In addition, the best kinetic model to describe the release would be Higuchi model.

Based on the new absorption band at 1584 cm^{-1} and TEM micrographs, κ -carrageenan-chitosan nanoparticle was shown to be successfully synthesized. The particle size, zeta

potential, yield percentage and swelling percentage are highly affected by the composition of polymers and the pH of solution. The encapsulation efficiency of κ -carrageenan-chitosan nanoparticle exhibited higher preference towards more water soluble active ingredients. Nevertheless, the release profile exhibit a reverse pattern whereby those which is less water soluble could release at faster rate. This is attributed by ionic interaction between the active ingredients and polymer whereby it could strongly retain in the κ -carrageenan-chitosan nanoparticle. The release profile suggested that κ -carrageenan-chitosan nanoparticle is suitable for prolonged release. The release kinetic follows Korsmeyer-Peppas model indicated that the release involved the swelling and relaxation of the polymers.

The properties of each delivery vehicles were summarized as in Table 5.1.

Table 5.1: The properties of each active ingredient's delivery vehicles

	NLC	Liposome	Water-in-oil microemulsion	κ -carrageenan-chitosan nanoparticle
Schematic diagram				
Disperse phase	Oil	Oil	Aqueous	Polymer in aqueous
Continuous phase	Aqueous	Aqueous	Oil	Aqueous
Average particle size	~250 nm	~100 nm	~30 nm	~400 nm
Morphology	Rounded to elongated	Rounded	Rounded	Rounded to irregular
Encapsulation efficiency	Excellent for hydrophobic active ingredients	Excellent for hydrophobic active ingredients	Excellent for hydrophilic active ingredients	Low encapsulation for all active ingredients
Kinetic models	First-order model	First-order model	Higuchi model	Korsmeyer-Peppas model

The pathways taken for the release of sparingly water soluble active ingredient in each delivery carrier from donor chamber to receptor chamber of NLC, liposome, water-in-oil microemulsion and κ -carrageenan-chitosan nanoparticle was illustrated as in the scheme as Figure 5.1(a), Figure 5.2(b), Figure 5.2(c) and Figure 5.2(d) respectively.

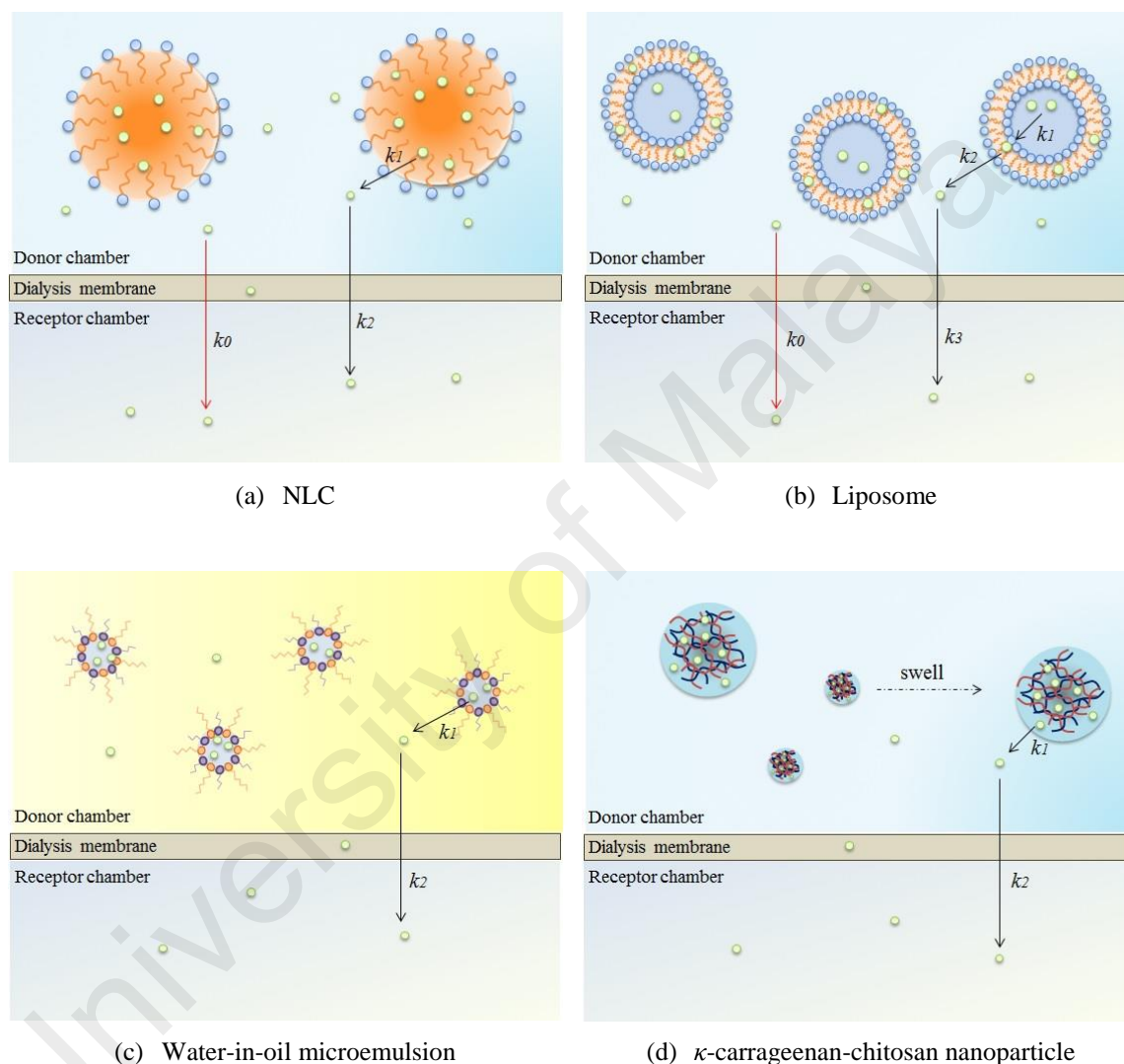


Figure 5.1: The proposed mechanism of the release of sparingly water soluble active ingredients in different delivery system. k_0 with red arrow indicates the release of unencapsulated active ingredients from donor chamber into receptor chamber. k_1 , k_2 , and k_3 with black arrow indicate the release of encapsulated active ingredients released from the respective delivery carrier. The color blue indicate aqueous phase whereas yellow color indicate oil phase. The size of the particle is in correlation to the size obtained from DLS.

5.2 Future work

As a continuum of this research work, there are more aspects that can be explored:

- *In vitro* cell culture studies to evaluate the possible cytotoxicity of the formulations on cell lines;
- Irritancy test to assess the safety of the formulation for topical application;
- *In vivo* animal studies to evaluate the efficacy and dosage for optimum therapeutic effect.

University of Malaya

REFERENCE

- Adibhatla, R. M., Hatcher, J., & Tureyen, K. (2005). CDP-choline liposomes provide significant reduction in infarction over free CDP-choline in stroke. *Brain Research*, 1058(1), 193-197.
- Aditya, N. P., Macedo, A. S., Doktorovova, S., Souto, E. B., Kim, S., Chang, P.-S., & Ko, S. (2014). Development and evaluation of lipid nanocarriers for quercetin delivery: A comparative study of solid lipid nanoparticles (SLN), nanostructured lipid carriers (NLC), and lipid nanoemulsions (LNE). *LWT-Food Science and Technology*, 59(1), 115-121.
- Agrawal, Y., Petkar, K. C., & Sawant, K. K. (2010). Development, evaluation and clinical studies of Acitretin loaded nanostructured lipid carriers for topical treatment of psoriasis. *International Journal of Pharmaceutics*, 401(1), 93-102.
- Ahmad, J., Mir, S. R., Kohli, K., & Amin, S. (2014). Effect of oil and co-surfactant on the formation of Solutol HS 15 based colloidal drug carrier by Box–Behnken statistical design. *Colloids and Surfaces A: Physicochemical and Engineering Aspects*, 453, 68-77.
- Ahmad, Z. (2010). The uses and properties of almond oil. *Complementary Therapies in Clinical Practice*, 16(1), 10-12.
- Akbarzadeh, A., Rezaei-Sadabady, R., Davaran, S., Joo, S. W., Zarghami, N., Hanifehpour, Y., Samiei, M., Kouhi, M., & Nejati-Koshki, K. (2013). Liposome: classification, preparation, and applications. *Nanoscale Research Letters*, 8(1), 102.
- Allen, T. M., & Martin, F. J. (2004). Advantages of liposomal delivery systems for anthracyclines. *Seminars in Oncology*, 31 (S13), 5-15.
- Almeida, A. J., & Souto, E. (2007). Solid lipid nanoparticles as a drug delivery system for peptides and proteins. *Advanced Drug Delivery Reviews*, 59(6), 478-490.
- Alves, N. M., & Mano, J. F. (2008). Chitosan derivatives obtained by chemical modifications for biomedical and environmental applications. *International Journal of Biological Macromolecules*, 43(5), 401-414.
- Andrade, L. M., de Fátima Reis, C., Maione-Silva, L., Anjos, J. L. V., Alonso, A., Serpa, R. C., Marreto, R. N., Lima, E. M., & Taveira, S. F. (2014). Impact of lipid dynamic behavior on physical stability, in vitro release and skin permeation of genistein-loaded lipid nanoparticles. *European Journal of Pharmaceutics and Biopharmaceutics*, 88(1), 40-47.
- Anjali, C. H., Dash, M., Chandrasekaran, N., & Mukherjee, A. (2010). Antibacterial activity of sunflower oil microemulsion. *International Journal of Pharmacy and Pharmaceutical Sciences*, 2, 123-128.

- Anusuya, S., & Sathiyabama, M. (2014). Preparation of β -d-glucan nanoparticles and its antifungal activity. *International Journal of Biological Macromolecules*, 70, 440-443.
- Apel, C. L., Deamer, D. W., & Mautner, M. N. (2002). Self-assembled vesicles of monocarboxylic acids and alcohols: conditions for stability and for the encapsulation of biopolymers. *Biochimica et Biophysica Acta (BBA)-Biomembranes*, 1559(1), 1-9.
- Araújo, J., Garcia, M. L., Mallandrich, M., Souto, E. B., & Calpena, A. C. (2012). Release profile and transscleral permeation of triamcinolone acetonide loaded nanostructured lipid carriers (TA-NLC): in vitro and ex vivo studies. *Nanomedicine: Nanotechnology, Biology and Medicine*, 8(6), 1034-1041.
- Auguste, D. T., Furman, K., Wong, A., Fuller, J., Armes, S. P., Deming, T. J., & Langer, R. (2008). Triggered release of siRNA from poly (ethylene glycol)-protected, pH-dependent liposomes. *Journal of Controlled Release*, 130(3), 266-274.
- Badolato, G. G., Aguilar, F., Schuchmann, H. P., Sobisch, T., & Lerche, D. (2008). Evaluation of long term stability of model emulsions by multisample analytical centrifugation. In Kremer, F. & Richtering, W. (Eds.), *Progress in Colloid and Polymer Science* (pp. 66-73). New York, USA: Springer.
- Banerjee, T., Mitra, S., Singh, A. K., Sharma, R. K., & Maitra, A. (2002). Preparation, characterization and biodistribution of ultrafine chitosan nanoparticles. *International Journal of Pharmaceutics*, 243(1), 93-105.
- Barrajón-Catalán, E., Menéndez-Gutiérrez, M. P., Falco, A., Carrato, A., Saceda, M., & Micol, V. (2010). Selective death of human breast cancer cells by lytic immunoliposomes: Correlation with their HER2 expression level. *Cancer Letters*, 290(2), 192-203.
- Basheer, H. S., Noordin, M. I., & Ghareeb, M. M. (2013). Characterization of microemulsion prepared using isopropyl palmitate with various surfactants and cosurfactants. *Tropical Journal of Pharmaceutical Research*, 12(3), 305-310.
- Berger, J., Reist, M., Mayer, J. M., Felt, O., Peppas, N., & Gurny, R. (2004). Structure and interactions in covalently and ionically crosslinked chitosan hydrogels for biomedical applications. *European Journal of Pharmaceutics and Biopharmaceutics*, 57(1), 19-34.
- Bhalekar, M. R., Pokharkar, V., Madgulkar, A., Patil, N., & Patil, N. (2009). Preparation and evaluation of miconazole nitrate-loaded solid lipid nanoparticles for topical delivery. *AAPS PharmSciTech*, 10(1), 289-296.
- Bilensoy, E., Sarisozen, C., Esendağlı, G., Doğan, A. L., Aktaş, Y., Şen, M., & Mungan, N. A. (2009). Intravesical cationic nanoparticles of chitosan and polycaprolactone for the delivery of Mitomycin C to bladder tumors. *International Journal of Pharmaceutics*, 371(1), 170-176.

- Boonsongrit, Y., Mitrevej, A., & Mueller, B. W. (2006). Chitosan drug binding by ionic interaction. *European Journal of Pharmaceutical and Biopharmaceutical*, 62(3), 267-274.
- Bravo-Osuna, I., Vauthier, C., Farabollini, A., Palmieri, G. F., & Ponchel, G. (2007). Mucoadhesion mechanism of chitosan and thiolated chitosan-poly (isobutyl cyanoacrylate) core-shell nanoparticles. *Biomaterials*, 28(13), 2233-2243.
- Brugè, F., Damiani, E., Puglia, C., Offerta, A., Armeni, T., Littarru, G. P., & Tiano, L. (2013). Nanostructured lipid carriers loaded with CoQ 10: Effect on human dermal fibroblasts under normal and UVA-mediated oxidative conditions. *International Journal of Pharmaceutics*, 455(1), 348-356.
- Bumajdad, A., & Eastoe, J. (2004). Conductivity of water-in-oil microemulsions stabilized by mixed surfactants. *Journal of Colloid and Interface Science*, 274(1), 268-276.
- Carafa, M., Marianecchi, C., Annibaldi, V., Di Stefano, A., Sozio, P., & Santucci, E. (2006). Novel O-palmitoylscleroglucan-coated liposomes as drug carriers: Development, characterization and interaction with leuprolide. *International Journal of Pharmaceutics*, 325(1), 155-162.
- Carbone, C., Campisi, A., Manno, D., Serra, A., Spatuzza, M., Musumeci, T., Bonfanti, R., & Puglisi, G. (2014). The critical role of didodecyldimethylammonium bromide on physico-chemical, technological and biological properties of NLC. *Colloids and surfaces B: Biointerfaces*, 121, 1-10.
- Carneiro, T. N., Novaes, D. S., Rabelo, R. B., Celebi, B., Chevallier, P., Mantovani, D., Beppu, M. M., & Vieira, R. S. (2013). BSA and fibrinogen adsorption on chitosan/ κ -carrageenan polyelectrolyte complexes. *Macromolecular Bioscience*, 13(8), 1072-1083.
- Castelli, F., Puglia, C., Sarpietro, M. G., Rizza, L., & Bonina, F. (2005). Characterization of indomethacin-loaded lipid nanoparticles by differential scanning calorimetry. *International Journal of Pharmaceutics*, 304(1), 231-238.
- Castro, G. A., Coelho, A. L. L., Oliveira, C. A., Mahecha, G. A. B., Oréfice, R. L., & Ferreira, L. A. M. (2009). Formation of ion pairing as an alternative to improve encapsulation and stability and to reduce skin irritation of retinoic acid loaded in solid lipid nanoparticles. *International Journal of Pharmaceutics*, 381(1), 77-83.
- Chang, H.-I., & Yeh, M.-K. (2012). Clinical development of liposome-based drugs: formulation, characterization, and therapeutic efficacy. *International Journal of Nanomedicine*, 7, 49-60.
- Charcosset, C., Juban, A., Valour, J.-P., Urbaniak, S., & Fessi, H. (2014). Preparation of liposomes at large scale using the ethanol injection method: Effect of scale-up and injection devices. *Chemical Engineering Research and Design*, 94, 508-515.

- Chattopadhyay, A., & Paila, Y. D. (2007). Lipid–protein interactions, regulation and dysfunction of brain cholesterol. *Biochemical and Biophysical Research Communications*, 354(3), 627-633.
- Chen, H., Chang, X., Weng, T., Zhao, X., Gao, Z., Yang, Y., Xu, H., & Yang, X. (2004). A study of microemulsion systems for transdermal delivery of triptolide. *Journal of Controlled Release*, 98(3), 427-436.
- Chen, M., Kumar, S., Anselmo, A. C., Gupta, V., Slee, D. H., Muraski, J. A., & Mitragotri, S. (2015). Topical delivery of Cyclosporine A into the skin using SPACE-peptide. *Journal of Controlled Release*, 199, 190-197.
- Chen, Y., Chen, Y., Nan, J., Wang, C., & Chu, F. (2011). Hollow poly(N-isopropylacrylamide)-co-poly(acrylic acid) microgels with high loading capacity for drugs. *Journal of Applied Polymer Science*, 124(6), 4678-4685.
- Chen, Y., Yang, X., Zhao, L., Almásy, L., Garamus, V. M., Willumeit, R., & Zou, A. (2014). Preparation and characterization of a nanostructured lipid carrier for a poorly soluble drug. *Colloids and Surfaces A: Physicochemical and Engineering Aspects*, 455, 36-43.
- Cheng, M.-B., Wang, J.-C., Li, Y.-H., Liu, X.-Y., Zhang, X., Chen, D.-W., Zhou, S.-F., & Zhang, Q. (2008). Characterization of water-in-oil microemulsion for oral delivery of earthworm fibrinolytic enzyme. *Journal of Controlled Release*, 129(1), 41-48.
- Chinsriwongkul, A., Chareanputtakhun, P., Ngawhirunpat, T., Rojanarata, T., Sila-on, W., Ruktanonchai, U., & Opanasopit, P. (2011). Nanostructured lipid carrier (NLC) for parenteral delivery of an anticancer drug. *AAPS PharmSciTech*, 13(1), 150-158.
- Cho, E. C., Lim, H. J., Kim, H. J., Son, E. D., Choi, H. J., Park, J. H., Kim, J.-W., & Kim, J. (2009). Role of pH-sensitive polymer–liposome complex in enhancing cellular uptake of biologically active drugs. *Materials Science and Engineering: C*, 29(3), 774-778.
- Cho, Y. I., Park, S., Jeong, S. Y., & Yoo, H. S. (2009). In vivo and in vitro anti-cancer activity of thermo-sensitive and photo-crosslinkable doxorubicin hydrogels composed of chitosan–doxorubicin conjugates. *European Journal of Pharmaceutics and Biopharmaceutics*, 73(1), 59-65.
- Cirri, M., Bragagni, M., Mennini, N., & Mura, P. (2012). Development of a new delivery system consisting in “drug-in cyclodextrin-in nanostructured lipid carriers” for ketoprofen topical delivery. *European Journal of Pharmaceutics and Biopharmaceutics*, 80(1), 46-53.
- Coimbra, M., Isacchi, B., van Bloois, L., Torano, J. S., Ket, A., Wu, X., Broere, F., Metselaar, J. M., Rijcken, C. J., & Storm, G. (2011). Improving solubility and

- chemical stability of natural compounds for medicinal use by incorporation into liposomes. *International Journal of Pharmaceutics*, 416(2), 433-442.
- Coimbra, P., Ferreira, P., De Sousa, H., Batista, P., Rodrigues, M., Correia, I., & Gil, M. (2011). Preparation and chemical and biological characterization of a pectin/chitosan polyelectrolyte complex scaffold for possible bone tissue engineering applications. *International Journal of Biological Macromolecules*, 48(1), 112-118.
- Ćurić, A., Reul, R., Möschwitzer, J., & Fricker, G. (2013). Formulation optimization of itraconazole loaded PEGylated liposomes for parenteral administration by using design of experiments. *International Journal of Pharmaceutics*, 448(1), 189-197.
- Daftarian, P. M., Stone, G. W., Kovalski, L., Kumar, M., Vosoughi, A., Urbietta, M., Blackwelder, P., Dikici, E., Serafini, P., Duffort, S., Boodoo, R., Rodríguez-Cortés, A., Lemmon, V., Deo, S., Alberola, J., Perez, V. L., Daunert, S., & Ager, A. L. (2013). A targeted and adjuvanted nanocarrier lowers the effective dose of liposomal amphotericin B and enhances adaptive immunity in murine cutaneous leishmaniasis. *The Journal of Infectious Diseases*, 208(11), 1914-1922.
- Dahan, A., Miller, J. M., & Amidon, G. L. (2009). Prediction of solubility and permeability class membership: Provisional BCS classification of the world's top oral drugs. *The AAPS Journal*, 11(4), 740-746.
- Dangi, A. A., Sorathiya, D., Sheth, N. R., Bagthariya, S. H., Solanki, S. M., & Chavda, A. (2011). Preparation and characteristic of solid lipid nanoparticles loaded with Rosiglitazone Maleate. *Inventi Rapid: NDDS*, 2011(3).
- Danhier, F., Feron, O., & Pr  at, V. (2010). To exploit the tumor microenvironment: Passive and active tumor targeting of nanocarriers for anti-cancer drug delivery. *Journal of Controlled Release*, 148(2), 135-146.
- Daniel-da-Silva, A. L., Lopes, A. B., Gil, A. M., & Correia, R. N. (2007). Synthesis and characterization of porous κ -carrageenan/calcium phosphate nanocomposite scaffolds. *Journal of Materials Science*, 42(20), 8581-8591.
- Dash, S., Murthy, P. N., Nath, L., & Chowdhury, P. (2010). Kinetic modelling on drug release from controlled drug delivery systems. *Acta Poloniae Pharmaceutica – Drug Research*, 67(3), 217-223.
- de Ara  jo, C. A., Nosed  , M. D., Cipriani, T. R., Goncalves, A. G., Duarte, M. E. R., & Ducatti, D. R. (2013). Selective sulfation of carrageenans and the influence of sulfate regiochemistry on anticoagulant properties. *Carbohydrate Polymers*, 91(2), 483-491.
- Deng, Y., Saucier-Sawyer, J. K., Hoimes, C. J., Zhang, J., Seo, Y-E., Andrejcsk, J. W., & Saltzman, W. M. (2014). The effect of hyperbranched polyglycerol coating on drug delivery using degradable polymer nanoparticles. *Biomaterials*, 35(24), 6595-6602.

- Doktorovová, S., Araújo, J., Garcia, M. L., Rakovský, E., & Souto, E. B. (2010). Formulating fluticasone propionate in novel PEG-containing nanostructured lipid carriers (PEG-NLC). *Colloids and Surfaces B: Biointerfaces*, 75(2), 538-542.
- Du, J., Dai, J., Liu, J.-L., & Dankovich, T. (2006). Novel pH-sensitive polyelectrolyte carboxymethyl Konjac glucomannan-chitosan beads as drug carriers. *Reactive and Functional Polymers*, 66(10), 1055-1061.
- Dudhani, A. R., & Kosaraju, S. L. (2010). Bioadhesive chitosan nanoparticles: Preparation and characterization. *Carbohydrate Polymers*, 81(2), 243-251.
- Dusastre, V. (2008). The invisible revolution. *Nature*, 451, 770-771.
- Eastoe, J. (2005). Surfactant aggregation and adsorption at interfaces. *Colloid Science: Principles, Methods and Applications*, 50-76.
- Eastoe, J. (2005). Microemulsion. *Colloid Science: Principles, Methods and Applications*, 77-97.
- Ekambaram, P., Sathali, A. A. H., & Priyanka, K. (2012). Solid lipid nanoparticles: a review. *Science Reviews & Chemical Communications*, 2(1), 80-102.
- Elbayoumi, T. A., & Torchilin, V. P. (2008). Tumor-specific antibody-mediated targeted delivery of Doxil[®] reduces the manifestation of auricular erythema side effect in mice. *International Journal of Pharmaceutics*, 357(1), 272-279.
- Fameau, A.-L., Arnould, A., & Saint-Jalmes, A. (2014). Responsive Self-assemblies based on Fatty acids. *Current Opinion in Colloid & Interface Science*, 19(5), 471-479.
- Fan, H., Liu, G., Huang, Y., Li, Y., & Xia, Q. (2014). Development of a nanostructured lipid carrier formulation for increasing photo-stability and water solubility of phenylethyl resorcinol. *Applied Surface Science*, 288, 193-200.
- Fan, L., Wu, H., Zhang, H., Li, F., Yang, T.-h., Gu, C.-h., & Yang, Q. (2008). Novel super pH-sensitive nanoparticles responsive to tumor extracellular pH. *Carbohydrate Polymers*, 73(3), 390-400.
- Fang, J.-Y., Fang, C.-L., Liu, C.-H., & Su, Y.-H. (2008). Lipid nanoparticles as vehicles for topical psoralen delivery: solid lipid nanoparticles (SLN) versus nanostructured lipid carriers (NLC). *European Journal of Pharmaceutics and Biopharmaceutics*, 70(2), 633-640.
- Fang, J.-Y., Hong, C.-T., Chiu, W.-T., & Wang, Y.-Y. (2001). Effect of liposomes and niosomes on skin permeation of enoxacin. *International Journal of Pharmaceutics*, 219(1), 61-72.
- Fang, J.-Y., Lee, W.-R., Shen, S.-C., & Huang, Y.-L. (2006). Effect of liposome encapsulation of tea catechins on their accumulation in basal cell carcinomas. *Journal of Dermatological Science*, 42(2), 101-109.

- Fettaka, M., Issaadi, R., Moulai-Mostefa, N., Dez, I., Le Cerf, D., & Picton, L. (2011). Thermo sensitive behavior of cellulose derivatives in dilute aqueous solutions: From macroscopic to mesoscopic scale. *Journal of Colloid and Interface Science*, 357(2), 372-378.
- Folmer, B. (2003). Fatty acid monoethanol amide ethoxylates. In Holmberg, K. (Ed.). *Novel surfactants: Preparation, methods and applications* (pp: 241-256). West Sussex, UK: John and Wiley & Sons Ltd.
- Franzen, U., Nguyen, T. T. T. N., Vermehren, C., Gammelgaard, B., & Østergaard, J. (2011). Characterization of a liposome-based formulation of oxaliplatin using capillary electrophoresis: Encapsulation and leakage. *Journal of Pharmaceutical and Biomedical Analysis*, 55(1), 16-22.
- Freemantle, E., Vandal, M., Tremblay-Mercier, J., Tremblay, S., Blachère, J.-C., Bégin, M. E., Brenna, J. T., Windust, A., & Cunnane, S. C. (2006). Omega-3 fatty acids, energy substrates, and brain function during aging. *Prostaglandins, leukotrienes and essential fatty acids*, 75(3), 213-220.
- Gainza, G., Bonafonte, D. C., Moreno, B., Aguirre, J. J., Gutierrez, F. B., Villullas, S., Pedraz, J. L., Igartua, M., & Hernandez, R. M. (2015). The topical administration of rhEGF-loaded nanostructured lipid carriers (rhEGF-NLC) improves healing in a porcine full-thickness excisional wound model. *Journal of Controlled Release*, 197, 41-47.
- Gan, Q., & Wang, T. (2007). Chitosan nanoparticle as protein delivery carrier—systematic examination of fabrication conditions for efficient loading and release. *Colloids and Surfaces B: Biointerfaces*, 59(1), 24-34.
- Gan, Q., Wang, T., Cochrane, C., & McCarron, P. (2005). Modulation of surface charge, particle size and morphological properties of chitosan–TPP nanoparticles intended for gene delivery. *Colloids and Surfaces B: Biointerfaces*, 44(2), 65-73.
- Giri, A., Ghosh, T., Panda, A. B., Pal, S., & Bandyopdhyay, A. (2012). Tailoring carboxymethyl guar gum hydrogel with nanosilica for sustained transdermal release of diclofenac sodium. *Carbohydrate Polymers*, 87(2), 1532-1538.
- Gong, R., Li, C., Zhu, S., Zhang, Y., Du, Y., & Jiang, J. (2011). A novel pH-sensitive hydrogel based on dual crosslinked alginate/N- α -glutaric acid chitosan for oral delivery of protein. *Carbohydrate Polymers*, 85(4), 869-874.
- Gonzalez-Mira, E., Egea, M. A., Garcia, M. L., & Souto, E. B. (2010). Design and ocular tolerance of flurbiprofen loaded ultrasound-engineered NLC. *Colloids and Surfaces B: Biointerfaces*, 81(2), 412-421.
- Grenha, A., Gomes, M. E., Rodrigues, M., Santo, V. E., Mano, J. F., Neves, N.M., & Reis, R. L. (2010). Development of new chitosan/carrageenan nanoparticles for drug delivery applications. *Journal of Biomedical Materials Research*, 92, 1265-1272.

- Grenha, A., Seijo, B., & Remunán-López, C. (2005). Microencapsulated chitosan nanoparticles for lung protein delivery. *European Journal of Pharmaceutical Sciences*, 25(4), 427-437.
- Guan, R., Ma, J., Wu, Y., Lu, F., Xiao, C., Jiang, H., & Kang, T. (2012). Development and characterization of lactoferrin nanoliposome: cellular uptake and stability. *Nanoscale Research Letters*, 7(1), 1-6.
- Guo, L., Fan, L., Pang, Z., Ren, J., Ren, Y., Li, J., Chen, J., Wen, Z., & Jiang, X. (2011). TRAIL and doxorubicin combination enhances anti-glioblastoma effect based on passive tumor targeting of liposomes. *Journal of Controlled Release*, 154(1), 93-102.
- Gupta, K., & Kumar, M. R. (2000). Drug release behavior of beads and microgranules of chitosan. *Biomaterials*, 21(11), 1115-1119.
- Gupta, V. K., Gnanarajan, G., & Kothiyal, P. (2012). A review article on colonic targeted drug delivery systems. *The Pharma Innovation*, 1(7), 14-24.
- Hamidi, M., Azadi, A., & Rafiei, P. (2008). Hydrogel nanoparticles in drug delivery. *Advanced Drug Delivery Reviews*, 60(15), 1638-1649.
- Hamman, J. H. (2010). Chitosan based polyelectrolyte complexes as potential carrier materials in drug delivery systems. *Marine Drugs*, 8(4), 1305-1322.
- Han, F., Yin, R., Che, X., Yuan, J., Cui, Y., Yin, H., & Li, S. (2012). Nanostructured lipid carriers (NLC) based topical gel of flurbiprofen: Design, characterization and in vivo evaluation. *International Journal of Pharmaceutics*, 439(1), 349-357.
- Han, H. D., Shin, B. C., & Choi, H. S. (2006). Doxorubicin-encapsulated thermosensitive liposomes modified with poly (N-isopropylacrylamide-co-acrylamide): Drug release behavior and stability in the presence of serum. *European Journal of Pharmaceutics and Biopharmaceutics*, 62(1), 110-116.
- Hatakeyama, H., Ito, E., Akita, H., Oishi, M., Nagasaki, Y., Futaki, S., & Harashima, H. (2009). A pH-sensitive fusogenic peptide facilitates endosomal escape and greatly enhances the gene silencing of siRNA-containing nanoparticles in vitro and in vivo. *Journal of Controlled Release*, 139(2), 127-132.
- Hejazi, R., & Amiji, M. (2003). Chitosan-based gastrointestinal delivery systems. *Journal of Controlled Release*, 89(2), 151-165.
- Hezaveh, H., & Muhamad, I. I. (2012). The effect of nanoparticles on gastrointestinal release from modified κ -carrageenan nanocomposite hydrogels. *Carbohydrate Polymers*, 89(1), 138-145.
- Hosny, K. M., & Hassan, A. H. (2014). Intranasal in situ gel loaded with saquinavir mesylate nanosized microemulsion: Preparation, characterization, and in vivo evaluation. *International Journal of Pharmaceutics*, 475(1), 191-197.

- Hsu, J.-P., & Nacu, A. (2003). Behavior of soybean oil-in-water emulsion stabilized by nonionic surfactant. *Journal of Colloid and Interface Science*, 259(2), 374-381.
- Hu, F.-Q., Zhang, Y., Du, Y.-Z., & Yuan, H. (2008). Nimodipine loaded lipid nanospheres prepared by solvent diffusion method in a drug saturated aqueous system. *International Journal of Pharmaceutics*, 348(1), 146-152.
- Hurler, J., & Škalko-Basnet, N. (2012). Potentials of chitosan-based delivery systems in wound therapy: bioadhesion study. *Journal of Functional Biomaterials*, 3(1), 37-48.
- Immordino, M. L., Dosio, F., & Cattel, L. (2006). Stealth liposomes: Review of the basic science, rationale, and clinical applications, existing and potential. *International Journal of Nanomedicine*, 1(3), 297.
- Inoh, Y., Tadokoro, S., Tanabe, H., Inoue, M., Hirashima, N., Nakanishi, M., & Furuno, T. (2013). Inhibitory effects of a cationic liposome on allergic reaction mediated by mast cell activation. *Biochemical Pharmacology*, 86(12), 1731-1738.
- Ishida, T., Ichihara, M., Wang, X. Y., Yamamoto, K., Kimura, J., Majima, E., & Kiwada, H. (2006). Injection of PEGylated liposomes in rats elicits PEG-specific IgM, which is responsible for rapid elimination of a second dose of PEGylated liposomes. *Journal of Controlled Release*, 112(1), 15-25.
- Ishida, T., & Kiwada, H. (2008). Accelerated blood clearance (ABC) phenomenon upon repeated injection of PEGylated liposomes. *International Journal of Pharmaceutics*, 354(1), 56-62.
- Ishida, T., Okada, Y., Kobayashi, T., & Kiwada, H. (2006). Development of pH-sensitive liposomes that efficiently retain encapsulated doxorubicin (DXR) in blood. *International Journal of pharmaceutics*, 309(1), 94-100.
- Ishida, T., Wang, X. Y., Shimizu, T., Nawata, K., & Kiwada, H. (2007). PEGylated liposomes elicit an anti-PEG IgM response in a T cell-independent manner. *Journal of Controlled Release*, 122(3), 349-355.
- Ishii, F. & Nii, T. (2014). Lipid emulsions and lipid vesicles prepared from various phospholipids as drug carrier. In Ohshima, H., & Makino, K. (Eds). *Colloid and Interface Science in Pharmaceutical Research and Development* (pp: 469-502). Oxford, UK: Elsevier.
- Jia, L., Zhang, D., Li, Z., Duan, C., Wang, Y., Feng, F., Wang, F., Liu, Y., & Zhang, Q. (2010). Nanostructured lipid carriers for parenteral delivery of silybin: Biodistribution and pharmacokinetic studies. *Colloids and Surfaces B: Biointerfaces*, 80(2), 213-218.
- Jiang, L., Li, L., He, X., Yi, Q., He, B., Cao, J., Pan, W., & Gu, Z. (2015). Overcoming drug-resistant lung cancer by paclitaxel loaded dual-functional liposomes with mitochondria targeting and pH-response. *Biomaterials*, 52, 126-139.

- Jin, Y.-H., Hu, H.-Y., Qiao, M.-X., Zhu, J., Qi, J.-W., Hu, C.-J., Zhang, Q., & Chen, D.-W. (2012). pH-sensitive chitosan-derived nanoparticles as doxorubicin carriers for effective anti-tumor activity: preparation and in vitro evaluation. *Colloids and Surfaces B: Biointerfaces*, 94, 184-191.
- Joshi, M., & Patravale, V. (2008). Nanostructured lipid carrier (NLC) based gel of celecoxib. *International Journal of Pharmaceutics*, 346(1), 124-132.
- Joye, I. J., & McClements, D. J. (2014). Biopolymer-based nanoparticles and microparticles: Fabrication, characterization, and application. *Current Opinion in Colloid & Interface Science*, 19(5), 417-427.
- Junyaprasert, V. B., Teeranachaidekul, V., Souto, E. B., Boonme, P., & Müller, R. H. (2009). Q 10-loaded NLC versus nanoemulsions: Stability, rheology and in vitro skin permeation. *International Journal of Pharmaceutics*, 377(1), 207-214.
- Jurcut, R., Wildiers, H., Ganame, J., D'hooge, J., De Backer, J., Denys, H., Paridaens, R., Rademakers, F., & Voigt, J.-U. (2008). Strain rate imaging detects early cardiac effects of pegylated liposomal Doxorubicin as adjuvant therapy in elderly patients with breast cancer. *Journal of the American Society of Echocardiography*, 21(12), 1283-1289.
- Justo, O. R., & Moraes, A. M. (2011). Analysis of process parameters on the characteristics of liposomes prepared by ethanol injection with a view to process scale-up: Effect of temperature and batch volume. *Chemical Engineering Research and Design*, 89(6), 785-792.
- Kalepu, S., Manthina, M., & Padavala, V. (2013). Oral lipid-based drug delivery systems—an overview. *Acta Pharmaceutica Sinica B*, 3(6), 361-372.
- Kaneda, Y., Tsutsumi, Y., Yoshioka, Y., Kamada, H., Yamamoto, Y., Kodaira, H., Tsunoda, S., Okamoto, T., Mukai, Y., Shibata, H., Nakagawa, S., & Mayumi, T. (2004). The use of PVP as a polymeric carrier to improve the plasma half-life of drugs. *Biomaterials*, 25(16), 3259-3266.
- Kanicky, J. R., & Shah, D. O. (2002). Effect of degree, type, and position of unsaturation on the pK_a of long-chain fatty acids. *Journal of Colloid and Interface Science*, 256(1), 201-207.
- Kaur, K., Hush, P., Pandey, R. S., Madan, J., Jain, U. K., & Katare, O. P. (2015). Stealth lipid coated aquasomes bearing recombinant human interferon- α -2b offered prolonged release and enhanced cytotoxicity in ovarian cancer cells. *Biomedicine & Pharmacotherapy*, 69, 267-276.
- Kawabata, Y., Wada, K., Nakatani, M., Yamada, S., & Onoue, S. (2011). Formulation design for poorly water-soluble drugs based on biopharmaceutics classification system: Basic approaches and practical applications. *International Journal of Pharmaceutics*, 420(1), 1-10.

- Keck, C. M., Anantaworasakul, P., Patel, M., Okonogi, S., Singh, K. K., Roessner, D., Scherrers, R., Schwabe, K., Rimpler, C., & Müller, R. H. (2014). A new concept for the treatment of atopic dermatitis: Silver–nanolipid complex (sNLC). *International Journal of Pharmaceutics*, 462(1), 44-51.
- Keck, C. M., Baisaeng, N., Durand, P., Prost, M., Meinke, M. C., & Müller, R. H. (2014). Oil-enriched, ultra-small nanostructured lipid carriers (usNLC): A novel delivery system based on flip–flop structure. *International Journal of Pharmaceutics*, 477(1), 227-235.
- Keppeler, S., Ellis, A., & Jacquier, J. (2009). Cross-linked carrageenan beads for controlled release delivery systems. *Carbohydrate Polymers*, 78(4), 973-977.
- Kim, H., Kim, Y., & Lee, J. (2013). Liposomal formulations for enhanced lymphatic drug delivery. *Asian Journal of Pharmaceutical Sciences*, 8(2), 96-103.
- Kim, I.-Y., Kang, Y.-S., Lee, D. S., Park, H.-J., Choi, E.-K., Oh, Y.-K., Son, H.-J., & Kim, J.-S. (2009). Antitumor activity of EGFR targeted pH-sensitive immunoliposomes encapsulating gemcitabine in A549 xenograft nude mice. *Journal of Controlled Release*, 140(1), 55-60.
- Kim, J.-H., Kim, Y.-S., Park, K., Lee, S., Nam, H. Y., Min, K. H., Jo, H. G., Park, J. H., Jeong, S. Y., Park, R. W., Kim, I. S., Kim, K., & Kwon, I. C. (2008). Antitumor efficacy of cisplatin-loaded glycol chitosan nanoparticles in tumor-bearing mice. *Journal of Controlled Release*, 127(1), 41-49.
- Kim, J.-Y., Kim, J.-K., Park, J.-S., Byun, Y., & Kim, C.-K. (2009). The use of PEGylated liposomes to prolong circulation lifetimes of tissue plasminogen activator. *Biomaterials*, 30(29), 5751-5756.
- Kim, S. J., Shin, S. R., Lee, K. B., Park, Y. D., & Kim, S. I. (2004). Synthesis and characteristics of polyelectrolyte complexes composed of chitosan and hyaluronic acid. *Journal of Applied Polymer Science*, 91(5), 2908-2913.
- Ko, J. A., Park, H. J., Hwang, S. J., Park, J. B., & Lee, J. S. (2002). Preparation and characterization of chitosan microparticles intended for controlled drug delivery. *International Journal of Pharmaceutics*, 249(1), 165-174.
- Kogan, A., & Garti, N. (2006). Microemulsions as transdermal drug delivery vehicles. *Advances in Colloid and Interface Science*, 123, 369-385.
- Kotikalapudi, L. S., Adepu, L., VijayaRatna, J., & Diwan, P. V. (2012). Formulation and in vitro characterization of domperidone loaded solid lipid nanoparticles. *International Journal of Pharmaceutical and Biomedical Research*, 3(1), 22-29.
- Koudelka, Š., & Turánek, J. (2012). Liposomal paclitaxel formulations. *Journal of Controlled Release*, 163(3), 322-334.
- Kovacevic, A., Savic, S., Vuleta, G., Müller, R. H., & Keck, C. M. (2011). Polyhydroxy surfactants for the formulation of lipid nanoparticles (SLN and NLC): Effects on

- size, physical stability and particle matrix structure. *International Journal of Pharmaceutics*, 406(1), 163-172.
- Kreilgaard, M. (2002). Influence of microemulsions on cutaneous drug delivery. *Advanced Drug Delivery Reviews*, 54, S77-S98.
- Krylova, O. O., Jahnke, N., & Keller, S. (2010). Membrane solubilisation and reconstitution by octylglucoside: Comparison of synthetic lipid and natural lipid extract by isothermal titration calorimetry. *Biophysical Chemistry*, 150(1), 105-111.
- Kulkarni, P. R., Yadav, J. D., & Vaidya, K. A. (2011). Liposomes: A novel drug delivery system. *International Journal of Current Pharmaceutical Research*, 3(2), 10-18.
- Kumar, R., & Sinha, V. R. (2014). Preparation and optimization of voriconazole microemulsion for ocular delivery. *Colloids and Surfaces B: Biointerfaces*, 117, 82-88.
- Kumar, S., Zakrewsky, M., Chen, M., Menegatti, S., Muraski, J. A., & Mitragotri, S. (2015). Peptides as skin penetration enhancers: Mechanisms of action. *Journal of Controlled Release*, 199, 168-178.
- Kunisawa, J., Masuda, T., Katayama, K., Yoshikawa, T., Tsutsumi, Y., Akashi, M., Mayumi, T., & Nakagawa, S. (2005). Fusogenic liposome delivers encapsulated nanoparticles for cytosolic controlled gene release. *Journal of Controlled Release*, 105(3), 344-353.
- Lajunen, T., Hisazumi, K., Kanazawa, T., Okada, H., Seta, Y., Yliperttula, M., Urtti, A., & Takashima, Y. (2014). Topical drug delivery to retinal pigment epithelium with microfluidizer produced small liposomes. *European Journal of Pharmaceutical Sciences*, 62, 23-32.
- Lavertu, M., Methot, S., Tran-Khanh, N., & Buschmann, M. D. (2006). High efficiency gene transfer using chitosan/DNA nanoparticles with specific combinations of molecular weight and degree of deacetylation. *Biomaterials*, 27(27), 4815-4824.
- Law, V., Knox, C., Djoumbou, Y., Jewison, T., Guo, A. C., Liu, Y., Maciejewski, A., Arndt, D., Wilson, M., Neveu, V., Tang, A., Gabriel, G., Ly, C., Adamjee, S., Dame, Z. T., Han, B., Zhou, Y., & Wishart, D. S. (2014). DrugBank 4.0: shedding new light on drug metabolism. *Nucleic Acids Research*, 42(1), D1091-1097.
- Lawrence, M. J., & Rees, G. D. (2000). Microemulsion-based media as novel drug delivery systems. *Advanced Drug Delivery Reviews*, 45(1), 89-121.
- Li, B., & Ge, Z.-Q. (2012). Nanostructured lipid carriers improve skin permeation and chemical stability of idebenone. *AAPS PharmSciTech*, 13(1), 276-283.

- Li, C., Hein, S., & Wang, K. (2013). Chitosan-carrageenan polyelectrolyte complex for the delivery of protein drugs. *ISRN Biomaterials*, 1-6. <http://dx.doi.org/10.5402/2013/629807>.
- Li, F., Li, Q.-H., Wang, J.-Y., Zhan, C.-Y., Xie, C., & Lu, W.-Y. (2012). Effects of interferon-gamma liposomes targeted to platelet-derived growth factor receptor-beta on hepatic fibrosis in rats. *Journal of Controlled Release*, 159(2), 261-270.
- Li, F., Wu, H., Zhang, H., Li, F., Gu, C.-h., & Yang, Q. (2009). Antitumor drug Paclitaxel-loaded pH-sensitive nanoparticles targeting tumor extracellular pH. *Carbohydrate Polymers*, 77(4), 773-778.
- Li, S-D., & Huang, L. (2008). Pharmacokinetics and biodistribution of nanoparticles. *Molecular Pharmaceutics*, 5(4), 496-504.
- Lichtenberg, D., Ahyayauch, H., Alonso, A., & Goñi, F. M. (2013). Detergent solubilization of lipid bilayers: A balance of driving forces. *Trends in Biochemical Sciences*, 38(2), 85-93.
- Lichtenberg, D., Ahyayauch, H., & Goñi, F. M. (2013). The mechanism of detergent solubilization of lipid bilayers. *Biophysical Journal*, 105(2), 289-299.
- Linhardt, R. J., & Liu, J. (2012). Synthetic heparin. *Current Opinion in Pharmacology*, 12(2), 217-219.
- Liu, C.-G., Chen, X.-G., & Park, H.-J. (2005). Self-assembled nanoparticles based on linoleic-acid modified chitosan: Stability and adsorption of trypsin. *Carbohydrate Polymers*, 62(3), 293-298.
- Liu, D., Kobayashi, T., Russo, S., Li, F., Plevy, S. E., Gambling, T. M., Carson, J. L., & Mumper, R. J. (2013). In vitro and in vivo evaluation of a water-in-oil microemulsion system for enhanced peptide intestinal delivery. *The AAPS Journal*, 15(1), 288-298.
- Liu, J., Hu, W., Chen, H., Ni, Q., Xu, H., & Yang, X. (2007). Isotretinoin-loaded solid lipid nanoparticles with skin targeting for topical delivery. *International Journal of Pharmaceutics*, 328(2), 191-195.
- Liu, W., Sun, D., Li, C., Liu, Q., & Xu, J. (2006). Formation and stability of paraffin oil-in-water nano-emulsions prepared by the emulsion inversion point method. *Journal of Colloid and Interface Science*, 303(2), 557-563.
- Liu, Z., Jiao, Y., Wang, Y., Zhou, C., & Zhang, Z. (2008). Polysaccharides-based nanoparticles as drug delivery systems. *Advanced Drug Delivery Reviews*, 60(15), 1650-1662.
- Long, J., Yu, X., Xu, E., Wu, Z., Xu, X., Jin, Z., & Jiao, A. (2015). In situ synthesis of new magnetite chitosan/carrageenan nanocomposite by electrostatic interactions for protein delivery applications. *Carbohydrate Polymers*, 131, 98-107.

- Luan, J., Zhang, D., Hao, L., Qi, L., Liu, X., Guo, H., Li, C., Guo, Y., Li, T., Zhang, Q., & Zhai, G. (2014). Preparation, characterization and pharmacokinetics of Amoitone B-loaded long circulating nanostructured lipid carriers. *Colloids and Surfaces B: Biointerfaces*, 114, 255-260.
- Luo, Y., & Wang, Q. (2014). Recent development of chitosan-based polyelectrolyte complexes with natural polysaccharides for drug delivery. *International Journal of Biological Macromolecules*, 64, 353-367.
- Luo, Y., Zhang, B., Cheng, W.-H., & Wang, Q. (2010). Preparation, characterization and evaluation of selenite-loaded chitosan/TPP nanoparticles with or without zein coating. *Carbohydrate Polymers*, 82(3), 942-951.
- Mahdavinia, G. R., Etemadi, H., & Soleymani, F. (2015). Magnetic/pH responsive beads based on carboxymethyl chitosan and κ -carrageenan and controlled release. *Carbohydrate Polymers*, 128, 112-121.
- Mai, J., Song, S., Rui, M., Liu, D., Ding, Q., Peng, J., & Xu, Y. (2009). A synthetic peptide mediated active targeting of cisplatin liposomes to Tie2 expressing cells. *Journal of Controlled Release*, 139(3), 174-181.
- Maitani, Y., Igarashi, S., Sato, M., & Hattori, Y. (2007). Cationic liposome (DC-Chol/DOPE= 1: 2) and a modified ethanol injection method to prepare liposomes, increased gene expression. *International Journal of Pharmaceutics*, 342(1), 33-39.
- Makhlof, A., Tozuka, Y., & Takeuchi, H. (2011). Design and evaluation of novel pH-sensitive chitosan nanoparticles for oral insulin delivery. *European Journal of Pharmaceutical Sciences*, 42(5), 445-451.
- Malmö, J., Sjørgård, H., Vårå, K. M., & Strand, S. P. (2012). siRNA delivery with chitosan nanoparticles: Molecular properties favoring efficient gene silencing. *Journal of Controlled Release*, 158(2), 261-268.
- Mansoori, M. A., Agrawal, S., Jawade, S., & Khan, M. I. (2010). A review on liposome. *International Journal of Advanced Research in Pharmaceutical & Bio Science*, 2(4), 453-464.
- Mansouri, S., Cuie, Y., Winnik, F., Shi, Q., Lavigne, P., Benderdour, M., Beaumont, E., & Fernandes, J. C. (2006). Characterization of folate-chitosan-DNA nanoparticles for gene therapy. *Biomaterials*, 27(9), 2060-2065.
- Marengo, E., Cavalli, R., Caputo, O., Rodriguez, L., & Gasco, M. R. (2000). Scale-up of the preparation process of solid lipid nanospheres. Part I. *International Journal of Pharmaceutics*, 205(1), 3-13.
- Marinova, K. G., Alargova, R. G., Denkov, N. D., Velez, O. D., Petsev, D. N., Ivanov, I. B., & Borwankar, R. P. (1996). Charging of oil-water interfaces due to spontaneous adsorption of hydroxyl ions. *Langmuir*, 12(8), 2045-2051.

- Martinac, A., Filipović-Grčić, J., Voinovich, D., Perissutti, B., & Franceschinis, E. (2005). Development and bioadhesive properties of chitosan-ethylcellulose microspheres for nasal delivery. *International Journal of Pharmaceutics*, 291(1), 69-77.
- Maruyama, K. (2011). Intracellular targeting delivery of liposomal drugs to solid tumors based on EPR effects. *Advanced Drug Delivery Reviews*, 63(3), 161-169.
- Mendes, A., Silva, A. C., Catita, J. A. M., Cerqueira, F., Gabriel, C., & Lopes, C. M. (2013). Miconazole-loaded nanostructured lipid carriers (NLC) for local delivery to the oral mucosa: improving antifungal activity. *Colloids and Surfaces B: Biointerfaces*, 111, 755-763.
- Meure, L. A., Foster, N. R., & Dehghani, F. (2008). Conventional and dense gas techniques for the production of liposomes: A review. *AAPS PharmSciTech*, 9(3), 798-809.
- Minagawa, T., Okamura, Y., Shigemasa, Y., Minami, S., & Okamoto, Y. (2007). Effects of molecular weight and deacetylation degree of chitin/chitosan on wound healing. *Carbohydrate Polymers*, 67(4), 640-644.
- Mirahmadi, N., Babaei, M. H., Vali, A. M., & Dadashzadeh, S. (2010). Effect of liposome size on peritoneal retention and organ distribution after intraperitoneal injection in mice. *International Journal of Pharmaceutics*, 383(1), 7-13.
- Mishra, B. K., Chauhan, M. K. G., & Patel, N. (2000). Behaviour of non-ionic Inicroelnsion containing Tween-80, iso-amyl alcohol, hexane and water. *Indian Journal of Chemical Technology*, 7, 338-341.
- Mitra, S., Gaur, U., Ghosh, P., & Maitra, A. (2001). Tumour targeted delivery of encapsulated dextran–doxorubicin conjugate using chitosan nanoparticles as carrier. *Journal of Controlled Release*, 74(1), 317-323.
- Mitri, K., Shegokar, R., Gohla, S., Anselmi, C., & Müller, R. H. (2011). Lutein nanocrystals as antioxidant formulation for oral and dermal delivery. *International Journal of Pharmaceutics*, 420(1), 141-146.
- Mojahedian, M. M., Daneshamouz, S., Samani, S. M., & Zargaran, A. (2013). A novel method to produce solid lipid nanoparticles using n-butanol as an additional co-surfactant according to the o/w microemulsion quenching technique. *Chemistry and Physics of Lipids*, 174, 32-38.
- Morozowich, W., & Gao, P. (2009). Improving the oral absorption of poorly soluble drugs using SEDDS and S-SEDDS formulations. In Qiu, Y., Chen, Y., Zhang, G. G. Z., Liu, L., & Porter, W. R. (Eds.), *Developing Solid Oral Dosage Forms: Pharmaceutical Theory and Practice* (pp. 443-468). Burlington, USA: Academic Press.

- Mukherjee, S., Ray, S., & Thakur, R. (2009). Solid lipid nanoparticles: A modern formulation approach in drug delivery system. *Indian Journal of Pharmaceutical Sciences*, 71(4), 349.
- Müller, R. H., Petersen, R. D., Hommos, A., & Pardeike, J. (2007). Nanostructured lipid carriers (NLC) in cosmetic dermal products. *Advanced Drug Delivery Reviews*, 59(6), 522-530.
- Müller, R. H., Radtke, M., & Wissing, S. A. (2002). Nanostructured lipid matrices for improved microencapsulation of drugs. *International Journal of Pharmaceutics*, 242(1), 121-128.
- Müller, R. H., Radtke, M., & Wissing, S. A. (2002). Solid lipid nanoparticles (SLN) and nanostructured lipid carriers (NLC) in cosmetic and dermatological preparations. *Advanced Drug Delivery Reviews*, 54, S131-S155.
- Muzaffar, F., Singh, U. K., & Chauhan, L. (2013). Review on microemulsion as futuristic drug delivery. *International Journal of Pharmacy and Pharmaceutical Sciences*, 5, 39-53.
- Nagaich, U., & Gulati, N. (2016). Nanostructured lipid carriers (NLC) based controlled release topical gel of clobetasol propionate: design and *in vivo* characterization. *Drug Delivery and Translational Research*, 6(3), 289-298.
- Nagpal, K., Singh, S. K., & Mishra, D. N. (2010). Chitosan nanoparticles: a promising system in novel drug delivery. *Chemical and Pharmaceutical Bulletin*, 58(11), 1423-1430.
- Nakano, K., Tozuka, Y., & Takeuchi, H. (2008). Effect of surface properties of liposomes coated with a modified polyvinyl alcohol (PVA-R) on the interaction with macrophage cells. *International Journal of Pharmaceutics*, 354(1), 174-179.
- Nam, H. Y., Kwon, S. M., Chung, H., Lee, S.-Y., Kwon, S.-H., Jeon, H., Kim, Y., Park, J. H., Kim, J., Her, S., Oh, Y. K., Kwon, I. C., Kim, K., & Jeong, S. Y. (2009). Cellular uptake mechanism and intracellular fate of hydrophobically modified glycol chitosan nanoparticles. *Journal of Controlled Release*, 135(3), 259-267.
- Nayak, A. P., Tiyaboonchai, W., Patankar, S., Madhusudhan, B., & Souto, E. B. (2010). Curcuminoids-loaded lipid nanoparticles: Novel approach towards malaria treatment. *Colloids and Surfaces B: Biointerfaces*, 81(1), 263-273.
- Neupane, Y. R., Srivastava, M., Ahmad, N., Kumar, N., Bhatnagar, A., & Kohli, K. (2014). Lipid based nanocarrier system for the potential oral delivery of decitabine: Formulation design, characterization, ex vivo, and in vivo assessment. *International Journal of Pharmaceutics*, 477(1), 601-612.
- Nguyen, T. T. T. N., Østergaard, J., Stürup, S., & Gammelgaard, B. (2013). Determination of platinum drug release and liposome stability in human plasma by CE-ICP-MS. *International Journal of Pharmaceutics*, 449(1), 95-102.

- Nicolosi, D., Cupri, S., Genovese, C., Nicolosi, V. M., Mattina, R., & Pignatello, R. (2015). Nanotechnology approaches for antibacterial drug delivery: preparation and microbiological evaluation of fusogenic liposomes carrying fusidic acid. *International Journal of Antimicrobial Agents*, 45(6), 622-626.
- Nikolova-Damyanova, B. (2009). Retention of lipids in silver ion high-performance liquid chromatography: Facts and assumptions. *Journal of Chromatography A*, 1216(10), 1815-1824.
- Nnamani, P. O., Hansen, S., Windbergs, M., & Lehr, C.-M. (2014). Development of artemether-loaded nanostructured lipid carrier (NLC) formulation for topical application. *International Journal of Pharmaceutics*, 477(1), 208-217.
- Noble, G. T., Stefanick, J. F., Ashley, J. D., Kiziltepe, T., & Bilgicer, B. (2014). Ligand-targeted liposome design: Challenges and fundamental considerations. *Trends in Biotechnology*, 32(1), 32-45.
- Nogueira, D. R., Tavano, L., Mitjans, M., Pérez, L., Infante, M. R., & Vinardell, M. P. (2013). In vitro antitumor activity of methotrexate via pH-sensitive chitosan nanoparticles. *Biomaterials*, 34(11), 2758-2772.
- Okur, N. Ü., Apaydın, Ş., Yavaşoğlu, N. Ü. K., Yavaşoğlu, A., & Karasulu, H. Y. (2011). Evaluation of skin permeation and anti-inflammatory and analgesic effects of new naproxen microemulsion formulations. *International Journal of Pharmaceutics*, 416(1), 136-144.
- Okur, N. Ü., Yavaşoğlu, A., & Karasulu, H. Y. (2014). Preparation and Evaluation of Microemulsion Formulations of Naproxen for Dermal Delivery. *Chemical and Pharmaceutical Bulletin*, 62(2), 135-143.
- Oldfield, C. (1994). Enzymes in water-in-oil microemulsions ('reversed micelles'): principle and applications. *Biotechnology and Genetic Engineering Review*, 12, 255-327.
- Ontiveros, J. F., Pierlot, C., Catté, M., Molinier, V., Salager, J.-L., & Aubry, J.-M. (2014). A simple method to assess the hydrophilic lipophilic balance of food and cosmetic surfactants using the phase inversion temperature of C 10 E 4/n-octane/water emulsions. *Colloids and Surfaces A: Physicochemical and Engineering Aspects*, 458, 32-39.
- Padamwar, M. N., & Pokharkar, V. B. (2006). Development of vitamin loaded topical liposomal formulation using factorial design approach: drug deposition and stability. *International Journal of Pharmaceutics*, 320(1), 37-44.
- Pan, Y., Li, Y.-J., Zhao, H.-Y., Zheng, J.-M., Xu, H., Wei, G., & Hao, J.-S. (2002). Bioadhesive polysaccharide in protein delivery system: Chitosan nanoparticles improve the intestinal absorption of insulin in vivo. *International Journal of Pharmaceutics*, 249(1), 139-147.

- Pandita, D., Kumar, S., Poonia, N., & Lather, V. (2014). Solid lipid nanoparticles enhance oral bioavailability of resveratrol, a natural polyphenol. *Food Research International*, 62, 1165-1174.
- Pardeike, J., Hommoss, A., & Müller, R. H. (2009). Lipid nanoparticles (SLN, NLC) in cosmetic and pharmaceutical dermal products. *International Journal of Pharmaceutics*, 366(1), 170-184.
- Pardeike, J., & Müller, R. H. (2007). Coenzyme Q10-loaded NLCs: preparation, occlusive properties and penetration enhancement. *Pharmaceutical Technology Europe*, 19(7), 46.
- Pardeike, J., Schwabe, K., & Müller, R. H. (2010). Influence of nanostructured lipid carriers (NLC) on the physical properties of the Cutanova Nanorepair Q10 cream and the in vivo skin hydration effect. *International Journal of Pharmaceutics*, 396(1), 166-173.
- Pardeike, J., Weber, S., Haber, T., Wagner, J., Zarfl, H., Plank, H. P., & Zimmer, A. (2011). Development of an itraconazole-loaded nanostructured lipid carrier (NLC) formulation for pulmonary application. *International Journal of Pharmaceutics*, 419(1), 329-338.
- Park, J. H., Kwon, S., Lee, M., Chung, H., Kim, J.-H., Kim, Y.-S., Park, R.-W., Kim, I.-S., Seo, S. B., Kwon, I. C., & Jeong, S. Y. (2006). Self-assembled nanoparticles based on glycol chitosan bearing hydrophobic moieties as carriers for doxorubicin: in vivo biodistribution and anti-tumor activity. *Biomaterials*, 27(1), 119-126.
- Park, J. H., Saravanakumar, G., Kim, K., & Kwon, I. C. (2010). Targeted delivery of low molecular drugs using chitosan and its derivatives. *Advanced Drug Delivery Reviews*, 62(1), 28-41.
- Park, J. W., Benz, C. C., & Martin, F. J. (2004). Future directions of liposome-and immunoliposome-based cancer therapeutics. *Seminars in oncology*, 31(S13), 196-205.
- Patel, A., & Velikov, K. P. (2011). Colloidal delivery systems in foods: A general comparison with oral drug delivery. *LWT-Food Science and Technology*, 44(9), 1958-1964.
- Patel, D., Dasgupta, S., Dey, S., Ramani, Y. R., Ray, S., & Mazumder, B. (2012). Nanostructured lipid carriers (NLC)-based gel for the topical delivery of aceclofenac: preparation, characterization, and in vivo evaluation. *Scientia Pharmaceutica*, 80(3), 749-764.
- Patel, M. P., Patel, R. R., & Patel, J. K. (2010). Chitosan mediated targeted drug delivery system: A review. *Journal of Pharmacy & Pharmaceutical Sciences*, 13(4), 536-557.
- Patel, R. B., Patel, M. R., Bhatt, K. K., & Patel, B. G. (2013). Formulation consideration and characterization of microemulsion drug delivery system for transnasal

- administration of carbamazepine. *Bulletin of Faculty of Pharmacy, Cairo University*, 51(2), 243-253.
- Patidar, A., Thakur, D. S., Kumar, P., & Verma, J. (2010). A review on novel lipid based nanocarriers. *International Journal of Pharmacy and Pharmaceutical Sciences*, 2(4), 30-35.
- Paul, W., & Sharma, C. P. (2004). Chitosan and alginate wound dressings: A short review. *Trends in Biomaterials & Artificial Organs*, 18(1), 18-23.
- Pham, H. L., Shaw, P. N., & Davies, N. M. (2006). Preparation of immuno-stimulating complexes (ISCOMs) by ether injection. *International Journal of Pharmaceutics*, 310(1), 196-202.
- Pinto, M. F., Moura, C. C., Nunes, C., Segundo, M. A., Lima, S. A. C., & Reis, S. (2014). A new topical formulation for psoriasis: Development of methotrexate-loaded nanostructured lipid carriers. *International Journal of Pharmaceutics*, 477(1), 519-526.
- Plapied, L., Vandermeulen, G., Vroman, B., Pr  at, V., & des Rieux, A. (2010). Bioadhesive nanoparticles of fungal chitosan for oral DNA delivery. *International Journal of Pharmaceutics*, 398(1), 210-218.
- Pople, P. V., & Singh, K. K. (2011). Development and evaluation of colloidal modified nanolipid carrier: application to topical delivery of tacrolimus. *European Journal of Pharmaceutics and Biopharmaceutics*, 79(1), 82-94.
- Porter, C. J., Pouton, C. W., Cuine, J. F., & Charman, W. N. (2008). Enhancing intestinal drug solubilisation using lipid-based delivery systems. *Advanced Drug Delivery Reviews*, 60(6), 673-691.
- Prieto, C., & Calvo, L. (2013). Performance of the Biocompatible Surfactant Tween 80, for the Formation of Microemulsions Suitable for New Pharmaceutical Processing. *Journal of Applied Chemistry*, 2013, 10. doi: 10.1155/2013/930356
- Prow, T. W., Grice, J. E., Lin, L. L., Faye, R., Butler, M., Becker, W., Wurm, E. M., Yoong, C., Robertson, T. A., Soyer, H. P., & Roberts, M. S. (2011). Nanoparticles and microparticles for skin drug delivery. *Advanced Drug Delivery Reviews*, 63, 470-491.
- Puglia, C., Blasi, P., Rizza, L., Schoubben, A., Bonina, F., Rossi, C., & Ricci, M. (2008). Lipid nanoparticles for prolonged topical delivery: An in vitro and in vivo investigation. *International Journal of Pharmaceutics*, 357(1), 295-304.
- Puglia, C., Damiani, E., Offerta, A., Rizza, L., Tirendi, G. G., Tarico, M. S., Curreri, S., Bonina, F., & Perrotta, R. E. (2014). Evaluation of nanostructured lipid carriers (NLC) and nanoemulsions as carriers for UV-filters: Characterization, in vitro penetration and photostability studies. *European Journal of Pharmaceutical Sciences*, 51, 211-217.

- Puglia, C., Frasca, G., Musumeci, T., Rizza, L., Puglisi, G., Bonina, F., & Chiechio, S. (2012). Curcumin loaded NLC induces histone hypoacetylation in the CNS after intraperitoneal administration in mice. *European Journal of Pharmaceutics and Biopharmaceutics*, 81(2), 288-293.
- Pujol, C. A., Estevez, J. M., Carlucci, M. J., Ciancia, M., Cerezo, A. S., & Damonte, E. B. (2002). Novel DL-galactan hybrids from the red seaweed *Gymnogongrus torulosus* are potent inhibitors of herpes simplex virus and dengue virus. *Antiviral Chemistry & Chemotherapy*, 13(2), 83-89.
- Rahman, M. H., Ramanathan, M., & Sankar, V. (2014). Preparation, characterization and in vitro cytotoxicity assay of curcumin loaded solid lipid nanoparticle in IMR32 neuroblastoma cell line. *Pakistan Journal of Pharmaceutical Sciences*, 27(5), 1281-1285.
- Rajaram, S., & Natham, R. (2013). Influence of formulation and process variables on the formation of rifampicin nanoparticles by ionic gelation technique. *Research Journal of Pharmaceutical, Biological and Chemical Sciences*, 4(4), 820-832.
- Ranpise, N. S., Korabu, S. S., & Ghodake, V. N. (2014). Second generation lipid nanoparticles (NLC) as an oral drug carrier for delivery of lercanidipine hydrochloride. *Colloids and Surfaces B: Biointerfaces*, 116, 81-87.
- Rodrigues, S., Rosa da Costa, A. M., & Grenha, A. (2012). Chitosan/carrageenan nanoparticles: Effect of cross-linking with tripolyphosphate and charge ratios. *Carbohydrate Polymers*, 89(1), 282-289.
- Rosada, R. S., Silva, C. L., Santana, M. H. A., Nakaie, C. R., & de la Torre, L. G. (2012). Effectiveness, against tuberculosis, of pseudo-ternary complexes: Peptide-DNA-cationic liposome. *Journal of Colloid and Interface Science*, 373(1), 102-109.
- Rowe, R. C., Sheskey, P. J., & Quinn, M. E. (Eds.). (2009). *Handbook of pharmaceutical excipients* (6th ed.). London, UK: Pharmaceutical Press.
- Sadiq, A. A., & Rassol, A. A. A. (2014). Formulation and evaluation of silibinin loaded solid lipid nanoparticles for peroral use targeting lower part of gastrointestinal tract. *International Journal of Pharmacy and Pharmaceutical Sciences*, 6(1), 55-67.
- Saengkrit, N., Saesoo, S., Srinuanchai, W., Phunpee, S., & Ruktanonchai, U. R. (2014). Influence of curcumin-loaded cationic liposome on anticancer activity for cervical cancer therapy. *Colloids and Surfaces B: Biointerfaces*, 114, 349-356.
- Sahoo, S., Chakraborti, C. K., & Behera, P. K. (2012). Development and evaluation of gastroretentive controlled release polymeric suspension containing ciprofloxacin and carbopol polymers. *Journal of Chemical and Pharmaceutical Research*, 4(4):2268-2284.

- Sandha, G. K., & Swami, V. K. (2009). Jojoba oil as an organic, shelf stable standard oil-phase base for cosmetic industry. *Rasayan Journal of Chemistry*, 2(2), 300-306.
- Sangsen, Y., Laochai, P., Chotsathidchai, P., & Wiwattanapatapee, R. (2015). Effect of solid lipid and liquid oil ratios on properties of nanostructured lipid carriers for oral curcumin delivery. *Advanced Materials Research*, 1060, 62-65.
- Sapra, P., & Allen, T. (2003). Ligand-targeted liposomal anticancer drugs. *Progress in Lipid Research*, 42(5), 439-462.
- Schwarz, J. C., Baisaeng, N., Hoppel, M., Löw, M., Keck, C. M., & Valenta, C. (2013). Ultra-small NLC for improved dermal delivery of coenzyme Q10. *International Journal of Pharmaceutics*, 447(1), 213-217.
- Severino, P., Andreani, T., Macedo, A. S., Fangueiro, J. F., Santana, M. H. A., Silva, A. M., & Souto, E. B. (2011). Current state-of-art and new trends on lipid nanoparticles (SLN and NLC) for oral drug delivery. *Journal of drug delivery*, 2012, 1-10. <http://dx.doi.org/10.1155/2012/750891>
- Severino, P., Pinho, S. C., Souto, E. B., & Santana, M. H. A. (2011). Polymorphism, crystallinity and hydrophilic-lipophilic balance of stearic acid and stearic acid-capric/caprylic triglyceride matrices for production of stable nanoparticles. *Colloids and Surfaces B: Biointerfaces*, 86(1), 125-130.
- Shi, J., Xue, S. J., Wang, B., Wang, W., Ye, X., & Quek, S. Y. (2015). Optimization of formulation and influence of environmental stresses on stability of lycopene-microemulsion. *LWT-Food Science and Technology*, 60(2), 999-1008.
- Shin, J., Shum, P., & Thompson, D. H. (2003). Acid-triggered release via dePEGylation of DOPE liposomes containing acid-labile vinyl ether PEG-lipids. *Journal of Controlled Release*, 91(1), 187-200.
- Shoaib, M. H., Tazeen, J., Merchant, H. A., & Yousuf, R. I. (2006). Evaluation of drug release kinetics from ibuprofen matrix tablets using HPMC. *Pakistan Journal of Pharmaceutical Sciences*, 19(2), 119-124.
- Sintov, A. C. (2015). Transdermal delivery of curcumin via microemulsion. *International Journal of Pharmaceutics*, 481(1), 97-103.
- Somasundaran, P., Wines, T. H., Mehta, S. C., Grati, N., & Farinato, R. (2007) Emulsion and their Behaviour. In Rhein, L. D. & Schlossman, M. (Eds.), *Surfactants in Personal Care Products and Decorative Cosmetics* (pp: 149-176) Florida, USA: Taylor & Francis Group.
- Souto, E. B., & Müller, R. H. (2008). Cosmetic features and applications of lipid nanoparticles (SLN[®], NLC[®]). *International Journal of Cosmetic Science*, 30(3), 157-165.

- Souto, E. B., Wissing, S. A., Barbosa, C. M., & Müller, R. H. (2004). Development of a controlled release formulation based on SLN and NLC for topical clotrimazole delivery. *International Journal of Pharmaceutics*, 278(1), 71-77.
- Souto, E. B., Wissing, S. A., Barbosa, C. M., & Müller, R. H. (2004). Evaluation of the physical stability of SLN and NLC before and after incorporation into hydrogel formulations. *European Journal of Pharmaceutics and Biopharmaceutics*, 58(1), 83-90.
- Souza, L. G., Silva, E. J., Martins, A. L., Mota, M. F., Braga, R. C., Lima, E. M., Valadares, M. C., Taveira, S. F., & Marreto, R. N. (2011). Development of topotecan loaded lipid nanoparticles for chemical stabilization and prolonged release. *European Journal of Pharmaceutics and Biopharmaceutics*, 79(1), 189-196.
- Špiclin, P., Gašperlin, M., & Kmetec, V. (2001). Stability of ascorbyl palmitate in topical microemulsions. *International Journal of Pharmaceutics*, 222(2), 271-279.
- Sripriya, R., Raja, K. M., Santhosh, G., Chandrasekaran, M., & Noel, M. (2007). The effect of structure of oil phase, surfactant and co-surfactant on the physicochemical and electrochemical properties of bicontinuous microemulsion. *Journal of Colloid and Interface Science*, 314(2), 712-717.
- Sudimack, J. J., Guo, W., Tjarks, W., & Lee, R. J. (2002). A novel pH-sensitive liposome formulation containing oleyl alcohol. *Biochimica et Biophysica Acta (BBA)-Biomembranes*, 1564(1), 31-37.
- Sugiura, S., Oda, T., Izumida, Y., Aoyagi, Y., Satake, M., Ochiai, A., Ohkohchi, N., & Nakajima, M. (2005). Size control of calcium alginate beads containing living cells using micro-nozzle array. *Biomaterials*, 26(16), 3327-3331.
- Suh, J.-K. F., & Matthew, H. W. (2000). Application of chitosan-based polysaccharide biomaterials in cartilage tissue engineering: A review. *Biomaterials*, 21(24), 2589-2598.
- Sułkowski, W. W., Pentak, D., Nowak, K., & Sułkowska, A. (2005). The influence of temperature, cholesterol content and pH on liposome stability. *Journal of Molecular Structure*, 744, 737-747.
- Syed, H. K., & Peh, K. K. (2014). Identification of phases of various oil, surfactant/co-surfactants and water system by ternary phase diagram. *Acta Poloniae Pharmaceutica – Drug Research*, 71(2), 301-309.
- Szu, S. C., Lin, K. F.-Y., Hunt, S., Chu, C., & Thinh, N. D. (2014). Phase I clinical trial of O-acetylated pectin conjugate, a plant polysaccharide based typhoid vaccine. *Vaccine*, 32(22), 2618-2622.
- Tagami, T., Suzuki, T., Matsunaga, M., Nakamura, K., Moriyoshi, N., Ishida, T., & Kiwada, H. (2012). Anti-angiogenic therapy via cationic liposome-mediated

- systemic siRNA delivery. *International Journal of Pharmaceutics*, 422(1), 280-289.
- Tan, H. W., & Misran, M. (2013). Polysaccharide-anchored fatty acid liposome. *International Journal of Pharmaceutics*, 441(1), 414-423.
- Tang, S. Y., Shridharan, P., & Sivakumar, M. (2013). Impact of process parameters in the generation of novel aspirin nanoemulsions—comparative studies between ultrasound cavitation and microfluidizer. *Ultrasonics Sonochemistry*, 20(1), 485-497.
- Teeranachaideekul, V., Boonme, P., Souto, E. B., Müller, R. H., & Junyaprasert, V. B. (2008). Influence of oil content on physicochemical properties and skin distribution of Nile red-loaded NLC. *Journal of Controlled Release*, 128(2), 134-141.
- Teeranachaideekul, V., Müller, R. H., & Junyaprasert, V. B. (2007). Encapsulation of ascorbyl palmitate in nanostructured lipid carriers (NLC) - Effects of formulation parameters on physicochemical stability. *International Journal of Pharmaceutics*, 340(1), 198-206.
- Telofski, L. S., Morello, A. P., Mack Correa, M. C., & Stamatas, G. N. (2012). The infant skin barrier: Can we preserve, protect, and enhance the barrier? *Dermatology Research and Practice*, 2012, 1-18. <http://dx.doi.org/10.1155/2012/198789>
- Teo, Y. Y., Misran, M., & Low, K. H. (2012). Effect of pH on physicochemical properties and encapsulation efficiency of PEGylated linoleic acid vesicles. *E-Journal of Chemistry*, 9(2), 729-738.
- Teo, Y. Y., Misran, M., Low, K. H., & Zain, S. M. (2011). Effect of unsaturation on the stability of C18 polyunsaturated fatty acids vesicles suspension in aqueous solution. *Bulletin of the Korean Chemical Society*, 32(1), 59-64.
- Tiyaboonchai, W. (2013). Chitosan nanoparticles: A promising system for drug delivery. *Naresuan University Journal: Science and Technology*, 11(3), 51-66.
- Torchilin, V. (2011). Tumor delivery of macromolecular drugs based on the EPR effect. *Advanced Drug Delivery Reviews*, 63(3), 131-135.
- Treiner, C. (2006). Adsorption of surfactants and induced adsorption at solid-liquid interfaces. In Somasundaran, P. (Ed.) *Encyclopedia of Surface and Colloid Science* (pp: 734-745). Florida, USA: Taylor and Francis Group.
- Trotta, M., Debernardi, F., & Caputo, O. (2003). Preparation of solid lipid nanoparticles by a solvent emulsification–diffusion technique. *International Journal of Pharmaceutics*, 257(1), 153-160.

- Tsai, Y.-H., Lee, K.-F., Huang, Y.-B., Huang, C.-T., & Wu, P.-C. (2010). In vitro permeation and in vivo whitening effect of topical hesperetin microemulsion delivery system. *International Journal of Pharmaceutics*, 388(1), 257-262.
- Ueno, H., Mori, T., & Fujinaga, T. (2001). Topical formulations and wound healing applications of chitosan. *Advanced Drug Delivery Reviews*, 52(2), 105-115.
- Üner, M., Karaman, E. F., & Aydoğmuş, Z. (2014). Solid lipid nanoparticles and nanostructured lipid carriers of loratadine for topical application: Physiochemical stability and drug penetration through rat skin. *Tropical Journal of Pharmaceutical Research*, 13(5), 653-660.
- Üner, M., Wissing, S. A., Yener, G., & Müller, R. H. (2004). Influence of surfactants on the physical stability of solid lipid nanoparticle (SLN) formulations. *Die Pharmazie-An International Journal of Pharmaceutical Sciences*, 59(4), 331-332.
- Üner, M., Wissing, S. A., Yener, G., & Müller, R. H. (2005). Solid lipid nanoparticles (SLN) and nanostructured lipid carriers (NLC) for application of ascorbyl palmitate. *Die Pharmazie-An International Journal of Pharmaceutical Sciences*, 60(8), 577-582.
- Urpi-Sarda, M., Casas, R., Chiva-Blanch, G., Romero-Mamani, E. S., Valderas-Martínez, P., Arranz, S., Andres-Lacueva, C., Llorach, R., Medina-Remón, A., Lamuela-Raventos, R. M., & Estruch, R. (2012). Virgin olive oil and nuts as key foods of the Mediterranean diet effects on inflammatory biomarkers related to atherosclerosis. *Pharmacological Research*, 65(6), 577-583.
- van Zutphen, S., & Reedijk, J. (2005). Targeting platinum anti-tumour drugs: Overview of strategies employed to reduce systemic toxicity. *Coordination Chemistry Reviews*, 249(24), 2845-2853.
- Varshosaz, J., Ghalaie, P. M., & Hassanzadeh, F. (2014). Hyaluronate targeted solid lipid nanoparticles of etoposide: optimization and in vitro characterization. *Journal of Nanomaterials*, 2014, 1-12. <http://dx.doi.org/10.1155/2014/345845>
- Viola, P., & Viola, M. (2009). Virgin olive oil as a fundamental nutritional component and skin protector. *Clinics in Dermatology*, 27(2), 159-165.
- Wakita, K., Kuwabara, H., Furusho, N., Tatebe, C., Sato, K., & Akiyama, H. (2014). A Comparative Study of the Hydroxyl and Saponification Values of Polysorbate 60 in International Food Additive Specifications. *American Journal of Analytical Chemistry*, 2014.
- Wang, J. J., Zeng, Z. W., Xiao, R. Z., Xie, T., Zhou, G. L., Zhan, X. R., & Wang, S. L. (2011). Recent advances of chitosan nanoparticles as drug carriers. *International Journal of Nanomedicine*, 6, 765-774.
- Wang, L.-H., Wang, C.-C., & Kuo, S.-C. (2007). Vehicle and enhancer effects on human skin penetration of aminophylline from cream formulations: Evaluation in vivo. *Journal of Cosmetic Science*, 58(3), 245-254.

- Wang, Q., Zhang, B., Lin, X., & Weng, W. (2011). Hybridization biosensor based on the covalent immobilization of probe DNA on chitosan–mutiwallled carbon nanotubes nanocomposite by using glutaraldehyde as an arm linker. *Sensors and Actuators B: Chemical*, 156(2), 599-605.
- Wang, X.-Q., & Zhang, Q. (2012). pH-sensitive polymeric nanoparticles to improve oral bioavailability of peptide/protein drugs and poorly water-soluble drugs. *European Journal of Pharmaceutics and Biopharmaceutics*, 82(2), 219-229.
- Wang, Y.-S., Liu, L.-R., Jiang, Q., & Zhang, Q.-Q. (2007). Self-aggregated nanoparticles of cholesterol-modified chitosan conjugate as a novel carrier of epirubicin. *European Polymer Journal*, 43(1), 43-51.
- Weiss, J., Decker, E. A., McClements, D. J., Kristbergsson, K., Helgason, T., & Awad, T. (2008). Solid lipid nanoparticles as delivery systems for bioactive food components. *Food Biophysics*, 3(2), 146-154.
- William, A. (2003). *Transdermal and Topical Drug Delivery from Theory to Clinical Practice*. London, UK: Pharmaceutical Press.
- Wissing, S. A., Kayser, O., & Müller, R. H. (2004). Solid lipid nanoparticles for parenteral drug delivery. *Advanced Drug Delivery Reviews*, 56(9), 1257-1272.
- Wissing, S. A., & Müller, R. H. (2002). Solid lipid nanoparticles as carrier for sunscreens: in vitro release and in vivo skin penetration. *Journal of Controlled Release*, 81(3), 225-233.
- Woo, J. O., Misran, M., Lee, P. F., & Tan, L. P. (2014). Development of a controlled release of salicylic acid loaded stearic acid-oleic acid nanoparticles in cream for topical delivery. *The Scientific World Journal*, 2014, 1-7. <http://dx.doi.org/10.1155/2014/205703>
- Wu, H., Long, X., Yuan, F., Chen, L., Pan, S., Liu, Y., Stowell, Y., & Li, X. (2014). Combined use of phospholipid complexes and self-emulsifying microemulsions for improving the oral absorption of a BCS class IV compound, baicalin. *Acta Pharmaceutica Sinica B*, 4(3), 217-226.
- Xu, X., Khan, M. A., & Burgess, D. J. (2012). Predicting hydrophilic drug encapsulation inside unilamellar liposomes. *International Journal of Pharmaceutics*, 423(2), 410-418.
- Xu, Y. X., Kim, K. M., Hanna, M. A., & Nag, D. (2005). Chitosan–starch composite film: preparation and characterization. *Industrial Crops and Products*, 21(2), 185-192.
- Yan, W., Chen, W., & Huang, L. (2007). Mechanism of adjuvant activity of cationic liposome: phosphorylation of a MAP kinase, ERK and induction of chemokines. *Molecular Immunology*, 44(15), 3672-3681.

- Yang, T., Choi, M.-K., Cui, F.-D., Kim, J. S., Chung, S.-J., Shim, C.-K., & Kim, D.-D. (2007). Preparation and evaluation of paclitaxel-loaded PEGylated immunoliposome. *Journal of Controlled Release*, 120(3), 169-177.
- Yang, T., Cui, F.-D., Choi, M.-K., Cho, J.-W., Chung, S.-J., Shim, C.-K., & Kim, D.-D. (2007). Enhanced solubility and stability of PEGylated liposomal paclitaxel: in vitro and in vivo evaluation. *International Journal of Pharmaceutics*, 338(1), 317-326.
- Yermak, I. M., Barabanova, A. O., Aminin, D. L., Davydova, V. N., Sokolova, E. V., Solov'eva, T. F., Kim, Y. H., & Shin, K. S. (2012). Effects of structural peculiarities of carrageenans on their immunomodulatory and anticoagulant activities. *Carbohydrate Polymers*, 87(1), 713-720.
- Yoo, H. S., Lee, J. E., Chung, H., Kwon, I. C., & Jeong, S. Y. (2005). Self-assembled nanoparticles containing hydrophobically modified glycol chitosan for gene delivery. *Journal of Controlled Release*, 103(1), 235-243.
- Yuan, H., Wang, L.-L., Du, Y.-Z., You, J., Hu, F.-Q., & Zeng, S. (2007). Preparation and characteristics of nanostructured lipid carriers for control-releasing progesterone by melt-emulsification. *Colloids and surfaces B: Biointerfaces*, 60(2), 174-179.
- Yuan, Y., Li, S.-M., Mo, F.-K., & Zhong, D.-F. (2006). Investigation of microemulsion system for transdermal delivery of meloxicam. *International Journal of Pharmaceutics*, 321(1), 117-123.
- Zhang, J., Li, G., Yang, F., Xu, N., Fan, H., Yuan, T., & Chen, L. (2012). Hydrophobically modified sodium humate surfactant: Ultra-low interfacial tension at the oil/water interface. *Applied Surface Science*, 259, 774-779.
- Zhang, P., Ling, G., Pan, X., Sun, J., Zhang, T., Pu, X., Yin, S., & He, Z. (2012). Novel nanostructured lipid-dextran sulfate hybrid carriers overcome tumor multidrug resistance of mitoxantrone hydrochloride. *Nanomedicine: Nanotechnology, Biology and Medicine*, 8(2), 185-193.
- Zhang, X., Pan, W., Gan, L., Zhu, C., Gan, Y., & Nie, S. (2008). Preparation of a dispersible PEGylate nanostructured lipid carriers (NLC) loaded with 10-hydroxycamptothecin by spray-drying. *Chemical and Pharmaceutical Bulletin*, 56(12), 1645-1650.
- Zhang, Y., Chen, J., Zhang, G., Lu, J., Yan, H., & Liu, K. (2012). Sustained release of ibuprofen from polymeric micelles with a high loading capacity of ibuprofen in media simulating gastrointestinal tract fluids. *Reactive and Functional Polymers*, 72(6), 359-364.
- Zhang, Y., Huo, M., Zhou, J., Zou, A., Li, W., Yao, C., & Xie, S. (2010). DDSolver: An add-in program for modelling and comparison of drug dissolution profiles. *The AAPS Journal*, 12(3), 263-271.

- Zhang, Y., Xu, Q., Liu, Y. H., Zhang, X. S., Wang, J., Yu, X. M., Zhang, R. X., Xue, C., Yang, X. Y., & Xue, C. Y. (2015). Medium-chain triglyceride activated brown adipose tissue and induced reduction of fat mass in C57BL/6J mice fed high-fat diet. *Biomedical and Environmental Sciences*, 28(2), 97-104.
- Zhao, X. B., & Lee, R. J. (2004). Tumor-selective targeted delivery of genes and antisense oligodeoxyribonucleotides via the folate receptor. *Advanced Drug Delivery Reviews*, 56(8), 1193-1204.
- Zheng, L.-Y., & Zhu, J.-F. (2003). Study on antimicrobial activity of chitosan with different molecular weights. *Carbohydrate Polymers*, 54(4), 527-530.
- Zhuang, Y., Ma, Y., Wang, C., Hai, L., Yan, C., Zhang, Y., Liu, F., & Cai, L. (2012). PEGylated cationic liposomes robustly augment vaccine-induced immune responses: role of lymphatic trafficking and biodistribution. *Journal of Controlled Release*, 159(1), 135-142.

LIST OF PUBLICATIONS AND PAPERS PRESENTED

Accepted publication

1. Yew, H.-C., Misran, M. (2016). Nonionic mixed surfactant stabilized water-in-oil microemulsions for active ingredient in vitro sustained release. *Journal of Surfactants and Detergents*, 19, 49-56.
2. Yew, H.-C., Misran, M. (2016). Preparation and characterization of pH dependent κ -carrageenan-chitosan nanoparticle as potential slow release delivery carrier. *Iranian Polymer Journal*, 25, 1037-1046.

Submitted publication

1. Yew, H.-C., Misran, M. Characterization of fatty acid based nanostructured lipid carrier (NLC) and their sustained release properties. (In review)
2. Yew, H.-C., Misran, M. Comparison of the effect of degree of unsaturation on C18 fatty acid liposome and its encapsulation efficiency (Revision)

Papers presented (Oral presentation)

1. Yew, H. C., Misran, M. (2013). The effect of unsaturated fatty acids on the size and encapsulation efficiency of nanostructured lipid carrier (NLC). International Post Graduate Conference on Science and Mathematics 2013, Universiti Pendidikan Sultan Idris, Perak, 5th to 6th October 2013.
2. Yew, H. C., Misran, M. (2015). Active ingredients with different water solubility loaded in fatty acid liposomes for sustained delivery. 5th International Polymer Conference of Thailand (PCT-5), Bangkok, Thailand, 18th to 19th June 2015.